DYNAMIC RESPONSE OF HIGH-SPEED RAIL DUE TO TRAIN BRAKING

TRAN MINH THI

(M. Eng., HCMUT)

A THESIS SUBMITTED

FOR THE DEGREE OF DOCTOR OF PHILOSOPHY

DEPARTMENT OF CIVIL AND ENVIRONMENTAL ENGINEERING

NATIONAL UNIVERSITY OF SINGAPORE

2016

DECLARATION

I hereby declare that this thesis is my original work and it has been written by me in its entirety. I have duly acknowledged all the sources of information which have been used in the thesis.

This thesis has also not been submitted for any degree in any university previously.

Tran Minh Thi
26 July 2016

ACKNOWLEDGMENTS

First of all, I would like to express my appreciation to my supervisor, Associate Professor Ang Kok Keng, for his encouragement and continuous guidance during my research. He was always willing to answer my questions, check my results and suggest new problems.

I am also grateful to my friend, Dr. Dai Jian, a former Ph.D. student at CEE department, NUS. He always shares his knowledge regarding train-track dynamics and this helps me a lot in my research.

I wish to express my sincere gratitude to the National University of Singapore for the financial aid given to support my study.

Finally, I want to acknowledge the support received from my family. I especially would like to dedicate this report with great respect and love to my parents, my wife Truong Thi Khanh Van and my son Tran Minh Khang for all things they have endured and sacrificed for my success.

TABLE OF CONTENTS

SUMMARY

The rapid increase in the use of high-speed rails (HSRs) for travels all over the world and the unfortunate occurrences of many catastrophic accidents involving HSRs are reasons why research on railway dynamics is becoming more and more important. The study on the response of high-speed trains subject to braking is particularly critical, as it contributes directly to ensuring better operational safety and superior train design. Heavy braking severely affects the dynamics of the train which could result in safety and train instability concerns. The former relates to the safe braking distance and the latter pertains to perilous occurrence of wheel sliding and potential disastrous derailment. Thus, the objective of this thesis is to formulate an efficient and reliable computational method for investigating the dynamics of high-speed trains subject to braking under various situations.

The challenge is to obtain efficient and accurate numerical strategies that can capture the details of the complex interaction between train system, wheels, rail track and the supporting system. In the commonly adopted Finite Element Method (FEM), the problem is complicated by the fact that the moving train will eventually reach and beyond the boundary of the truncated finite element domain. This problem is even more serious for HSR systems whereby the speed is much higher than normal trains, which means the finite element domain has to be very large (hence computationally expensive).

For these reasons, the recently developed Moving Element Method (MEM) has been adopted. The method has been shown by several researchers to be novel and efficient for modeling moving train/load on rail track supported continuously on uniform viscoelastic foundation. In addition to overcoming the train running out of the truncated domain, the MEM permits non-uniform mesh (for better efficiency) which is not possible when using the FEM for moving train/load problems.

In this thesis, numerical modeling and parametric studies have been carried out to investigate the dynamic response of high-speed train subject to braking. Compared to previous works on the MEM, the main findings in enhancing the method can be summarized as follows:

(1) A solution strategy to deal with non-uniform speed. This is necessary to solve problems where acceleration or deceleration is not known apriori, which is the case for braking, especially unplanned deceleration due to emergency braking.

(2) In achieving point 1 above, the system dynamics has to include forces on moving train such as running resistance, wheel-rail contact force (nonlinear Hertz model), wheel-rail adhesion force. This enables the study of effects of braking on wheel sliding. When the train is subject to braking under emergency situation, it is found that the applied braking torque should be at the so-called optimal torque as it represents a good compromise between train instability and safety. The optimal braking torque is one when all wheels are rolling and one of the wheels is at impending sliding condition.

(3) The MEM is extended to include interaction of multiple railcars accounting for couplers with slack action, which is the relative motion between railcars. Based on parametric studies, it is found that model with minimum three railcars is sufficient to capture the response of a multiple railcar train.

LIST OF TABLES

LIST OF FIGURES

NOTATIONS

3-DOF train model

m_1 , m_2 , m_3	Mass of the car body, bogie and wheel-axle, respectively
k_1 , c_1	Spring and dashpot of a secondary suspension system, respectively
k_2 , c_2	Spring and dashpot of a primary suspension system, respectively
k_3 , c_3	Spring and dashpot of the contact between the wheel and rail beam, respectively
u_1, u_2, u_3	Vertical displacements of the car body, bogie and wheel-axle, respectively
g	Acceleration due to the gravity

15-DOF train model

m_c , m_b , m_w	Mass of the car body, each bogie and each wheel, respectively
J_c , J_b, J_w	Moment of inertia about the pitch of car body, each bogie and each wheel, respectively
k_s , c_s	Spring and dashpot of a secondary suspension system, respectively
k_p , c_p	Spring and dashpot of a primary suspension system, respectively
l_1, l_2	Positions of the secondary and primary suspension spring-damping units measured with respect to the centre of mass of the bogies and car body, respectively
u_c , θ_c	Vertical and pitch displacements of the car body, respectively
u_{br} , θ_{br}	Vertical and pitch displacements of the rear bogie, respectively
u_{bf} , θ_{bf}	Vertical and pitch displacements of the front bogie, respectively

u_{wi} $(i = 1 \text{ to } 4)$	Vertical displacement of the i^{th} wheel
$\theta_{wi}\left(i = 1 \text{ to } 4\right)$	Pitch displacement of the i^{th} wheel
h_1	Vertical distance between car body's center of gravity and horizontal internal forces interlocking between car body and bogies
h_2	Vertical distance between the horizontal internal forces and center of gravity of bogies
h_3	Vertical distance between center of gravity of bogies and internal horizontal forces connecting bogies to wheels
h_4	Vertical distance between the coupler and the car body's centre of mass

Running resistance

F_r	Total running resistance force acting on car body
c_0, c_v, c_a	Aerodynamic coefficients obtained from wind tunnel test

Wheel-rail interaction

F_c	Contact force between the wheel and rail
F_{ci}	Contact force between the i^{th} wheel and rail
Δy	Indentation at the contact surface
Δy_i	Indentation at the contact surface at the i^{th} wheel
K_H	Hertzian spring constant
R_w, R_r	Radii of the wheel and railhead, respectively
υ	Poisson's ratio of the material
K_L	Linear Hertzian spring constant
W	Self-weight of the upper structure of the train-track system
y_r, y_t	Rail displacements and the magnitude of the track

	irregularity at the contact point, respectively
y_{ri} , y_{ti}	Rail displacements and the magnitude of the track irregularity at the i^{th} contact point, respectively
a_t , λ_t	Amplitude and wavelength of track irregularity, respectively.

Wheel-rail adhesion force

f_i	Adhesion force between the i^{th} wheel and rail
ε_i	Gradient of tangential stress in the longitudinal direction
k_A, k_S	Reduction factors in the adhesion and slip areas, respectively
a_i , b_i	Semi-axes of the contact ellipse at the i^{th} wheel
c_{11}	Coefficient from Kalker's linear theory
G	Shear modulus of rigidity
μ_i	Friction coefficient between the i^{th} wheel and rail
c_{li}	Longitudinal creep at the i^{th} wheel
A	Ratio of limit friction coefficient μ_∞ at infinity slip velocity to maximum friction coefficient μ_0 at the zero slip velocity
B	Coefficient of the exponential friction decrease.

Coupler force

F_{cf} , F_{cr}	Coupler forces exerted on the car body at the front and rear, respectively
g_{cf} , g_{cr}	Coupler gaps of the front and rear couplers, respectively;
s_f , s_r	Relative motions of the typical railcar relative to the front and rear railcars, respectively
c_{cf} , k_{cf}	Damping and stiffness of the coupler between the typical railcar and front neighbouring railcar, respectively
c_{cr} , k_{cr}	Damping and stiffness of the coupler between the typical

	railcar and rear neighbouring railcar, respectively

Track-foundation model

α , ϕ, λ	Damping parameters
s , $\dot{s}$, $\ddot{s}$	Travel, velocity and acceleration of the train at any instant, respectively
k , k_{sm}	Vertical Winkler springs and shear modulus, respectively
y	Vertical displacement of the track
E , I , m	Young's modulus, moment of inertia and mass per unit length of rail beam, respectively
t	Time
δ	Dirac-delta function
x, r	Fixed and moving relative coordinate, respectively

Moving element method

$\mathbf{M}_e$, $\mathbf{C}_e$, $\mathbf{K}_e$	Mass, damping and stiffness matrices of the moving element, respectively
$(\ )_{,r}$	Partial derivative with respect to r
L	Length of a typical moving element
$\mathbf{N}$	Element nodal displacement shape function for beam element
a_0, a_1	Factors in calculating Rayleigh damping
ω_m, ζ_m	Fundamental frequency and damping ratio of the system, respectively
ω_n, ζ_n	Higher frequencies and damping ratios of the modes that contribute significantly to the dynamic response, respectively
ξ	Damping ratio

Governing equations of motion

$\ddot{\mathbf{z}}$, $\dot{\mathbf{z}}$, $\mathbf{z}$	Global acceleration, velocity and displacement vectors of the train-track-foundation system, respectively
$\mathbf{M}$, $\mathbf{C}$, $\mathbf{K}$	Global mass, damping and stiffness matrices, respectively
$\mathbf{P}$	Global load vector

Analytical solution

y_i	Generalized coordinate of the i^{th} vibration mode of the rail

Newmark integration method

$\ddot{\mathbf{z}}_{n+1}$, $\dot{\mathbf{z}}_{n+1}$, $\mathbf{z}_{n+1}$	Global displacement, velocity and acceleration vectors at time t_{n+1}, respectively
$\ddot{\mathbf{z}}_n$, $\dot{\mathbf{z}}_n$, $\mathbf{z}_n$	Global displacement, velocity and acceleration vectors at time t_n, respectively
Δt	Interval of time
γ , β	How much the acceleration at the end of the interval enters into the velocity and displacement equations at the end of the interval Δt, respectively
$\mathbf{P}_{n+1}$	Global force vectors at time t_{n+1}

Newton-Raphson scheme

f	Equilibrium function
f^{i+1}, f^i	Values for f at iteration step $i+1$ and i, respectively
U	Vector of variables
U^{i+1}, U^i	Values for U at iteration step $i+1$ and i, respectively
τ	Numerical tolerance

ACRONYMS

2-D	Two-dimensional
3-D	Three-dimensional
DAF	Dynamic amplification factor
DOF	Degree of freedom
FEM	Finite element method
FTM	Fourier transformation method
HSR	High-speed rail
MEM	Moving element method

CHAPTER 1. INTRODUCTION

1.1 Background

Railway transportation is one of the key modes of travel today. The advancement in train technology leading to faster and faster trains is without doubt a positive development, which makes the HSR more attractive as an alternative to other modes of transportation for long distance travel. As early as 1978, an electric train manufactured in France reached a record high speed of 260 km h^{-1}. In October 1981, another high speed train named "TGV" began operation in France and rewrote the record for maximum speed when it managed to achieve a speed of 380 km h^{-1}. Presently in China, a new series of high-speed trains named "CRH-3" can reach an average speed of 350 km h^{-1}, and is becoming widely used. At the same time, the population of people who are travelling by high-speed trains regularly has grown. By 2020, a new high-speed line between Kuala Lumpur and Singapore would have been constructed and commuters would enjoy a short travel time of only 90 minutes. The number of commuters using this high-speed line is expected to be significant.

While train technology has greatly advanced since the introduction of the first HSR and the network of high-speed tracks has grown considerably, there is unfortunately insufficient research done to understand the dynamics of the HSRs. The lack of research might be cited as a contributing reason why there are many accidents involving HSRs all over the world. Figure 1.1 shows

the Eschede train disaster that occurred on 3rd June 1998 in Germany. It was the world's deadliest HSR accident with a recorded toll of 101 deaths and estimated 88 injured. It was caused by a single fatigue crack in one wheel, which caused the train to derail at a switch. Figure 1.2 shows CRH accident occurred in China on 23rd July 2011, in which two high-speed trains collided and derailed each other. More than 40 people were killed, at least 192 were injured, 12 of which were severe injuries. Figure 1.3 presents the Shinkansen accident in Japan on 2nd March 2013. A high speed Shinkansen train carrying 130 people derailed when going through the Akita Province. Apparently, the derailment may be due to thick snow sticking to the rails. Figure 1.4 presents another tragedy involving HSR accidents resulting in 78 deaths and 131 injured, which took place recently on 25 July 2013 in the northern Spanish region of Galicia. The accident involved a HSR train derailing due it travelling at a speed higher than the allowed speed over a curved part of the journey.

The catastrophic nature of all the above-cited accidents involving HSRs emphasizes the importance of understanding the dynamic response of train-track systems. Various safety concerns have to be addressed in order to minimize or eradicate such accidents from ever happening. Derailment is a key safety concern that arises mainly due to high vibrations produced. Some of the factors that affect the dynamic response are the speed of the train, the magnitude of the applied wheel braking torques, the severity of railhead irregularities and foundation stiffness. The high speed of trains do results in a

set of safety, design and maintenance issues not previously noted in trains travelling at moderate or low speeds.

Figure 1.1. ICE accident (1998).

Figure 1.2. CRH accident (2011).

Figure 1.3. Japan (2013).

Figure 1.4. Spain (2013).

While it is important to understand the response of HSR travelling at uniform high speed, it is also critical to study the response of non-uniform motion of HSR due to braking. A derailment study (China Academy of Railway Science 1998) revealed that 30% of derailments in Russia occurred due to emergency braking under poor wheel-rail contact condition. Forced high decelerations in order to safeguard the train to come to a halt quickly to avoid other possible catastrophes may be necessary under emergency situations. Such trains would then be subject to so-called ‘abnormal’ braking.

Unlike normal braking, when a train decelerates under moderate to heavy braking condition, instability due to train wheels sliding over the rails could occur. Also, unsafe levels of high dynamic response may be induced due to abnormal braking, which may lead to failure of structural components. Many of the above-cited factors influencing the dynamics of HSRs have not been adequately addressed in the literature. There is thus an urgent need to investigate the dynamics of HSRs subject to braking in order to safeguard the safety of HSR travels and ensure that its popularity as a viable means of safe and reliable transportation continues to grow.

1.2 Literature review

The HSR has been investigated as a track beam resting on a visco-elastic foundation subject to moving loads varying both in time and space. As early as 1926, Timoshenko proposed the use of a moving coordinate system to obtain the quasi-steady state solution of an infinite beam resting on an elastic foundation subject to a constant-velocity moving point load. In this study, the Fourier Transform Method (FTM) is used for solving the differential equation.

Various researchers have investigated the problem of loads travelling at non-uniform velocities. Suzuki (1977) employed the energy method to derive the governing equation of a finite beam subject to traveling loads involving acceleration. Involved integrations are carried out using Fresnel integrals and analytical solutions are presented. Yadav (1991) investigated the vibration response of a train-track-foundation system resulting from a vehicle travelling

at variable velocities over finite track. Analytical solutions were obtained and the response characteristics of the system examined. Karlstrom (2006) used the FTM to obtain analytical solutions for the investigation of ground vibrations due to accelerating and decelerating trains traveling over an infinitely long track. The solution is based on Fourier transforms in time and along the track. Although analytical solutions are elegant which provide clear physical insights into the nature of the problem, they are limited in dealing with practical applications involving multi-degrees of freedom train models and realistic railway tracks that suffer from railhead roughness.

The Finite Element Method (FEM) is a well-established numerical method widely used to solve many complicated problems, including problems involving moving loads. For example, Frýba et al. (1993) presented a stochastic finite element analysis of an infinite beam resting on an elastic foundation subject to a constant load travelling at constant speed. Another research study carried out based on the FEM was done by Thambiratnam and Zhuge (1996). They performed a dynamic analysis of a simply supported beam resting on an elastic foundation subjected to moving point loads and extended the study to the analysis of a railway track modeled as an infinitely long beam.

However, the FEM encounters difficulty when the moving load approaches the boundary of the finite domain and travels beyond the boundary. These difficulties can be overcome by employing a large enough domain size but at the expense of significant increase in computational time.

In an attempt to overcome the complication encountered by FEM, Krenk et al. (1999) proposed the use of FEM in convected coordinates, similar to the moving coordinate system proposed by Timoshenko (1926), to obtain the response of an elastic half-space subject to a moving load. The key advantage of this approach is its ability to overcome the problem produced by the moving load travelling over a finite domain. Andersen et al. (2001) provided an FEM formulation in resolving the problem of a beam on a Kelvin foundation subject to a harmonic moving load. Koh et al. (2003) adopted the convected coordinate system for solving train-track problems, and named the numerical algorithm the moving element method (MEM). The method was subsequently applied to the analysis of in-plane dynamic response of annular disk (Koh et al. 2006) and moving loads on a viscoelastic half space (Koh et al. 2007). Ang and Dai (2013) extended the MEM to investigate the "jumping wheel" phenomenon in high-speed train motion at constant velocity over a transition region where there is a sudden change of foundation stiffness. The phenomenon occurs when there is momentary loss of contact between the wheel and rail.

In the above-cited studies, the HSR has so far been investigated as a rail beam resting on a Winkler foundation which is a rather simplistic model of the foundation. Interaction between the Winkler springs is not considered and thus may not accurately represent the characteristics of actual foundations. To overcome the deficiency of the single-parameter Winkler foundation, various researchers have proposed the use of a more accurate two-parameter soil

model (Filonenko–Borodich 1940; Pasternak 1954; Kerr 1964; Vlasov and Leont'ev 1966). This model differs from the Winkler foundation due to use of a shearing layer to connect the top of the Winkler springs and the adoption of a second foundation parameter to account for the stiffness of the shear layer. The accuracy and advantages of the two-parameter foundation in modeling the effects of elastic foundation support on structures have been investigated and described by Feng and Cook (1983). More recently, Kumari et al. (2012) investigated the dynamic response of infinite Euler-Bernoulli beam resting on two-parameter viscoelastic foundation subject to a constant-velocity moving point load. They obtained the solution of the governing differential equation analytically.

Lixin and Haitao (2001) studied the 3-D dynamic response of heavy trains travelling at a low speed subject to normal braking, in which the occurrence of wheel sliding was not investigated. Handoko and Dhanasekar (2007) predicted the dynamics of simplified two-axle bogies of low-speed train both under constant speed and under variable speed due to traction and braking. Zhang and Dhanasekar (2009) presented a low-speed train model under braking conditions in order to investigate car body pitch, derailment, and wheel-set skid. The influence of wheel-rail contact condition and track geometry defects on car body pitch was also discussed.

The aforementioned works mostly focused on the single-railcar train. As a typical train comprises of several railcars, it is important to investigate the longitudinal interaction between railcars connected by couplers, especially

when the train is subject to braking. The relative motion between railcars, known as "slack action", plays a significant effect on the response of the train-track system. During braking, the coupler between consecutive railcars develops cyclical compressive and tensile forces. The maximum compressive force developed in the coupler depends on many factors, such as the coupler stiffness and the coupler gap. Under adverse conditions, the coupler force developed may be large enough to cause failure in the couplers resulting in catastrophic train derailments (Garg and Dukkipati 1984). Pugi et al. (2007) developed a simple model of the longitudinal dynamics of a freight train due to normal braking. Vehicles are modeled as simple lumped masses connected by coupling system subject to normal braking. Dhanasekar et al. (2007) studied the longitudinal bogie dynamics of low-speed train under applied braking torque using an experimental method. In this study, controlling braking pressure and its application time were used to evaluate the occurrence of wheel sliding. Ansari et al. (2009) presented a comprehensive parametric study on the longitudinal dynamics of low-speed freight trains subject to traction and braking. The effect of the coupler properties on the dynamic response of a ten-railcar train model was investigated. Recently, Ahmad (2013) developed a dynamic model of a low-speed freight train due to normal braking. A three-railcar train model was used for performing a parametric study to investigate the effect of various factors on the braking distance.

1.3 Motivation of research

As can be seen from the literature review, many researchers focused their studies on a high-speed train travelling at uniform velocity. Some research has been carried out on a train subject to braking but these are confined to heavy train traveling at low-speed under normal braking condition with the railhead assumed to be perfectly smooth. However, real train-track systems are likely to have various degrees of railhead roughness and thus it is important to account for the effect of track irregularity on the dynamic response of HSRs. Also, high-speed trains do travel at non-uniform velocities, especially when accelerating to attain maximum operational speed or decelerating to reduce speed. Controlled levels of deceleration are encountered when normal braking is applied such as when the train approaches a curved track or coming to a halt at a station. However, high deceleration may be necessary when abnormal braking occurs, such as under emergency situations, that requires the train to come to a halt quickly to avoid other possible catastrophes. In order to investigate a high-speed train subject to abnormal braking, it is necessary to include in the formulation of the governing equations the possibility of wheel sliding over the rail.

Most previous works in the literature investigated the dynamics of a single-railcar train. Limited research works carried out on multiple-railcar train dynamics however mostly focused on a long heavy train traveling at low-speed over a smooth track subject to normal braking. Due to the gap in the literature, it is thus important to investigate the dynamic response of high-

speed multiple-railcar train subject to abnormal braking, in particular, the interaction between railcars which could result in spikes in the forces developed in the train couplers.

From the above literature review, it can be seen that the MEM has been successfully used in solving problems involving trains travelling on tracks resting on viscoelastic foundation. The method, which is a variation of the FEM, is elegant and has several advantages as compared to the FEM when dealing with problems involving moving loads. However, the method has so far been limited in applications involving rail beams resting on Winkler foundation subject to a constant-velocity moving train. The constant velocity-based MEM has been employed to deal with non-uniform motion of train but confined to cases where the train speed-time profile is given or assumed (Koh et al. 2003). This is achieved by dividing the total time duration into small time intervals and assuming that the speed of the train during each time interval is constant. As time changes, the constant velocity of the train in the MEM formulation is updated based on this piecewise approximation of the speed-time profile. However, under train braking conditions, the speed-time history of the train is unknown in advance and thus using the constant velocity-based MEM, as described above, is not feasible. It is thus necessary to extend the MEM to account for the instantaneous acceleration/deceleration of the train in order to investigate the dynamics of the HSR subject to braking.

1.4 Objective and scope of study

The objective of the present study is to investigate the dynamic response of high-speed train subject to braking. The results of the study will be useful in the safe operation, maintenance and design of HSRs. The scope of the research work includes:

(1) Efficient computational method

The constant velocity-based MEM is inadequate for dealing with train dynamics involving braking. It is thus necessary to extend the MEM to account for the instantaneous acceleration/deceleration of the moving train.

(2) Two-parameter elastic damped foundation

The foundation in which the track rests on forms a crucial component of the HSR. Thus, an accurate model of the foundation is important in obtaining a correct prediction of the response of the HSR. While the Winkler foundation is able to reasonably model the behavior of the foundation, it may be too simplified to account for the actual foundation. Thus, it is necessary to adopt a more accurate two-parameter soil model.

Dissipation mechanisms in the track-foundation model needs to be addressed appropriately. There are three mechanisms of physical damping in a realistic track-foundation, namely (1) external or viscous damping (interaction with surrounding medium or interface with other physical systems), (2) so-called structural damping (shear diffusion damping) and (3) internal or Kelvin-Voigt damping (caused by processes within the system, i.e. increase of heat

energy to the detriment of mechanical energy by means of internal friction and thermo-elastic effects).

(3) Wheel-rail contact model

The accuracy of the dynamic analysis of the HSRs depends significantly on the correctness of the contact model accounting for the normal wheel-rail interaction. Two models based on Hertz contact theory are employed, namely a simple linearized and a more sophisticated nonlinear version. Due to the nature of high speed of the train, the contact models are extended to account for the possible occurrence of the jumping wheel phenomenon, where there is a momentary loss of contact between wheels and rail.

(4) Response of non-uniform motion of HSR

The proposed MEM is employed to first investigate the response of non-uniform motion of HSR, in which the speed-time profile of the train is given. The profile consists of three phases, namely (1) an accelerating phase in which the train accelerates uniformly to attain an operational speed, (2) a constant-speed phase and (3) a decelerating phase in which the train decelerates uniformly from operational speed to a halt. The accuracy of results obtained by the proposed MEM is verified against available results in the literature. A parametric study is carried out to understand the effects of various factors on the dynamic response of HSR including the occurrence of jumping wheel phenomenon. Parameters considered include the magnitude of train acceleration/deceleration, the severity of railhead roughness (track irregularity) and the wheel load.

(5) Response of single-railcar train subject to braking

A realistic train model that accounts for the effect of pitching moment arising from the longitudinal inertia effects and wheel adhesion forces is employed in order to deal with the case when a train is subject to braking. The modified nonlinear Hertz contact theory and Polach adhesive model are employed to account for the normal and tangential wheel-rail contact forces, respectively. Braking torques of constant amplitude are applied at all wheels in order to decelerate the train till to a halt. The effects of parameters such as braking torque, wheel-rail contact condition and initial train speed on the single-railcar train dynamics, including the dynamic amplification factor (DAF) in wheel-rail contact force as well as the occurrence of wheel sliding and jumping wheel phenomenon, will be examined.

(6) Response of multiple-railcar train subject to braking

A multiple-railcar train is employed in order to investigate the longitudinal interaction between railcars when the high-speed train is subject to abnormal braking. A parametric study is performed to understand the effects of magnitude of braking torque, coupler stiffness, coupler gap, wheel load, wheel-rail contact condition and initial train speed. The effect of partial failure in the train braking mechanism on the response of the multiple-railcar train subject to braking was also investigated.

1.5 Outline of study

The thesis is organized into following chapters as follows:

Chapter 1: The background, literature review as well as the motivation of the present study are presented. This is followed by the statement of the objective and some details on the scope of work carried out.

Chapter 2: Various mathematical models of the components of the HSR including the train, track-foundation, normal wheel-rail interaction model are presented. The derivation of the governing equations of motion of the system is also presented.

Chapter 3: This chapter mainly focuses on the computational method employed in this study. The MEM is employed to model the track-foundation, where element matrices are formulated based on a convected coordinate system attached to the center of mass of the moving train. Analytical formulas for simple cases of moving loads over tracks are presented for the purpose of comparison with the proposed computational method. Verification of the accuracy of the proposed scheme for simple case of moving load problem through comparison with available analytical and FEM results is presented.

Chapter 4: A computational study is carried out to investigate the dynamic response of HSR travelling at non-uniform speeds, in which the speed-time profile is specified. Verification of the accuracy of the proposed MEM for non-uniform motion of a 3-DOF train model through comparison with available results in the literature is presented and discussed. The effects of various factors on the dynamic response of the system such as the magnitude of train acceleration/deceleration, train speed, severity of track irregularity and wheel load are presented.

Chapter 5: This chapter presents the proposed computational scheme for investigating single-railcar train dynamics subject to braking with allowance for the possible occurrence of wheel sliding. A more realistic 15-DOF train model that accounts for the effect of pitching moment arising from the longitudinal inertia effects and wheel adhesion forces is presented. Solutions obtained using the proposed MEM for dynamic response of a single-railcar train subject to braking with possible sliding of wheels are verified through comparison with results obtained via the FEM. Results of a parametric study to understand the effects of various factors such as braking torque, initial train speed and wheel-rail contact condition on the dynamic response of the system, duration of wheel sliding and braking distance are presented.

Chapter 6: This chapter is concerned with the dynamics of multiple-railcar train subject to braking. The mathematical model of a multiple-railcar train traveling on a two-parameter elastic damped foundation is described and the governing equations are derived. The formulation of the coupler force connecting neighboring railcars is also presented. Solutions obtained using the proposed MEM for dynamic response of a multiple-railcar train subject to braking in which sliding of wheels occurs are verified through comparison with results obtained via the FEM. Results of a parametric study to investigate the effects of various factors such as the magnitude of braking torque, coupler stiffness, coupler gap, wheel load, wheel-rail contact condition, initial train speed and partial failure in braking mechanism on the multiple-railcar train dynamics are presented.

Chapter 7: This chapter summarizes the key findings of the thesis and presents the recommendations for future works.

CHAPTER 2. MATHEMATICAL MODELING

2.1 Introduction

In this chapter, mathematical modeling of train-track-foundation system is introduced. Various train models ranging from the simplest moving load model to the 3-DOF train model are employed. The train and track-foundation are coupled through the normal wheel-rail contact force. Two normal wheel-rail contact problems accounting for occurrence of the jumping wheel phenomenon are presented, namely a simple linearized and a more sophisticated nonlinear version. The railhead is assumed to have some imperfections resulting in the so-called "track irregularity". The railway track is treated as an Euler-Bernoulli beam resting on a two-parameter elastic damped foundation. The governing equation of motion of the train-track-foundation system is derived based on Newton's second Law of motion.

2.2 Train model

In view that the track gauge is large enough and that the track is straight, it is reasonable to assume there is little interaction between the pair of wheels of each wheel set and there is negligible rolling displacement of the centroid of the wheel-set of the wheel axle. Thus, a 2-D model of the train-track system comprising of one rail and half the train is considered.

2.2.1 Moving load model

Figure 2.1 shows a moving load model involving track-foundation subject to a single or sequence of moving loads F_i travelling a distance s over the railway track. This model is suitable for the cases involving less inertia effect and less wheel-rail interaction. Thus, the model may be good for the case when the mass of the train is much smaller as compared to the lower structure.

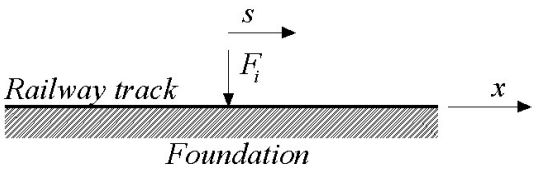

Figure 2.1. Moving load model.

2.2.2 3-DOF train model

In the 3-DOF model, the train is modeled as a system of three rigid components, namely the car body, bogie and wheel-set, inter-connected by spring-damper units as shown in Figure 2.2. The topmost mass m_1 represents the car body where the passengers are. The car body is supported by the bogie of mass m_2 through a secondary suspension system modeled by the spring k_1 and dashpot c_1. The bogie is in turn supported by the wheel-axle system of mass m_3 through a primary suspension system modeled by the spring k_2 and dashpot c_2. F_c is the contact force exerted between the train and track. The

vertical displacements of the car body, bogie and wheel-axle are denoted by u_1, u_2 and u_3, respectively.

Accounting for the effects of moving gravity loads and letting g be the acceleration due to the gravity, governing equations for the train model are written as

$$m_1\ddot{u}_1 + k_1\left(u_1 - u_2\right) + c_1\left(\dot{u}_1 - \dot{u}_2\right) = -m_1 g \tag{2.1}$$

$$m_2\ddot{u}_2 + k_2\left(u_2 - u_3\right) + c_2\left(\dot{u}_2 - \dot{u}_3\right) - k_1\left(u_1 - u_2\right) - c_1\left(\dot{u}_1 - \dot{u}_2\right) = -m_2 g \tag{2.2}$$

$$m_3\ddot{u}_3 - k_2\left(u_2 - u_3\right) - c_2\left(\dot{u}_2 - \dot{u}_3\right) = -m_3 g + F_c \tag{2.3}$$

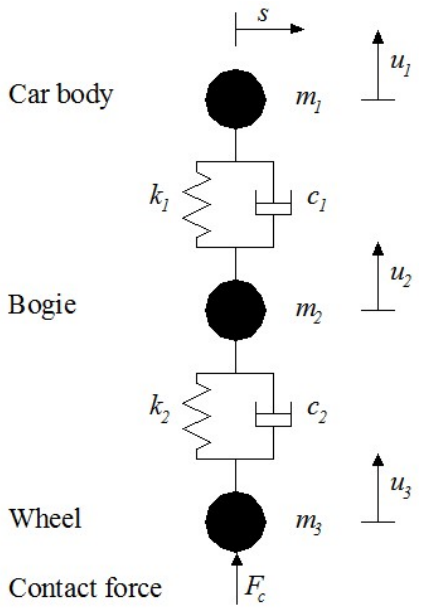

Figure 2.2. Moving 3-DOF model.

2.3 Wheel-rail contact force

Based on the nonlinear Hertz contact model (Esveld 2001), the contact force F_c between the wheel and rail may be expressed as

$$F_c = \begin{cases} K_H \Delta y^{\frac{3}{2}} & for \quad \Delta y \geq 0 \\ 0 & for \quad \Delta y < 0 \end{cases} \tag{2.4}$$

where K_H is the Hertzian spring constant given by

$$K_H = \frac{2}{3}\sqrt{\frac{E^2\sqrt{R_w R_r}}{(1-\upsilon^2)^2}} \tag{2.5}$$

in which R_w and R_r denote the radii of the wheel and railhead, respectively, υ the Poisson's ratio of the material and Δy the indentation at the contact surface. The latter may be expressed as

$$\Delta y = y_r + y_t - u_3 \tag{2.6}$$

in which y_r, y_t denote the vertical displacement of the rail and track irregularity at the contact point, respectively, and u_3 the vertical displacement of the wheel.

Track irregularity is a major source of the dynamic excitation. The corrugation of the rail surface and weld imperfections are the most important factors accounting for irregularities with short and moderate wavelengths in the order of centimeters up to about 3 m. For irregularities with larger wavelengths in the order of 3 m and more, the key causes are due to rail rolling defects and uneven settlement of the foundation (Esveld 2001 and Clark et al. 1982). The track irregularity describes the vertical unevenness in the railhead surface which arises due to various factors such as wear, tear and plastic deformation; and is widely assumed to take the following sinusoidal form (Nielsen and Abrahamsson 1992)

$$y_t = a_t \sin \frac{2\pi x}{\lambda_t} \tag{2.7}$$

where a_t and λ_t denote the amplitude and wavelength of track irregularity, respectively.

To avoid high computational cost and complexity of the nonlinear contact problem, many researchers have adopted a simplified approach based on a linear Hertz contact model in which F_c is given by

$$F_c = \begin{cases} K_L \Delta y & for \quad \Delta y \geq 0 \\ 0 & for \quad \Delta y < 0 \end{cases} \tag{2.8}$$

where K_L is the linear Hertzian spring constant (Esveld 2001) and may be computed as

$$K_L = \sqrt[3]{\frac{3E^2 W \sqrt{R_w R_r}}{2(1-\upsilon^2)^2}} \tag{2.9}$$

in which it is assumed that the reaction force at the contact point equals the self-weight of the upper structure W of the train-track system.

2.4 Shear modulus of foundation

Mathematically, the foundation reaction may be written as follows

$$p(x) = ky(x) - k_{sm} \frac{d^2 y(x)}{dx^2} \tag{2.10}$$

where $y(x)$ denotes the transverse deflection of the foundation; k and k_{sm} the Winkler modulus and second-parameter foundation (namely shear modulus)

coefficients, respectively. Note that shear modulus k_{sm} may be called by other ways:

- *a constant tension* by connecting the Winkler springs to a thin elastic membrane (Filonenko–Borodich 1940);
- *shear interaction* between the springs by connecting the ends of the springs to a layer consisting of incompressible vertical elements which deform only by transverse shearing (Pasternak 1954);
- *an equivalent line load* may be transformed by moment load from the foundation (Kerr 1964).

Although there is a difference from the definition of the parameters, the above formulations of foundation reactions proposed are equivalent. Therefore, it is not need to pay attention to this difference when solving the problems relating to a beam resting on a elastic foundation.

2.5 Dissipation mechanisms

Naturally, the presence of energy dissipation mechanisms is accepted in all models used for simulation of mechanical vibrations in elastic systems. In general, Herrmann (2008) presented three types of dissipation mechanisms

$$(a) \quad \alpha \frac{\partial y}{\partial t}; \qquad (b) \quad -\lambda \frac{\partial^3 y}{\partial x^2 \partial t}; \qquad (c) \quad \phi \frac{\partial^5 y}{\partial x^4 \partial t} \tag{2.11}$$

where the term (a) denotes the so-called external or viscous damping (interaction with surrounding medium, interface with other physical system); the term (b) the so-called structural damping (shear diffusion damping); and

the term (c) the so-called internal or Kelvin-Voigt damping (caused by processes within the system, i.e. increase of heat energy to the detriment of mechanical energy by means of internal friction and thermo-elastic effects).

2.6 Track-foundation model

The rail track is modeled as an infinite Euler-Bernoulli beam resting on a two-parameter elastic damped foundation. The beam is subject to a moving load arising from the wheel contact force F_c of the 3-DOF train model, as illustrated in Figure 2.3. The track-foundation is discretized into finite moving elements, in which the formulation of the element equations are based on adopting a convected coordinate r-axis with origin fixed at the origin of the moving load, as shown in Figure 2.3.

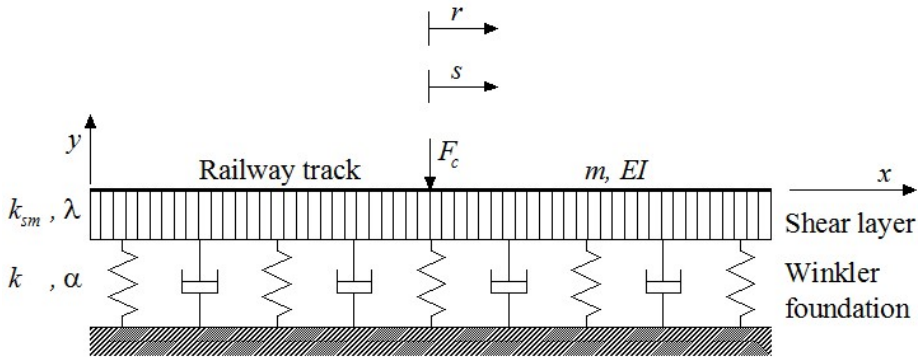

Figure 2.3. A track-foundation model.

The governing differential equation of motion of the track-foundation may be written as

$$EI\frac{\partial^4 y}{\partial x^4}+\phi EI\frac{\partial^4 \dot{y}}{\partial x^4}-\lambda\frac{\partial^2 \dot{y}}{\partial x^2}-k_{sm}\frac{\partial^2 y}{\partial x^2}+m\ddot{y}+\alpha\dot{y}+ky=-F_c\delta(x-s) \qquad (2.12)$$

where δ is the Dirac-delta function; and s the travel distance at any instant t of the origin of the r-axis measured with respect to the origin of the x-coordinate; E, I, m are the Young's modulus, second moment of inertia, mass per unit length of the track, respectively; k, k_{sm} the Winkler stiffness and shear modulus of foundation, respectively; α, ϕ, λ the so-called damping parameters of Winkler foundation, rail beam and shear layer, respectively.

Interestingly, it can be seen in Eq. (2.12) that $\left(EI\frac{\partial^4 y}{\partial x^4}, \phi EI\frac{\partial^4 \dot{y}}{\partial x^4} \right)$, $\left(k_{sm}\frac{\partial^2 y}{\partial x^2}, \lambda\frac{\partial^2 \dot{y}}{\partial x^2} \right)$ and $\left(ky, \alpha\dot{y} \right)$ denote so-called spring and damping forces of rail beam, shear layer and Winkler foundation, respectively. Mathematically, the three damping forces are the results of differentiation respect to time of the respective spring forces.

Considering the special case, the train is assumed to traverse the rail beam on a viscoelastic Winkler foundation at constant velocity $\dot{s}_0$, i.e. $\lambda = \phi = 0$, $k_{sm} = 0$, Eq. (2.12) becomes

$$EI\frac{\partial^4 y}{\partial x^4} + m\ddot{y} + \alpha\dot{y} + ky = -F_c\delta\left(x - \dot{s}_0 t \right) \tag{2.13}$$

which is noted to be identical to governing equation of motion of the track-foundation model derived by Koh et al. (2003).

2.7 Concluding remarks

In this chapter, mathematical models of various components of the system, namely the train, track-foundation and wheel-rail contact, are presented. Various train models ranging from the simplest moving load model to the 3-DOF train model are employed. The track is modeled as an Euler-Bernoulli beam resting on a two-parameter elastic damped foundation. The train and track-foundation are coupled through the normal wheel-rail contact force. Two normal wheel-rail contact models adopting for the "jumping wheel" phenomenon are presented, namely a simple linearized and a more sophisticated nonlinear version. The governing equation of motion of the train-track-foundation system is derived based on Newton's second Law of motion.

CHAPTER 3. METHODOLOGY

3.1 Introduction

In the previous chapter, the governing equations of motion of the train-track-foundation system were presented in details. Thus, appropriate approaches need to be employed to solve the governing equations in both spatial and time domain. This chapter aims to introduce the proposed computational method for the purpose of solving the governing equations. The MEM is employed to model the track-foundation, where element matrices are formulated based on the convected coordinate system attached to the center of mass of the moving train. As an illustration, the response of an Euler-Bernoulli beam resting on a two-parameter elastic damped foundation subject to a moving load is investigated. The Newmark method is a powerful tool adopted to solve equations of motion of the systems. The Newton-Raphson's scheme is employed for solving nonlinear equation arising from the nonlinear wheel-rail contact model. The accuracy of the proposed scheme for the problem of a moving load travelling at non-uniform motion, results obtained is verified against analytical solutions and FEM results.

3.2 Moving element method

The MEM was first proposed with the idea of attaching the origin of the r-axis moving at the same speed as the train. The relationship of the fixed coordinate and moving coordinate is given by

$$r = x - s \tag{3.1}$$

In view of Eq. (3.1), Eq. (2.12) may be rewritten as

$$\begin{aligned} &EI\frac{\partial^4 y}{\partial r^4} + \phi EI\frac{\partial^4}{\partial r^4}\left(\dot{y} - \dot{s}\frac{\partial y}{\partial r}\right) - \lambda\frac{\partial^2}{\partial r^2}\left(\dot{y} - \dot{s}\frac{\partial y}{\partial r}\right) - k_{sm}\frac{\partial^2 y}{\partial r^2} \\ &+ m\left(\dot{s}^2\frac{\partial^2 y}{\partial r^2} - 2\dot{s}\frac{\partial \dot{y}}{\partial r} - \ddot{s}\frac{\partial y}{\partial r} + \ddot{y}\right) + \alpha\left(\dot{y} - \dot{s}\frac{\partial y}{\partial r}\right) + ky = -F_c\delta(r) \end{aligned} \tag{3.2}$$

By adopting Galerkin's approach, the generalized mass $\mathbf{M}_e$, damping $\mathbf{C}_e$ and stiffness $\mathbf{K}_e$ matrices for a typical moving element of length L may be proposed as

$$\mathbf{M}_e = m\int_0^L \mathbf{N}^{\mathrm{T}}\mathbf{N}\,\mathrm{d}r \tag{3.3}$$

$$\mathbf{C}_e = \phi EI\int_0^L \mathbf{N}_{,rr}^{\mathrm{T}}\mathbf{N}_{,rr}\,\mathrm{d}r + \lambda\int_0^L \mathbf{N}_{,r}^{\mathrm{T}}\mathbf{N}_{,r}\,\mathrm{d}r - 2m\dot{s}\int_0^L \mathbf{N}^{\mathrm{T}}\mathbf{N}_{,r}\,\mathrm{d}r + \alpha\int_0^L \mathbf{N}^{\mathrm{T}}\mathbf{N}\,\mathrm{d}r \tag{3.4}$$

$$\begin{aligned} \mathbf{K}_e = {} & EI\int_0^L \mathbf{N}_{,rr}^{\mathrm{T}}\mathbf{N}_{,rr}\,\mathrm{d}r - \dot{s}\lambda\int_0^L \mathbf{N}_{,r}^{\mathrm{T}}\mathbf{N}_{,rr}\,\mathrm{d}r - \dot{s}\phi EI\int_0^L \mathbf{N}_{,rr}^{\mathrm{T}}\mathbf{N}_{,rrr}\,\mathrm{d}r \\ & - \left(m\dot{s}^2 - k_{sm}\right)\int_0^L \mathbf{N}_{,r}^{\mathrm{T}}\mathbf{N}_{,r}\,\mathrm{d}r - \left(m\ddot{s} + \alpha\dot{s}\right)\int_0^L \mathbf{N}^{\mathrm{T}}\mathbf{N}_{,r}\,\mathrm{d}r + k\int_0^L \mathbf{N}^{\mathrm{T}}\mathbf{N}\,\mathrm{d}r \end{aligned} \tag{3.5}$$

where $\mathbf{N}$ is the shape function based on Hermitian cubic polynomials and $(\ )_{,r}$ denotes partial derivative with respect to r.

By adopting Rayleigh damping (Clough and Penzien 1993), the damping matrix $\mathbf{C}_e$ may be expressed as

$$\begin{aligned}\mathbf{C}_e &= a_0\mathbf{M}_e + a_1\mathbf{K}_e \\ &= a_1 EI\int_0^L \mathbf{N}_{,rr}^{\mathrm{T}}\mathbf{N}_{,rr}\,\mathrm{d}r + k_{sm}a_1\int_0^L \mathbf{N}_{,r}^{\mathrm{T}}\mathbf{N}_{,r}\,\mathrm{d}r + \left(a_0 m + a_1 k\right)\int_0^L \mathbf{N}^{\mathrm{T}}\mathbf{N}\,\mathrm{d}r\end{aligned} \tag{3.6}$$

where $\mathbf{M}_e$, $\mathbf{K}_e$ are determined at the *initial elastic state.* By equating Eq. (3.6) to Eq. (3.4), which is also determined at the *initial elastic state,* the damping parameters are proposed as follows

$$\alpha = a_0 m + a_1 k \quad ; \quad \phi = a_1 \quad ; \quad \lambda = a_1 k_{sm} \tag{3.7}$$

It can be seen that the viscous damping parameter α is noted to be identical to the value derived by Clough and Penzien (1993). Note that other damping parameters ϕ and λ proposed in this study have not been adequately addressed in the literature.

Considering the special case, the train is assumed to traverse the rail beam on a viscoelastic Winkler foundation at constant velocity $\dot{s}_0$, i.e. $\ddot{s} = 0;\ \lambda = \phi = 0$, $k_{sm} = 0$, the Eqs. (3.3), (3.4) and (3.5) thus becomes:

$$\mathbf{M}_e = m\int_0^L \mathbf{N}^{\mathrm{T}}\mathbf{N}\,\mathrm{d}r \tag{3.8}$$

$$\mathbf{C}_e = -2m\dot{s}_0\int_0^L \mathbf{N}^{\mathrm{T}}\mathbf{N}_{,r}\,\mathrm{d}r + \alpha\int_0^L \mathbf{N}^{\mathrm{T}}\mathbf{N}\,\mathrm{d}r \tag{3.9}$$

$$\mathbf{K}_e = EI\int_0^L \mathbf{N}_{,rr}^{\mathrm{T}}\mathbf{N}_{,rr}\,\mathrm{d}r - m\dot{s}_0^{\,2}\int_0^L \mathbf{N}_{,r}^{\mathrm{T}}\mathbf{N}_{,r}\,\mathrm{d}r - \alpha\dot{s}_0\int_0^L \mathbf{N}^{\mathrm{T}}\mathbf{N}_{,r}\,\mathrm{d}r + k\int_0^L \mathbf{N}^{\mathrm{T}}\mathbf{N}\,\mathrm{d}r \tag{3.10}$$

which are noted to be identical to the matrices derived by Koh et al. (2003).

By assembling the element matrices, the equation of motion for the combined train-track-foundation (HSR) model can be written as

$$\mathbf{M}\ddot{\mathbf{z}} + \mathbf{C}\dot{\mathbf{z}} + \mathbf{K}\mathbf{z} = \mathbf{P} \tag{3.11}$$

where $\ddot{\mathbf{z}}$, $\dot{\mathbf{z}}$, $\mathbf{z}$ denote the global acceleration, velocity and displacement vectors of the train-track-foundation system, respectively; $\mathbf{M}$, $\mathbf{C}$ and $\mathbf{K}$ the global mass, damping and stiffness matrices, respectively; and $\mathbf{P}$ the global load vector. The above dynamic equation can be solved by any direct integration methods such as the Newmark-β method (Bathe 1996), which is discussed in Section 3.3.

3.3 The Newmark method

In order to solve the differential equations of motion in Eq. (3.11), many numerical methods such as the Euler method, Improved Euler method, Taylor series method, Runge-Kutta method, Central Difference method, Houbolt method, Wilson method and Newmark method can be used. In this study, the Newmark method (Bathe 1996) is employed for solving the problems.

The Newmark method is based on the assumption that the acceleration varies linearly between two instants of time. The resulting expressions for the velocity $\dot{\mathbf{z}}_{n+1}$ and displacement $\mathbf{z}_{n+1}$ at time t_{n+1} are written as

$$\dot{\mathbf{z}}_{n+1} = \dot{\mathbf{z}}_n + \left[\left(1-\gamma\right)\ddot{\mathbf{z}}_n + \gamma\ddot{\mathbf{z}}_{n+1} \right]\Delta t \tag{3.12}$$

$$\mathbf{z}_{n+1} = \mathbf{z}_n + \Delta t\dot{\mathbf{z}}_n + \left[\left(\frac{1}{2} - \beta \right)\ddot{\mathbf{z}}_n + \beta\ddot{\mathbf{z}}_{n+1} \right]\left(\Delta t\right)^2 \tag{3.13}$$

where $\mathbf{z}_n$, $\dot{\mathbf{z}}_n$ and $\ddot{\mathbf{z}}_n$ denote the displacement, velocity and acceleration at time t_n, respectively; the parameters γ and β indicate how much the acceleration at the end of the interval enters into the velocity and displacement equations at the end of the interval Δt. In fact, γ and β can be chosen to

obtain the desired accuracy and stability characteristics. When $\gamma = \frac{1}{2}$ and $\beta = \frac{1}{6}$, Eqs. (3.12) and (3.13) correspond to the linear acceleration method. When $\gamma = \frac{1}{2}$ and $\beta = \frac{1}{4}$, Eqs. (3.12) and (3.13) correspond to the assumption of constant acceleration between t_n and t_{n+1}.

Solving Eqs. (3.12) and (3.13), the velocity $\dot{\mathbf{z}}_{n+1}$ and acceleration $\ddot{\mathbf{z}}_{n+1}$ at time t_n can be obtained by

$$\ddot{\mathbf{z}}_{n+1} = \frac{1}{\beta(\Delta t)^2}(\mathbf{z}_{n+1} - \mathbf{z}_n) - \frac{1}{\beta \Delta t}\dot{\mathbf{z}}_n - \left(\frac{1}{2\beta} - 1\right)\ddot{\mathbf{z}}_n \tag{3.14}$$

$$\dot{\mathbf{z}}_{n+1} = \frac{\gamma}{\beta \Delta t}(\mathbf{z}_{n+1} - \mathbf{z}_n) + \left(1 - \frac{\gamma}{\beta}\right)\dot{\mathbf{z}}_n + \left(1 - \frac{\gamma}{2\beta}\right)\Delta t \ddot{\mathbf{z}}_n \tag{3.15}$$

In the case of linear dynamic problems for the purpose of finding the value of $\mathbf{z}_{n+1}$, Eq. (3.11) is thus considered at time t_{n+1}

$$\mathbf{M}\ddot{\mathbf{z}}_{n+1} + \mathbf{C}\dot{\mathbf{z}}_{n+1} + \mathbf{K}\mathbf{z}_{n+1} = \mathbf{P}_{n+1} \tag{3.16}$$

By substituting Eqs. (3.14) and (3.15) into Eq. (3.16), a relation for finding the value of displacement $\mathbf{z}_{n+1}$ may be rewritten as

$$\begin{aligned} &\mathbf{M}\left[\frac{1}{\beta(\Delta t)^2}(\mathbf{z}_{n+1} - \mathbf{z}_n) - \frac{1}{\beta \Delta t}\dot{\mathbf{z}}_n - \left(\frac{1}{2\beta} - 1\right)\ddot{\mathbf{z}}_n\right] \\ &+ \mathbf{C}\left[\frac{\gamma}{\beta \Delta t}(\mathbf{z}_{n+1} - \mathbf{z}_n) + \left(1 - \frac{\gamma}{\beta}\right)\dot{\mathbf{z}}_n + \left(1 - \frac{\gamma}{2\beta}\right)\Delta t \ddot{\mathbf{z}}_n\right] + \mathbf{K}\mathbf{z}_{n+1} = \mathbf{P}_{n+1} \end{aligned} \tag{3.17}$$

or

$$\mathbf{z}_{n+1} = R^{-1}F \tag{3.18}$$

where

$$R = \frac{1}{\beta\left(\Delta t\right)^2}\mathbf{M} + \frac{\gamma}{\beta\Delta t}\mathbf{C} + \mathbf{K} \tag{3.19}$$

$$\begin{aligned} F = \mathbf{P}_{n+1} &+ \left(\frac{1}{\beta\left(\Delta t\right)^2}\mathbf{z}_n + \frac{1}{\beta\Delta t}\dot{\mathbf{z}}_n + \left(\frac{1}{2\beta} - 1\right)\ddot{\mathbf{z}}_n \right)\mathbf{M} \\ &+ \left(\frac{\gamma}{\beta\Delta t}\mathbf{z}_n + \left(\frac{\gamma}{\beta} - 1\right)\dot{\mathbf{z}}_n + \left(\frac{\gamma}{2\beta} - 1\right)\Delta t\ddot{\mathbf{z}}_n \right)\mathbf{C} \end{aligned} \tag{3.20}$$

Finally, the acceleration $\ddot{\mathbf{z}}_{n+1}$ and velocity $\dot{\mathbf{z}}_{n+1}$ can be computed according to Eqs. (3.14) and (3.15), respectively.

3.4 The Newton-Raphson scheme

The MEM is the first proposed to solve sets of simultaneous linear equations. Unfortunately, the nonlinear Hertz contact theory accounting for the normal wheel-rail interaction is employed in this study, resulting in complications in numerical implementation. In an attempt to overcome the aforementioned complication, the Newton-Raphson's scheme (Bathe 1996) may be employed for solving nonlinear equation arising from the nonlinear wheel-rail contact model. Thus, this section presents the procedure of adopting the approach in the treatment of the nonlinear equation.

Upon closer combination of Eqs. (2.1), (2.2) and (2.3), the governing equation of the 3-DOF train model may be rewritten as

$$m_1\ddot{u}_1 + m_2\ddot{u}_2 + m_3\ddot{u}_3 = F_c - \left(m_1 + m_2 + m_3\right)g \tag{3.21}$$

Substituting the contact force F_c in Eq. (2.4) into Eq. (3.21)

$$
\begin{aligned}
&m_1\ddot{u}_1 + m_2\ddot{u}_2 + m_3\ddot{u}_3 \\
&= \begin{cases} K_H\left(y_r + y_t - u_3\right)^{\frac{3}{2}} - \left(m_1 + m_2 + m_3\right)g, & \left(y_r + y_t - u_3\right) \geq 0 \\ -\left(m_1 + m_2 + m_3\right)g, & \left(y_r + y_t - u_3\right) < 0 \end{cases}
\end{aligned} \tag{3.22}
$$

For the purpose of linearizing Eq. (3.22), an assumed equilibrium function $f(X)$ may be written as

$$
\begin{aligned}
&f\left(X\right) = \\
&\begin{cases} K_H\left(y_r + y_t - u_3\right)^{\frac{3}{2}} - m_1\left(\ddot{u}_1 + g\right) - m_2\left(\ddot{u}_2 + g\right) - m_3\left(\ddot{u}_3 + g\right), & \left(y_r + y_t - u_3\right) \geq 0 \\ -m_1\left(\ddot{u}_1 + g\right) - m_2\left(\ddot{u}_2 + g\right) - m_3\left(\ddot{u}_3 + g\right), & \left(y_r + y_t - u_3\right) < 0 \end{cases}
\end{aligned} \tag{3.23}
$$

where $X = X\left(u_1, u_2, u_3, y_r, y_t, \ddot{u}_1, \ddot{u}_2, \ddot{u}_3\right)$ is the vector of variables.

The aim is to find values for the variables so that $f\left(X\right) = 0$ by doing an iterative procedure. In view that the speed of convergence study depends on the nonlinearity of the equation as well as the initial trial values, there is a need to repeat the procedure with more iteration steps until the equilibrium function $f^{i+1}\left(X\right)$ at the $(i+1)^{th}$ iteration step satisfies $f^{i+1}\left(X\right) = 0$. Based on the Taylor series expansion, the equilibrium function $f^{i+1}\left(X\right)$ may be linearized as

$$
f^{i+1}\left(X\right) = f^{i}\left(X\right) + \frac{\partial f^{i}\left(X\right)}{\partial X^{T}}\left(X^{i+1} - X^{i}\right) \tag{3.24}
$$

To find solutions satisfying the equation $f^{i+1}\left(X\right) = 0$, the increment in X should be within a given numerical tolerance τ as follows

$$
\left\| \frac{X^{i+1} - X^{i}}{X^{i+1}} \right\| \leq \tau \tag{3.25}
$$

3.5 Analytical solution

For purpose of comparison with the proposed computational method, the analytical solution for simple cases of moving loads over tracks is also presented in this study. The analytical steady-state response of a curved beam on a viscously damped foundation subjected to a sequence of moving loads was firstly proposed by Dai and Ang (2014). By setting the radius of the curved beam to zero and adding the effects of dissipation mechanisms and shear modulus of the foundation, the analytical solution is extended to solve the problems involving a straight rail beam resting on a two-parameter elastic damped foundation subject to moving loads.

As this study mainly focuses on the response of the rail when the moving load is away from the truncated ends, the rail displacement and reaction force at the boundaries are usually negligible. Thus, the rail displacement can be reasonably expressed as

$$y = \sum_{i=1}^{n} y_i(t) \sin\left(\frac{i\pi x}{L}\right) \tag{3.26}$$

where y_i denotes the generalized coordinate of the i^{th} vibration mode of the railway track.

As the mode of vibration is orthogonal with each other, the governing equation in Eq. (2.12) by adopting Galerkin's approach can be rewritten as

$$\frac{\partial^2 y_i}{\partial t^2} + c_i \frac{\partial y_i}{\partial t} + d_i y_i = -\frac{2F_c}{mL} \sin\left(\frac{i\pi s}{L}\right) \tag{3.27}$$

where $c_{\mathrm{i}} = \frac{\alpha}{m} + \frac{\phi EI}{m}\left(\frac{i\pi}{L}\right)^4 + \frac{\lambda}{m}\left(\frac{i\pi}{L}\right)^2$; $d_{\mathrm{i}} = \frac{k}{m} + \frac{EI}{m}\left(\frac{i\pi}{L}\right)^4 + \frac{k_{sm}}{m}\left(\frac{i\pi}{L}\right)^2$.

The steady-state response of Eq. (3.27) may be written as

$$y_i = \sum_{i=1}^{n}\left(A_{\mathrm{i}} \sin\left(\frac{i\pi s}{L}\right) + B_{\mathrm{i}} \cos\left(\frac{i\pi s}{L}\right)\right)\sin\left(\frac{i\pi x}{L}\right) \tag{3.28}$$

where A_{i} and B_{i} are coefficients determined by substituting Eq. (3.28) into Eq. (3.27)

$$\begin{bmatrix} d_{\mathrm{i}} - \left(\frac{i\pi\dot{s}}{L}\right)^2 & -\frac{i\pi\ddot{s}}{L} - c_{\mathrm{i}}\frac{i\pi\dot{s}}{L} \\ \frac{i\pi\ddot{s}}{L} + c_{\mathrm{i}}\frac{i\pi\dot{s}}{L} & d_{\mathrm{i}} - \left(\frac{i\pi\dot{s}}{L}\right)^2 \end{bmatrix} \begin{Bmatrix} A_i \\ B_i \end{Bmatrix} = \begin{Bmatrix} \frac{-2F_c}{mL} \\ 0 \end{Bmatrix} \tag{3.29}$$

In sum, the analytical steady-state response of a beam resting on two-parameter elastic damped foundation subject to a moving load F_c is obtained in Eq. (3.28). For the case of multiple moving loads of more realistic complicated train models, the superposition technique should be employed.

3.6 Verification of results

In an attempt to test the accuracy of proposed MEM for the problem of a moving load travelling at non-uniform motion, results obtained will be verified against analytical solutions and FEM results. Note that the analytical method is limited in solving only the problem of a moving load travelling at a constant speed. For other more complicated travelling load problems, it was necessary to resort to writing a FEM code for the purpose of comparison.

Figure 3.1 shows the general train speed profile adopted in the analysis. The train is assumed to be travelling initially at a constant speed $\dot{s}_0 = 70$ m s^{-1}. After time t_1, which is taken to be long enough for the vibration of the train-track-foundation system to attain steady-state, the train is then assumed to decelerate uniformly at 2 m s^{-2} before coming to a halt at time t_2. This deceleration magnitude is typical during heavy braking. For simplicity, results are obtained based on a moving wheel load of 1 kN. The foundation supporting the track is modelled as a two-parameter elastic damped foundation. Values of parameters related to the properties of the track and foundation (Koh et al. 2003) are summarized in Table 3.1. Note that the value of shear modulus k_{sm} is taken from Feng and Cook (1983). The equations of motion are solved using Newmark's constant acceleration method employing a time step of 0.0005 s.

In the FEM model, a sufficiently long segment of the railway track is discretized uniformly with 0.25 m size elements, which has been found to be adequately small enough to attain converged accurate results. The segment may be divided into three sub-portions, a central portion and two end portions. The central portion, where the train travels during the period considered, is taken to be 140.5 m. The central portion is padded by two end portions of sufficient length in order to mitigate the erroneous boundary effects due to the moving train load approaching the boundaries of the FEM model. Through a convergence study, the length of the end portions is taken to be 24 m. Due to the advantage enjoyed by the MEM in dealing with moving load problems, a

relatively shorter segment is required. Also from a convergence study made, the length required for the truncated railway track in the MEM model is 50 m that is discretized non-uniformly with elements ranging from a coarse 1 m to a more refined 0.25 m size.

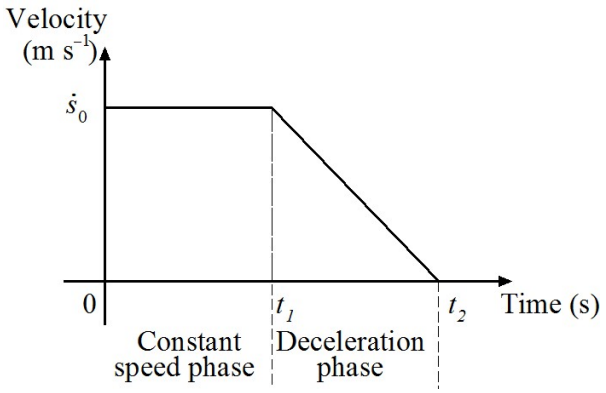

Figure 3.1. Train speed profile.

Table 3.1. Parameters for track-foundation model.

Parameter	Value
Flexural stiffness	6.12×10^6 N m^2
Track section	UIC 60 (60 E1)
Stiffness of Winkler foundation k	1×10^7 N m^{-2}
Shear modulus k_{sm}	8.12×10^6 N
Damping ratio ξ	0.1

Figures 3.2(a) and (b) show the rail displacement profiles in the vicinity of the wheel-rail contact point when the train travels at constant speed and after the train decelerates for 1 s, respectively. Results in Figure 3.2(a) are predicted by the analytical solution, FEM and MEM while results in Figure 3.2(b) are obtained by the two latter methods. As can be seen in Figure 3.2, good agreement between all results is obtained. In view that the FEM requires a longer domain length as compared to the MEM, it is not surprising that the computational time required is much higher than that needed in the MEM.

This comparison study clearly illustrated that the MEM is accurate as well as computationally efficient and is more suited generally for the study of moving load problems as compared to the FEM.

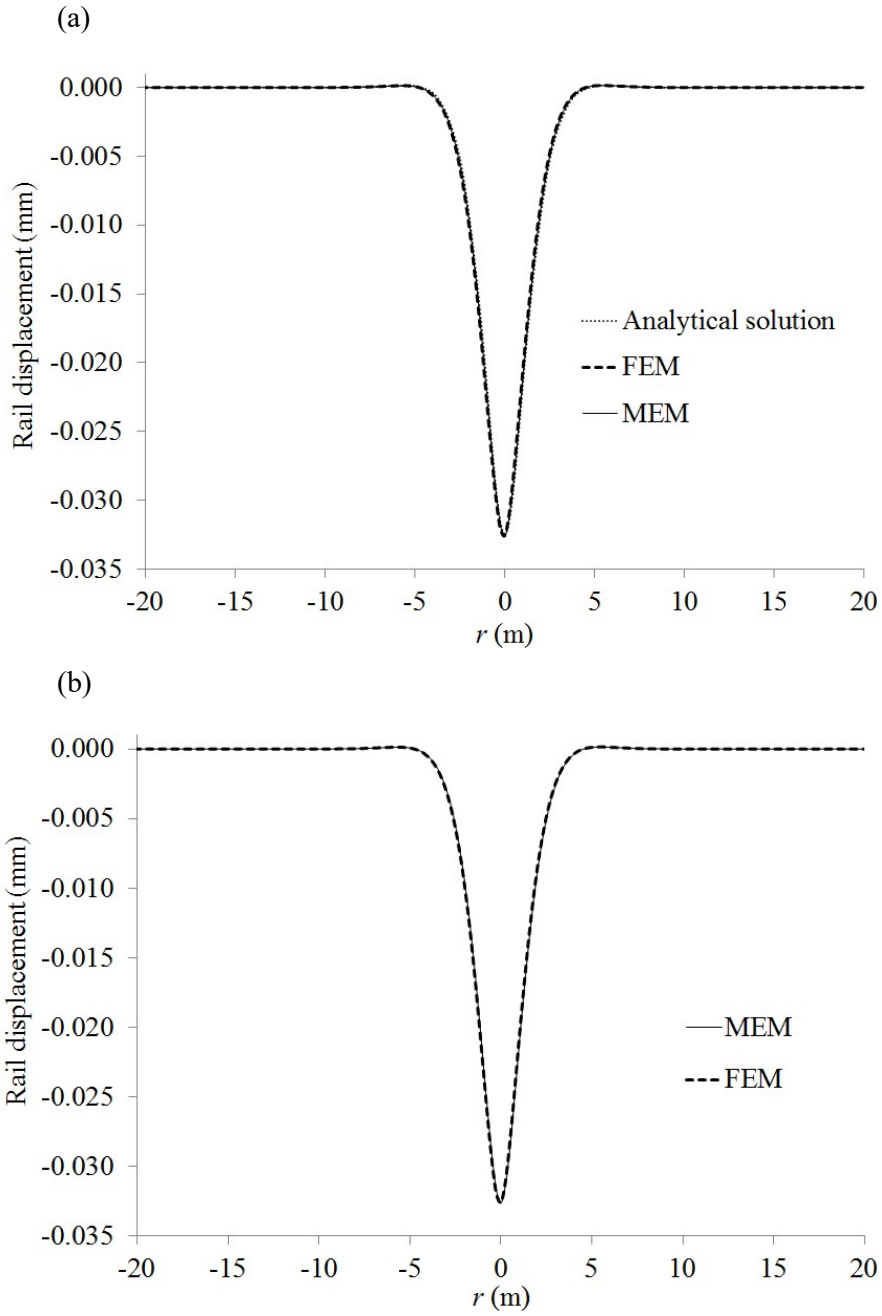

Figure 3.2. Rail displacement profiles during: (a) Constant speed phase and (b) Deceleration phase.

3.7 Concluding remarks

This chapter presented the computational method for solving the governing equations of motion of the HSR. The MEM is employed to model the track-foundation and is extended to account for the instantaneous acceleration/deceleration of the moving train. The proposed computational scheme based on the MEM for the problem of a moving load travelling at non-uniform motion is verified against available analytical solutions and FEM results. Results from all methods are found to be agreeable thereby validating the proposed MEM adopted in the present study. The MEM, which is a variation of the FEM, however enjoys significant computational efficiency over the FEM and overcomes the inherent complications faced by the FEM. Also, analytical formulas are derived for simple cases of moving loads over tracks for the purpose of comparison with the proposed computational method. The Newton-Raphson's scheme is employed for solving nonlinear equation arising from the nonlinear wheel-rail contact model and the Newmark method is adopted to solve governing equations of motion of the systems.

CHAPTER 4. NON-UNIFORM MOTION OF HIGH-SPEED TRAIN

4.1 Introduction

In the previous chapter, the methodology for the dynamic analysis of the HSR is presented. Aforementioned results revealed that the MEM is effective in solving the case of an Euler-Bernoulli railway track beam resting on two-parameter elastic damped foundation subject to a moving load travelling at a constant speed. However, the moving load model is obviously an over-simplified representation of a moving train. To capture the inertia effect of the moving train mass, a more complex 3-DOF train model needs to be employed.

When a train travels at a cruising speed higher than the resonant speed of the HSR, the dynamic response is found to be significantly larger when the speed of the train crosses the resonant speed as the train decelerates to come to a halt. The momentary spike in the dynamic response, including the higher chance of occurrences of the jumping wheel phenomenon, needs to be considered in the safe operation of the HSR. Thus, this chapter presents the results of a study on the dynamic response of non-uniform motion of HSR, in which the speed-time profile of the train is given or assumed.

4.2 Literature review

In reality, high-speed trains do also travel at non-uniform velocities, especially when accelerating to attain maximum operational speed or decelerating when approaching a curved track or coming to a halt at a station. Various researchers have investigated the problem of loads travelling at non-uniform velocities. Suzuki (1977), Yadav (1991) and Karlstrom (2006) employed the analytical solutions to investigate the response of a train-track-foundation system due to accelerating and decelerating trains traveling over a/an finite/infinite track. Although analytical solutions are elegant which provide clear physical insights into the nature of the problem, they are limited in dealing with practical applications involving complicated multi-degrees of freedom system and the railhead roughness.

The finite element method (FEM) is a well-known powerful numerical method for solving a wide range of complex problems, including problems of beams subject to moving loads (Frýba et al. 1993; Thambiratnam and Zhuge 1996). However, the FEM encounters difficulty when the moving load approaches the boundary of the finite domain and travels beyond the boundary. These difficulties can be overcome by employing a large enough domain size but at the expense of significant increase in computational time. In an attempt to overcome the complication encountered by FEM, Krenk et al. (1999) proposed the use of FEM in convected coordinates, similar to the moving coordinate system proposed by Timoshenko (1926), to obtain the response of an elastic half-space subject to a moving load. The key advantage

of this approach is its ability to overcome the problem produced by the moving load travelling over a finite domain. Andersen et al. (2001) provided an FEM formulation in resolving the problem of a beam on a Kelvin foundation subject to a harmonic moving load. Koh et al. (2003) adopted the convected coordinate system for solving train-track problems, and named the numerical algorithm the moving element method (MEM). Ang and Dai (2013) extended the MEM to investigate the "jumping wheel" phenomenon in high-speed train motion at constant velocity over a transition region where there is a sudden change of foundation stiffness.

Safety concerns during the acceleration and deceleration phases of a high-speed train journey have not been adequately addressed in the literature. One major concern is the possible occurrence of resonance of the system when the frequency of the external force, in this case the rail corrugation, coincides with the natural frequency of a significant vibration mode of the system. When this happens, the response of the system is dynamically amplified and becomes significant large. This chapter is concerned with a computational study of the dynamic response of HSR systems involving accelerating or decelerating trains using the proposed MEM. As the dynamic response of the track depends significantly on the contact between wheel and track, this study is also concerned with examining the suitability of two contact models.

4.3 Problem definition

In this chapter, the HSR system, as shown in Figure 4.1, comprises of a 3-DOF train traveling at non-uniform motion over a rail track, which is modeled as an infinite Euler-Bernoulli beam, resting on a two-parameter elastic damped foundation in the positive x-direction. The origin of the fixed x-axis is arbitrarily located along the beam. However, for convenience, its origin is taken such that the train is at $x = 0$ when $t = 0$. The railhead is assumed to have some imperfections resulting in the so-called "track irregularity".

The train is modeled as a system of three rigid components, namely the car body, bogie and wheel-set, inter-connected by spring-damper units. The topmost mass m_1 represents the car body where the passengers are. The car body is supported by the bogie of mass m_2 through a secondary suspension system modeled by the spring k_1 and dashpot c_1. The bogie is in turn supported by the wheel-axle system of mass m_3 through a primary suspension system modeled by the spring k_2 and dashpot c_2. F_c is the contact force exerted between the train and track. The vertical displacements of the car body, bogie and wheel-axle are denoted by u_1, u_2 and u_3, respectively.

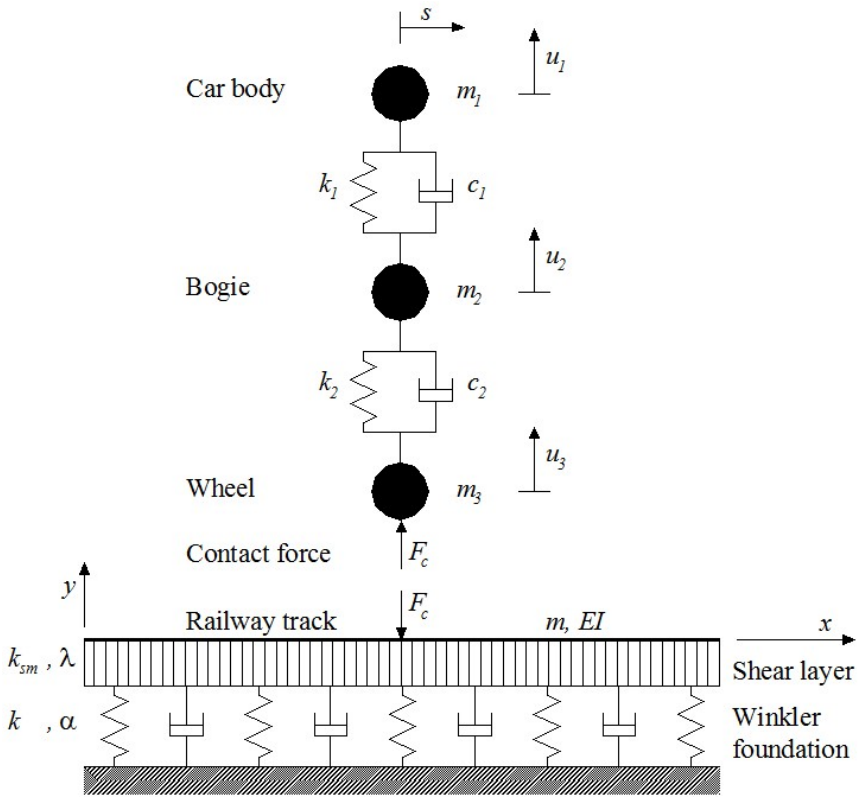

Figure 4.1. A HSR model.

4.4 Proposed computational technique

The MEM has so far been limited in applications involving rail beams resting on Winkler foundation subject to a constant-velocity moving train. The constant velocity-based MEM has been employed to deal with non-uniform motion of train but confined to cases where the train speed-time profile is given or assumed (Koh et al. 2003). This is achieved by dividing the total time duration into small time intervals and assuming that the speed of the train during each time interval is constant. As time changes, the constant velocity of the train in the MEM formulation is updated based on this piecewise

approximation of the speed-time profile. However, under train braking conditions, the speed-time history of the train is unknown in advance and thus using the constant velocity-based MEM, as described above, is not feasible. It is thus necessary to extend the MEM to account for the instantaneous acceleration/deceleration of the train in order to investigate the dynamics of HSRs subject to braking, as presented earlier in section 3.2.

In this chapter, the proposed MEM is employed to first investigate the response of non-uniform motion of HSR, in which the speed-time profile of the train is given or assumed. The profile consists of three phases, namely (1) an accelerating phase in which the train accelerates uniformly to attain an operational speed, (2) a constant-speed phase and (3) a decelerating phase in which the train decelerates uniformly from operational speed to a halt.

The numerical procedure based on the Newton-Raphson's approach presented in Chapter 3 is proposed to solve the nonlinear equations of the train produced by the nonlinear contact force exerted on the wheel. For the nonlinear equations of the track-foundation arising from the nonlinear contact force exerted on the track, this approach was however found to be too cumbersome to use. Thus, the explicit scheme is proposed by adopting the nonlinear contact force exerted on the track, which is determined by employing constants of known values at the current step, for that at the next step during the iterative procedure till to satisfy the convergence requirement. As the contact forces produced at the wheel and track do not match, there is however a spurious 'time lag' effect in the computational procedure. Thus, it

is a need to use a very refined time step size in order to minimize this spurious effect, but at the expense of significant increase in computational effort.

Alternatively, the implicit scheme may be employed by replacing the nonlinear Hertz contact force exerted on the track by a linear combination of the vertical accelerations of the train components. For the ease of reference, the governing equations of the 3-DOF train model presented in Eqs. (2.1), (2.2) and (2.3) may be rewritten as

$$m_1\ddot{u}_1 + k_1\left(u_1 - u_2\right) + c_1\left(\dot{u}_1 - \dot{u}_2\right) = -m_1 g \tag{4.1}$$

$$m_2\ddot{u}_2 + k_2\left(u_2 - u_3\right) + c_2\left(\dot{u}_2 - \dot{u}_3\right) - k_1\left(u_1 - u_2\right) - c_1\left(\dot{u}_1 - \dot{u}_2\right) = -m_2 g \tag{4.2}$$

$$m_3\ddot{u}_3 - k_2\left(u_2 - u_3\right) - c_2\left(\dot{u}_2 - \dot{u}_3\right) = -m_3 g + F_c \tag{4.3}$$

Substituting Eqs. (4.1) and (4.2) into Eq. (4.3), the nonlinear contact force F_c exerted on the track is eliminated as

$$F_c = m_1\ddot{u}_1 + m_2\ddot{u}_2 + m_3\ddot{u}_3 + \left(m_1 + m_2 + m_3\right) g \tag{4.4}$$

Substituting Eq. (4.4) into Eq. (3.2), the governing equation of track-foundation becomes an equation without nonlinear terms.

By assembling the element matrices, the equation of motion for the combined train-track-foundation (HSR) model can be written as

$$\mathbf{M}\ddot{\mathbf{z}} + \mathbf{C}\dot{\mathbf{z}} + \mathbf{K}\mathbf{z} = \mathbf{P} \tag{4.5}$$

where $\ddot{\mathbf{z}}$, $\dot{\mathbf{z}}$, $\mathbf{z}$ denote the global acceleration, velocity and displacement vectors of the train-track-foundation system, respectively; $\mathbf{M}$, $\mathbf{C}$ and $\mathbf{K}$ the global mass, damping and stiffness matrices, respectively; and $\mathbf{P}$ the global

load vector. The above equation of motion can be solved by using Newmark's constant acceleration method (Bathe 1996).

4.5 Verification of results

4.5.1 The accuracy study

In the proposed MEM, the stiffness matrix of the moving element depends on the magnitude of the train acceleration/deceleration as can be seen from Eq. (3.5). It is thus necessary to investigate the contribution from such components on the dynamic response of HSRs.

In an attempt to test the effectiveness and the accuracy of proposed MEM in the problem involving variable train speed, the solution obtained by present study is compared against the FEM as well as the MEM by Koh et al. (2003). A FEM code was written that is matched in capability as the proposed MEM code. The latter used the MEM formulation based on piecewise constant velocity by dividing the time into small time intervals and assuming that the travel during each time interval is at constant velocity. For the purpose of comparison, the train is modeled as a 3-DOF model traveling on a viscoelastic Winkler foundation. The same train speed profile and all technical data adopted by Koh et al. (2003) are employed. This speed profile is shown in Figure 4.2 where it can be seen that there are three phases of travel.

The speed profile parameters for this case are presented in Table 4.1 under Case I. The initial phase considers the train to be moving at a constant acceleration of travel and reaching a maximum speed of 20 m s^{-1} after 2 s.

During the second phase of travel, the train moves at the maximum constant speed for another 2 s. In the final phase, the train decelerates at a constant magnitude to come to a complete halt after another 2 s of travel. Results obtained using the proposed method are found to be in excellent agreement with those obtained by the MEM by Koh et al. (2003) as well as the FEM. Figure 4.3 shows a typical comparison of the rail displacement profile at 5 s that shows virtually no difference in the results.

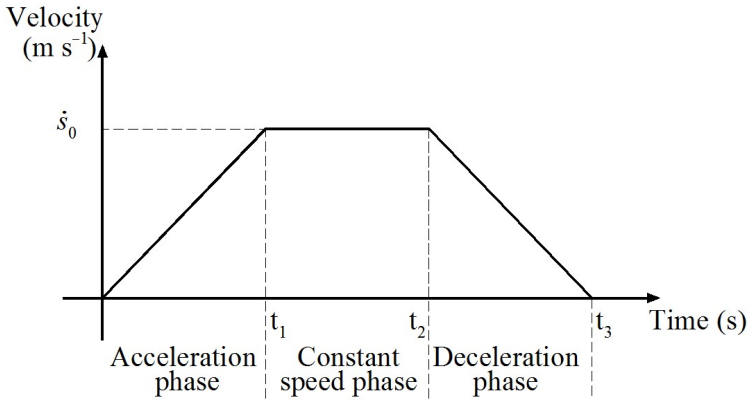

Figure 4.2. Profile of train speed.

Table 4.1. Profiles of train velocities.

Case	Maximum train velocity $\dot{s}_0$ (m s^{-1})	Magnitude of train acceleration/deceleration $\lvert\ddot{s}\rvert$ (m s^{-2})	Time parameters		
			t_1 (s)	t_2 (s)	t_3 (s)
I	20	10.000	2.0	4.0	6.0
II	70	10.000	7.0	9.0	16.0
III	70	2.222	31.5	33.5	65.0
IV	70	0.720	98.0	100.0	198.0

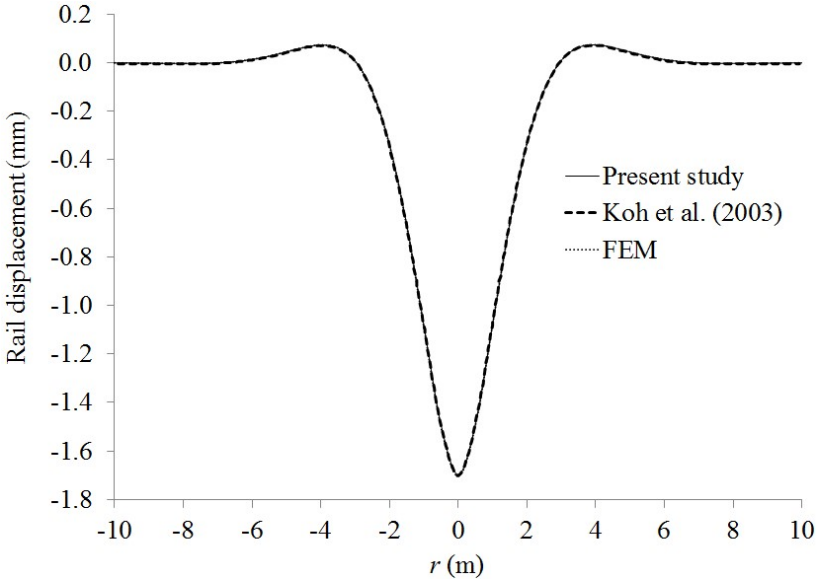

Figure 4.3. Comparison of the rail displacement profiles at 5 s.

In the present study, the stiffness matrix of the moving element depends on the additional term involving the magnitude of the train acceleration/deceleration and mass of rail beam, as can be seen from Eq. (3.5). However, upon close examination of the various terms contributing to the stiffness, the contribution from the acceleration component is expected to be small compared to other terms, especially the main term of foundation stiffness. The additional term may be significant when the train travels at enough large acceleration/deceleration amplitude on a sufficiently large structure (i.e. slab track is modeled as beam with total mass 3675 kg (Lei and Wang 2013) resting on the soft foundation. In view of this, only three values of acceleration/deceleration of train will be considered in the study. These are designated as Cases II, III and IV in Table 4.1 corresponding to acceleration/deceleration magnitudes of 10.000, 2.222 and 0.720 m s^{-2},

respectively. And subgrade stiffness is employed from soft to stiff (Dimitrovova´ and Varandas 2009). Note that the amplitude and wavelength of all track irregularities are chosen to be 0.5 mm and 0.5 m, respectively. Figure 4.4 shows the variation of maximum discrepancy of rail displacement against subgrade stiffness for various acceleration/deceleration amplitudes. All analyses are carried out twice, each using the MEM by Koh et al. (2003) and present study. It can be seen that there is virtually no difference in the results except for the cases that the difference is significant (by 30% and 1.5%) when subgrade stiffness is small, i.e. 427×10^3 and 854×10^3 (N m^{-2}), respectively and the train travels at 10.000 m s^{-2}.

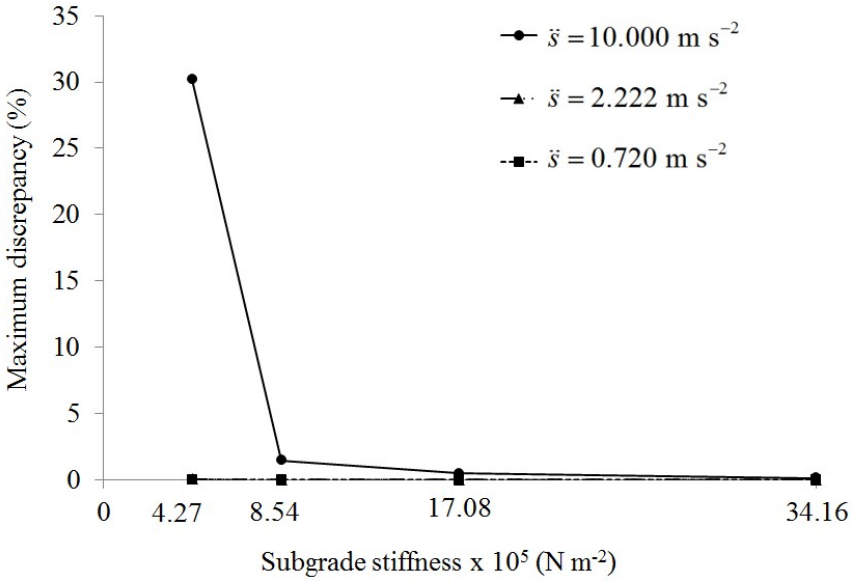

Figure 4.4. Comparison of maximum discrepancy of rail displacement between solutions by Koh et al. (2003) and present study.

In next investigations, the MEM model adopted comprises of a truncated railway track of 50 m length discretized non-uniformly with elements ranging from a coarse 1 m to a more refined 0.25 m size. Note that refined element

sizes are employed in the vicinity of the moving train load in order to capture accurately the maximum response of the train-track system. The train modeled as the moving 3-DOF model travels over an Euler-Bernoulli railway beam resting on a two-parameter elastic damped foundation. Parameters relating to the properties of the train-track-foundation used for this study are listed in Table 4.2 and Table 3.1. Note that the radii of the wheel R_w, railhead R_r and the Poisson's ratio of the wheel/rail material υ used in determining the nonlinear and linearized Hertz spring constants are taken to be 460 mm, 300 mm and 0.3, respectively.

Table 4.2. Parameters for high-speed train model (Wu et al. 2001).

Parameters	Value
m_1	5218.75 kg
k_1	1.325×10^5 N m^{-1}
c_1	22.55×10^3 N s m^{-1}
m_2	760 kg
k_2	5.9×10^5 N m^{-1}
c_2	19.6×10^3 N s m^{-1}
m_3	890 kg

4.5.2 Effective computational scheme

As presented earlier in section 4.4, two computational schemes namely the explicit and implicit approaches, have been proposed to account for the nonlinear contact force exerted on the rail. This section presents a numerical study on the comparison of results obtained by both schemes as well as discusses their computational effectiveness.

Figure 4.5 shows the time histories of the wheel-rail contact force obtained by these two schemes. Note that the train travels at a cruising speed

of 70 m s^{-1}. It can be seen in this figure that results obtained are found to be virtually the same. When adopting the explicit approach, it is found that a time step size less than 0.0002 s is necessary to achieve the convergence requirement. For the implicit scheme adopted, a time step size of 0.0005 s is good enough to satisfy the convergence study. In view that the explicit approach requires a refined time step size as compared to the implicit scheme, it is not surprising that the computational time required is substantially higher than that needed in the implicit approach. This comparison study clearly illustrated that the implicit scheme is accurate as well as computationally efficient as compared to the explicit scheme, but is restricted only to simple train models. Due to the simple train model employed in this chapter, subsequent studies will thus be carried out based on the implicit scheme to obtain the dynamic response of non-uniform motion of the HSR.

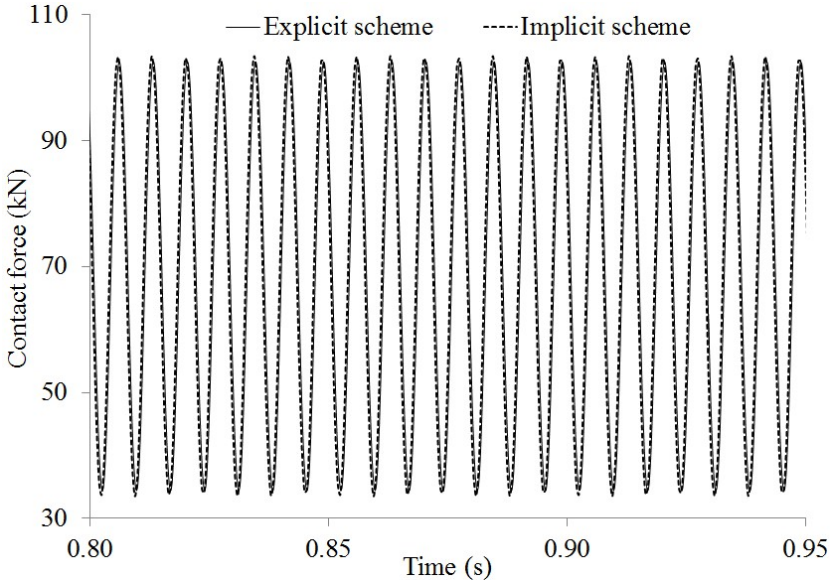

Figure 4.5. Time-histories of wheel-rail contact force.

4.6 Numerical results

In the following sections, results from the study of two cases of HSR travel using the proposed MEM approach are presented. The first case studies the response of high speed train moving over a two-parameter elastic damped foundation at constant speed. The effects of track irregularity and wheel load on the dynamic response of train-track system and the occurrence of the jumping wheel phenomenon will be investigated using the Hertz nonlinear and linearized contact models. In the second case, the response of train-track system moving at varying speed will be investigated. Safety concerns during the acceleration and deceleration phases of a high speed train journey have not been adequately addressed in the literature. One major concern is the possible occurrence of resonance of the system when the frequency of the external force, in this case the rail corrugation, coincides with the natural frequency of a significant vibration mode of the system. When this happens, the response of the system is dynamically amplified and becomes significantly large. The aim of this study is to determine whether the magnitude of train acceleration or deceleration affects the dynamic response of the train-track system when the HSR travels at resonant speed. The effects of track irregularity and wheel load on the occurrence of the jumping wheel phenomenon and dynamic response of the system during the acceleration/deceleration phases will also be examined.

4.6.1 Uniform motion of HSR

4.6.1.1 Effect of track irregularity

As the dynamic response of the train-track system depends significantly on the accuracy in modeling the contact between the wheel and track, it would be important to examine the suitability of the aforementioned nonlinear and linearized contact models. The effects of train speed and track irregularity amplitude are investigated. The wavelength of all track irregularities considered is taken to be 0.5 m (Thompson 2008).

Figure 4.6 shows the variation of dynamic amplification factor (DAF) in wheel-rail contact force against track irregularity amplitude for various train speeds typically associated with today's HSR travels. All analyses are carried out twice, each using the nonlinear and linearized contact models. Note that DAF is defined as the ratio of the maximum dynamic contact force to the static wheel load which is the sum of the self-weights of car body, bogie and wheel-set. For the perfectly smooth ($a_t = 0$ mm) track, the DAF is found be 1 as to be expected in view that there is no dynamic load. Consequently, the linearized contact model based on spring properties computed in Eq. (2.9) according to the static wheel load condition (Esveld 2001) can be used.

The results in Figure 4.6 also show that when the amplitude of track irregularity and/or train speed increase, the DAF is increased. Both the linearized and nonlinear contact models were found to produce results, which are in good agreement for low vehicle speeds regardless of the amplitude of

the track irregularity. Good agreement was also noted to occur at higher speeds provided the amplitudes of track irregularity are smaller than certain critical values, approximately 1.2 mm and 0.8 mm for $\dot{s}_0 =$ 70 and 90 m s^{-1}, respectively. Beyond these critical values, the difference in the DAF results becomes significant between the two contact models. The above results clearly indicate that the simple linearized contact model may be used only when there is no large dynamic load involved. This is to be expected since the spring property used in the linearized contact model is based on the static wheel load. Thus, when the train speed is high and/or the track irregularity is considered to be severe, it is necessary to use the more computationally intensive nonlinear contact model in view of the expected high dynamic load.

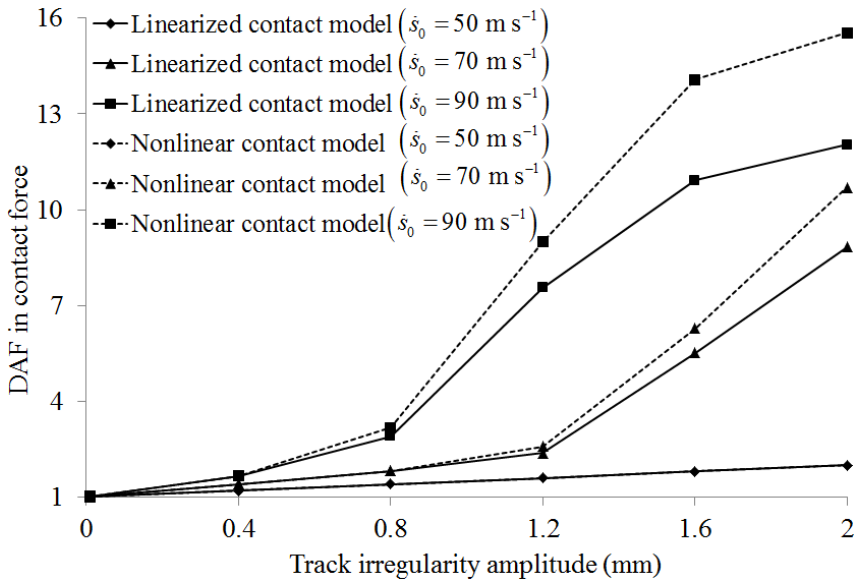

Figure 4.6. Effects of irregularity amplitude and train speed on the DAF.

As the response of high-speed rails system strongly depends on the severity of track irregularity, it is expected that shorter irregularity wavelength

would lead to larger vibrations. Therefore, it would be useful to investigate the effects of irregularity wavelengths and train speeds on the response of the HSRs. The amplitude of all track irregularities considered in this investigation is taken to be 1.5 mm.

Figure 4.7 shows the effects of irregularity wavelength and train speed on the DAF of HSRs. It can be seen that the DAF is generally close to 1.0 for irregularity wavelengths larger than some critical values. This critical value depends on the train speed, being larger when the speed is larger. As to be expected, when the wavelength is large enough, the track may be considered to be in a near smooth condition. Consequently, there is little dynamic amplification effect. Conversely, when the wavelength is small resulting in a more severe track irregularity condition, the DAF is noted to be significantly larger than 1 especially when the wavelength is less than 1.0 m and the train speed is high. However, when the train speed is low such as at 50 m s^{-1}, there is little dynamic effect despite that the track irregularity is considered to be severe. Whenever the DAF is large, it can be seen that the difference in results between the linearized and nonlinear contact models is significant. As the linearized contact model results are consistently smaller, it may be concluded that it is not conservative to adopt this model especially when the dynamic response of the HSR is expected to be high.

Figure 4.7 also shows that there are some localized peaks in the DAF at certain values of the irregularity wavelength for each train speed. The

frequency of the dynamic excitation f_e due to track irregularity depends on the train speed $\dot{s}_0$ and irregularity wavelength λ_t and may be expressed as

$$f_e = \frac{\dot{s}_0}{\lambda_t} \tag{4.6}$$

The natural frequency of the linearized train model

$$f_n = \frac{\omega}{2\pi} \tag{4.7}$$

may be determined by solving the associated characteristic equation

$$\det\left(\mathbf{K} - \omega^2 \mathbf{M}\right) = 0 \tag{4.8}$$

for the circular natural frequency ω, where $\mathbf{M}$, $\mathbf{K}$ are the global mass and stiffness matrices of linearized train-track-foundation system, respectively. Resonance occurs when the exciting frequency f_e due to track irregularity coincides with the natural frequency f_n and this occurs when the train speed matches the resonant speed $\dot{s}_r$ given by

$$\dot{s}_r = \lambda_t f_n \tag{4.9}$$

For the train-track-foundation system considered, the natural frequency f_n of the wheel-set is found to be 27.61 (Hz). The frequencies of the dynamic excitation computed from Eq. (4.7) for train speeds of 50, 70 and 90 m s^{-1} and track irregularity wavelengths ranging from 0.5 m to 5.0 m are presented in Table 4.3. As can be seen from the table, the frequency of the dynamic excitation approaches the natural frequency of the wheel-set when the track irregularity wavelengths are 2.0, 2.5 and 3.5 m (values in bold) corresponding

to the train speeds of 50, 70 and 90 m s^{-1}, respectively. This explains why Figure 4.7 shows peak dynamic responses occurring at these combinations of train speed and track irregularity wavelength due to the occurrence of near resonance. For other wavelength track irregularities, the exciting frequency is noted to be appreciably different in value from the natural frequency of the wheel-set.

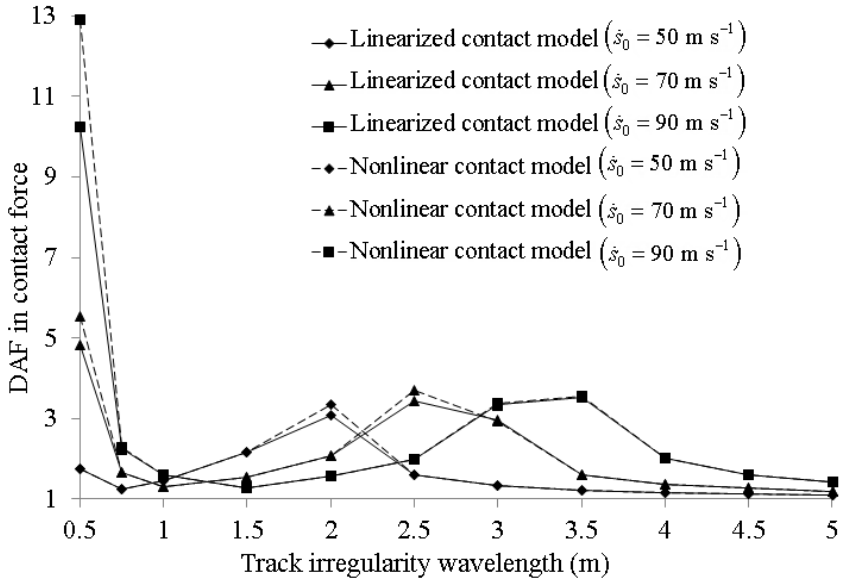

Figure 4.7. Effects of irregularity wavelength and train speed on the DAF.

Table 4.3. Exciting frequencies f_e (Hz) due to track irregularities.

Train speed (m s^{-1})	Track irregularity wavelength (m)									
	0.5	1.0	1.5	2.0	2.5	3.0	3.5	4.0	4.5	5.0
50	100.0	50.0	33.3	**25.0**	20.0	16.7	14.3	12.5	11.1	10.0
70	140.0	70.0	46.7	35.0	**28.0**	23.3	20.0	17.5	15.6	14.0
90	180.0	90.0	60.0	45.0	36.0	30.0	**25.7**	22.5	20.0	18.0

4.6.1.2 Effect of wheel load

It has been shown that the accuracy of the contact force depends on the contact model. In order to further establish when it would be important to adopt the more accurate but computationally more intensive nonlinear contact model, it would be critical to investigate the effect of the wheel load parameter. In practice, there is a varying range of wheel loads for high-speed train. Wheel loads of 55 kN (Tokunaga and Sogabe 2012) and 75 kN (Chen and Li 2000) correspond to the empty passenger railcar and locomotive, respectively.

Figures 4.8(a), (b) and (c) illustrate the effect of wheel load on the accuracy of the linearized contact model as compared to the nonlinear contact model in predicting the DAF in contact force of HSRs for train speed equal to 50, 70 and 90 m s^{-1}, respectively. All plots show the variation of DAF in contact force against track irregularity amplitude for the two cases of wheel loads considered using the linearized and nonlinear contact models.

It can be seen from Figure 4.8(a) that when the train speed is small at 50 m s^{-1}, there is virtually no difference in results obtained by both contact models for all track irregularities and wheel loads considered. This is not surprising in view that the dynamic effect is expected to be small when the train speed is low and hence the linearized contact model is accurate enough to capture the dynamic response of the HSR system.

However, when the train speed is larger as the case in Figures 4.8(b) and (c), the difference in solutions between the two contact models become

appreciable especially for larger amplitudes track irregularities. For a given track irregularity condition, the difference is also larger when the wheel load is small. On the other hand, when the wheel load is large, it appears that the linearized contact model is able to produce results close to the nonlinear contact model. Note that when the wheel load is large, dynamic effect is mitigated as can be seen by lower values of DAF in contact force. Under such a condition, it is expected that the linearized contact model is able to give good results, as the contact force magnitude would be largely due to the static wheel load effect.

(a)

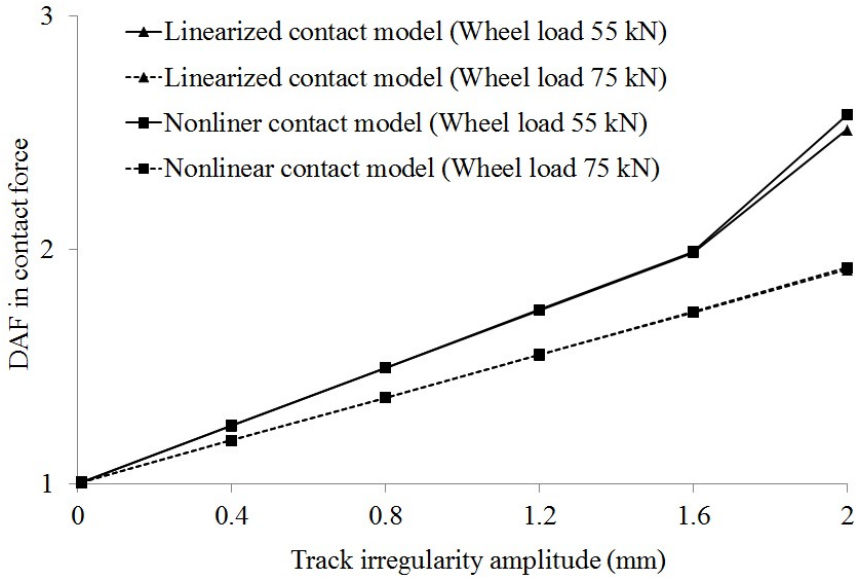

(b)

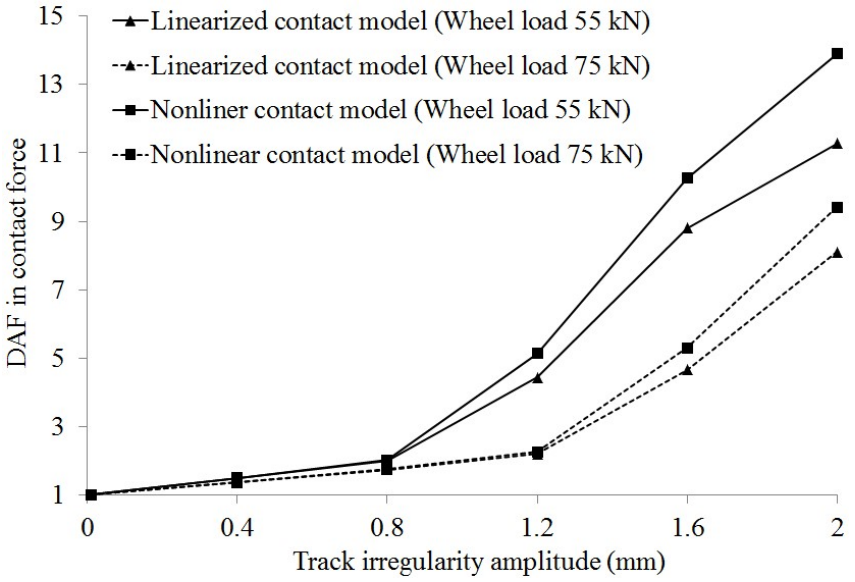

(c)

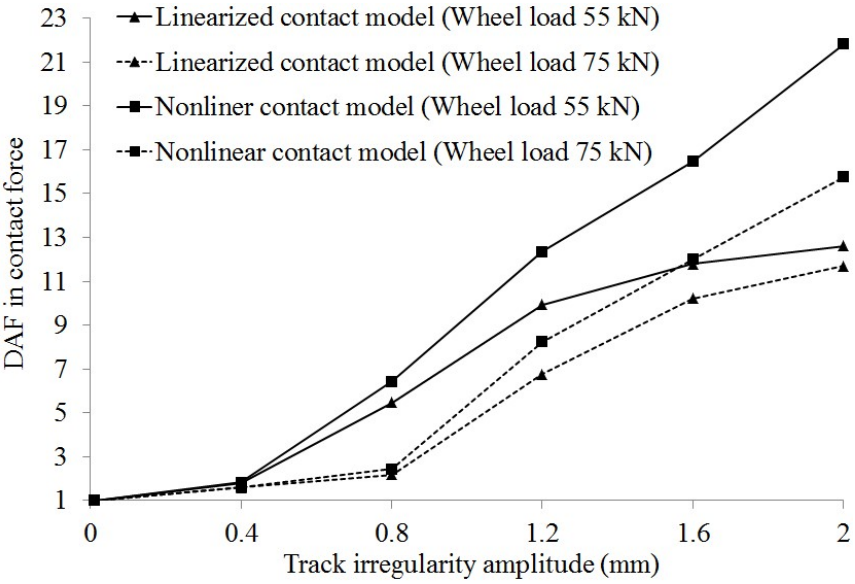

Figure 4.8. Effects of wheel load and irregularity amplitude on the DAF in contact force: (a) $\dot{s}_0 = 50$ m s^{-1}, (b) $\dot{s}_0 = 70$ m s^{-1} and (c) $\dot{s}_0 = 90$ m s^{-1}.

From the results presented in sections 4.6.1.1 to 4.6.1.2, it can be concluded that the computationally cheaper linearized contact model is

accurate enough to be used whenever the expected dynamic effect of the HSR system is not large. In general, when the train speed is low, track irregularity is near smooth and/or wheel load is large, the DAF in contact wheel force is expected to be low, and hence the use of the linearized contact model would be acceptable. On the other hand, it should be emphasized that the computationally more expensive but more accurate nonlinear contact model must be employed whenever the dynamic effect of the HSR system is expected to be significant.

4.6.1.3 Occurrence of jumping phenomenon

As presented earlier, the contact force between the wheel and rail strongly depends on the train speed, track irregularity and wheel load. When the condition is such that the DAF is relatively large, the possibility of the occurrence of the jumping wheel phenomenon, where there is momentary loss of contact between wheel and rail, becomes high. Thus, the aforementioned factors are also critical in affecting the occurrence of the jumping wheel phenomenon. Tables 4.4 and 4.5 show the occurrence or non-occurrence of the jumping wheel phenomenon for various train speeds, track irregularity and wheel load. Note that track irregularity condition is affected by two parameters, namely track irregularity amplitude and wavelength. In general, when the wavelength is small and/or amplitude is large, the track irregularity condition may be rated as severe, and vice-versa. Table 4.4 shows the results for a track irregularity wavelength of 0.5 m, which is deemed to be small, for three cases of track irregularity amplitudes ranging from very small to large.

Table 4.5 presents the results for a track irregularity amplitude of 2 mm, which is deemed to be large, for three cases of track irregularity wavelength ranging from small to large. Note that all results presented are obtained through the use of the nonlinear contact model.

It can be seen in Tables 4.4 and 4.5 that when the track condition is deemed near smooth, there is no occurrence of the jumping wheel phenomenon for all train speeds and wheel loads. On the other hand, when the track condition is considered to be severe, the jumping wheel phenomenon occurs for all wheel loads when the train speed is large enough. For the case when the train speed is low at 50 m s^{-1}, the jumping wheel phenomenon is suppressed when the wheel load is large. When the track condition is rated as moderate that is it is neither near smooth or severe, the jumping wheel phenomenon may or may not occur. It tends to occur when the train speed is high enough and when the wheel load is small. This observation is consistent with earlier results that a combination of small wheel load and high train speed promote larger dynamic effects and hence the greater chance of occurrence of the jumping wheel phenomenon.

Table 4.4. Occurrence of jumping phenomenon ($\lambda_t = 0.5$ m).

Train speed (m s^{-1}) / Track irregularity amplitude (mm)	0.01		1		2	
Wheel load (kN)	55	75	55	75	55	75
50	N	N	N	N	Y	N
70	N	N	Y	N	Y	Y
90	N	N	Y	Y	Y	Y

Table 4.5. Occurrence of jumping phenomenon ($a_t = 2$ mm)

Train speed (m s^{-1}) / Wheel load (kN)	Track irregularity wavelength (m)					
	0.5		2.5		4	
	55	75	55	75	55	75
50	Y	N	N	N	N	N
70	Y	Y	Y	Y	N	N
90	Y	Y	Y	Y	Y	Y

Note that "N" denotes non-occurrence of jumping wheel phenomenon. "Y" non-occurrence of jumping wheel phenomenon.

4.6.2 Non-uniform motion of HSR

In the following sections, the effects of amplitudes of train acceleration/deceleration, track irregularity and wheel load on dynamic response of the train-track system during the accelerating/decelerating phases using the proposed MEM approach are presented. The parameters for various train speed profiles considered are presented in Table 4.6 under Cases 1 to 2.

Table 4.6. Profiles of train velocities.

Case	Maximum velocity $\dot{s}_0$ (m s^{-1})	Amplitude of acceleration/deceleration $\lvert\ddot{s}\rvert$ (m s^{-2})	Time parameters		
			t_1 (s)	t_2 (s)	t_3 (s)
1	70	0.720	98.0	100.0	198.0
2	70	2.222	31.5	33.5	65.0

4.6.2.1 Effect of magnitude of train acceleration/acceleration

In the moving element method, the stiffness matrix of the moving element depends on the magnitude of the train acceleration/deceleration, as can be seen from Eq. (3.5). In view of this, only two values of acceleration/deceleration of train will be considered in the study. These are

designated as Cases 1 and 2 in Table 4.6 corresponding to acceleration/deceleration magnitudes of 0.720 and 2.222 m s^{-2}, respectively. Note that the amplitude and wavelength of all track irregularities are chosen to be 2 mm and 1 m (Thompson 2008), respectively. Figures 4.9(a) to (d) show the force factor-time history plots for Case 2 during the acceleration phase of the travel. Note that the force factor (FF) in contact force is defined as the ratio of dynamic force to static force. The vertical lines drawn in Figure 4.9(a) demarcate the time duration in which the jumping wheel phenomenon occurs. Figures 4.9(b) and (d) show blow-up views of the force factor-time history plot in the vicinity of the onset and ending of the jumping wheel phenomenon, respectively. Figure 4.9(c) shows a similar blow-up view over a typical period where there is sustained jumping wheel. Note that when the FF equals to -1, there is momentary loss of contact between the wheel and rail, which is what is known as jumping wheel. As the plots are similar during the deceleration phase for Case 1 as well as for both phases in Case 2, these are thus not presented. It should be noted that when the instantaneous speed of the train is close to the resonant speed of the HSR, high dynamic response is expected to occur leading to the occurrence of the jumping wheel phenomenon. Hence, the magnitude of the acceleration/deceleration will only affect the duration in which jumping wheel occurs. Thus, it is not surprising that the interval of time in which jumping wheel occurs is found to be longer in Case 1 when the acceleration/deceleration amplitude is smaller as compared to Case 2. Thus, subject to meeting the comfort level of passengers, it is recommended that

HSR trains should travel at its highest possible acceleration/deceleration to attain its final speed in order to minimize the duration of the jumping wheel phenomenon. However, it is important to note that other ill effects relating to high acceleration/deceleration have not been considered. The maximum FF for both cases are found to be virtually the same thereby confirming the fact that the magnitude of acceleration/deceleration has negligible effect on the stiffness of the system and hence the dynamic response. In view of this finding, all other results to be subsequently presented shall pertain to Case 1, considered to be the typical speed profile of today's HSR travels.

(a)

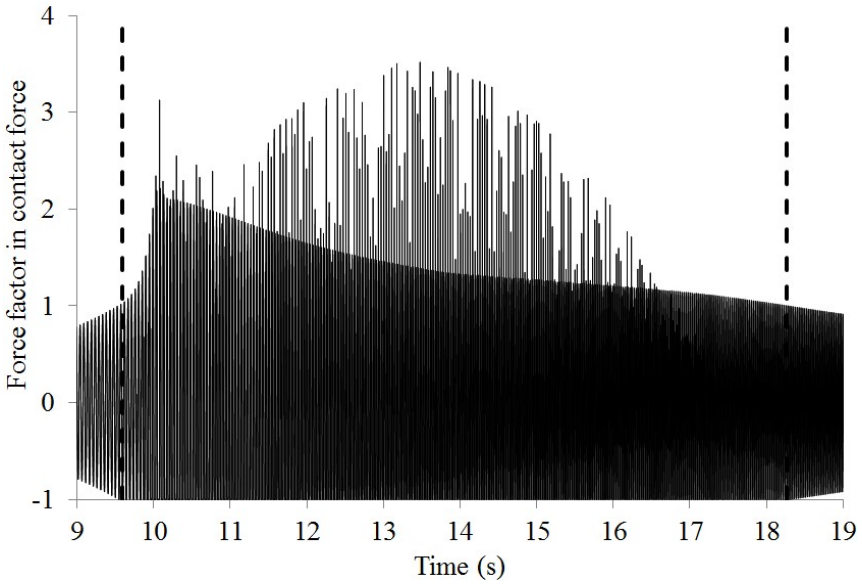

(b)

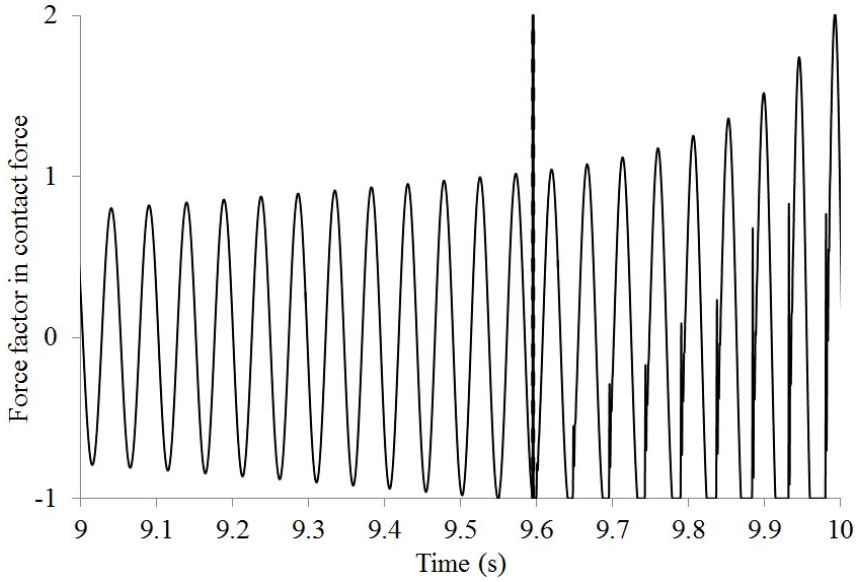
2
1
0
-1
Force factor in contact force
9
9.1
9.2
9.3
9.4
9.5
9.6
9.7
9.8
9.9
10
Time (s)

(c)

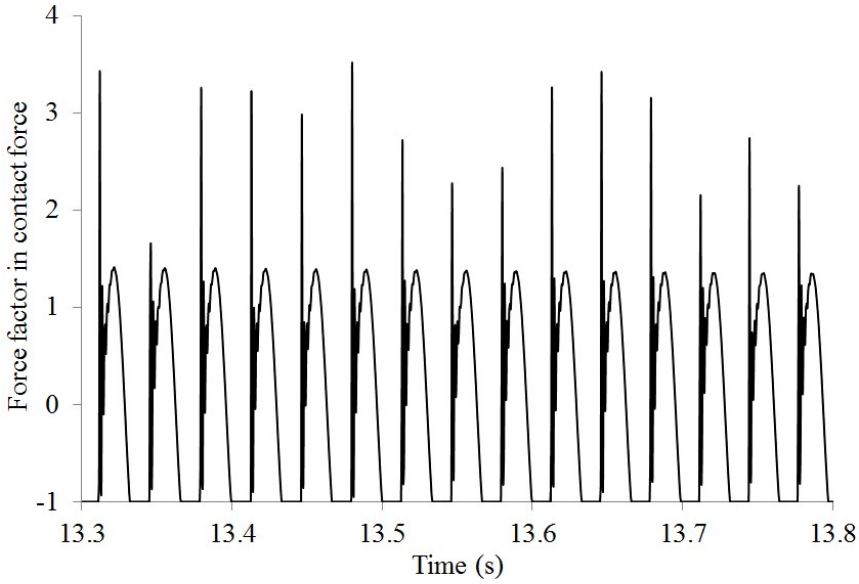
4
3
2
1
0
-1
Force factor in contact force
13.3
13.4
13.5
13.6
13.7
13.8
Time (s)

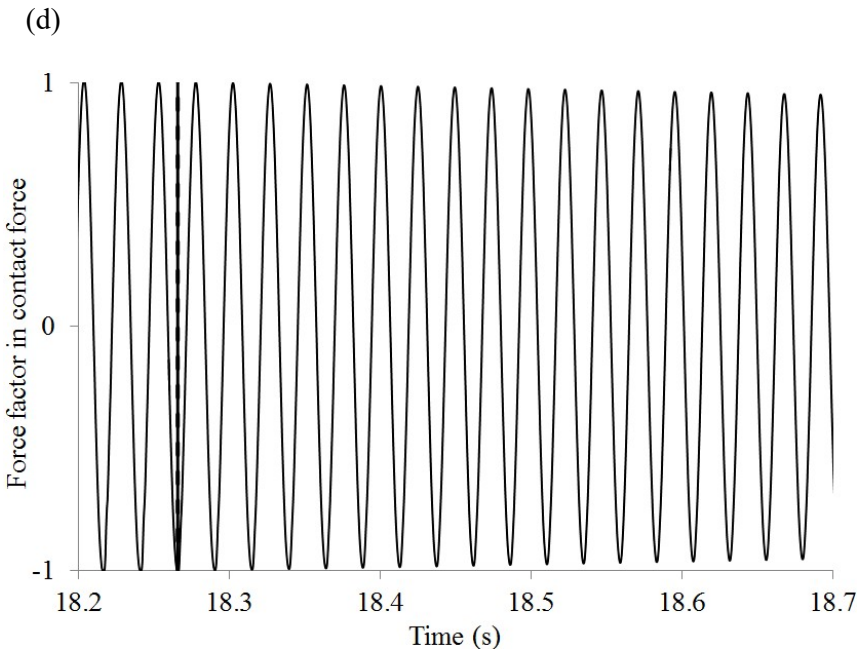

Figure 4.9 Force factor-time history: (a) in the time duration in which the jumping wheel phenomenon occurs, (b) in the vicinity of the onset of the jumping wheel phenomenon, (c) over a typical period where there is sustained jumping, and (d) in the vicinity of the ending of the jumping wheel phenomenon.

4.6.2.2 Effect of track irregularity

The effect of track irregularity amplitude on the DAF is next investigated. The results are plotted in Figure 4.10. The 3 curves drawn correspond to the 3 phases of travel, namely during the acceleration, constant speed and deceleration phases. Note that the wavelength λ_t of all track irregularities is chosen to be 1 m. For a near smooth track ($a_t = 0.01$ mm), the DAF is found to be approximately 1, as to be expected. When the amplitude of track irregularity increases, the DAF is noted to increase gradually and then significantly for the acceleration/deceleration phases. For these two phases, when the track irregularity amplitude is large enough for the track condition to

be considered as moderate or severe, the DAF increases significantly due to the occurrence of the jumping wheel phenomena for the brief interval in which the train speed is in the vicinity of the resonant speed. Note that the frequency of the dynamic excitation due to the track irregularity depends on the train speed and irregularity wavelength. Thus, when the train speed and wavelength are such that the frequency of the dynamic excitation approaches the natural frequency of the wheel-set, there will be expected resonance effect. The DAF is also noted to be slightly larger during the deceleration phase as compared to the acceleration phase. For the constant speed phase, the DAF is observed to increase gradually as the track irregularity amplitude increases. No jumping wheel is noted to occur during this phase.

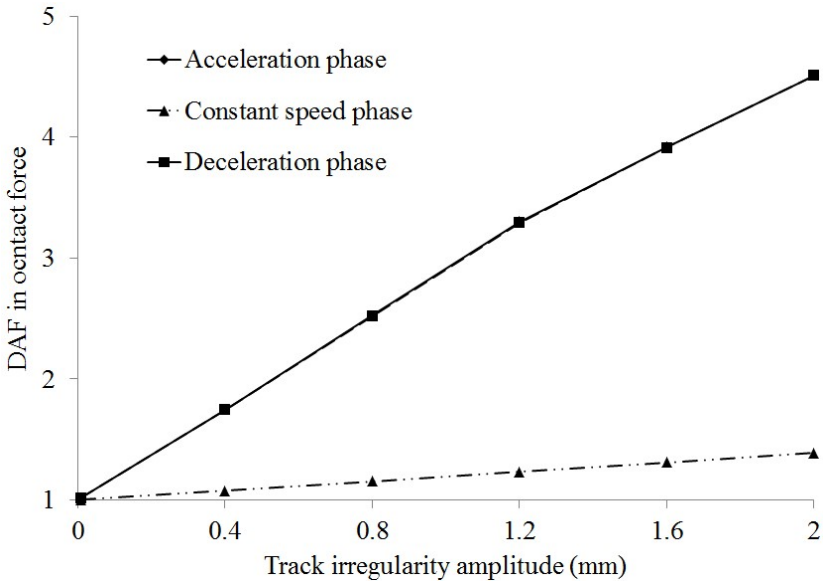

Figure 4.10. Effect of track irregularity amplitude on the DAF.

As the natural frequency of the wheel-set system is fixed, the magnitude of track irregularity wavelength is a significant factor in affecting the

occurrence of the resonant phenomenon during the acceleration/deceleration phases. As already mentioned, resonance occurs briefly during these two phases when the train speed reaches the magnitude of the resonant speed. This occurs only when the maximum train speed is higher than the resonant speed.

Figure 4.11 shows the effect of track irregularity wavelength on the DAF for the 3 phases of train travel. Note that all track irregularity amplitudes are 2 mm for this study. When the wavelength is large, it is noted that the DAF is relatively low, as to be expected. As the wavelength decreases, the DAF is found to increase gradually and then abruptly when it approaches 2.5 m for all phases. It should be noted that the frequency of the wheel-set is close to the exciting frequency when the track irregularity wavelength is 2.5 m. Thus, resonance is noted to occur for all phases which accounts why the DAF increases abruptly. Also, note that when the track irregularity wavelength is greater than approximately 3 m, the resonant phenomenon does not occur, as the theoretical resonant speed is larger than the maximum train speed attained during the travel.

During the acceleration/deceleration phases, the DAF seems to be initially constant as the track irregularity wavelength decreases below 2.5 m. Note that the DAF tends to increase with decreasing track irregularity wavelength since small values of wavelength are associated with more severe track irregularity conditions. However, as the resonant speed decreases with decreasing wavelength, the DAF tends to decrease since the train speed, as it crosses the resonant speed during the acceleration/deceleration phases, are

smaller. These two opposing effects on the DAF thus explain why the DAF is observed to be approximately constant when the wavelength is between 0.75 m and 2.5 m. As the wavelength decreases further below 0.75 m, the effect of severity of track condition becomes more pronounced and thus the DAF is seen to increase abruptly. Note that the trend for the constant speed phase of travel is similar to the acceleration/deceleration phases except that the DAF decreases abruptly as the track irregularity wavelength decreases below 2.5 m.

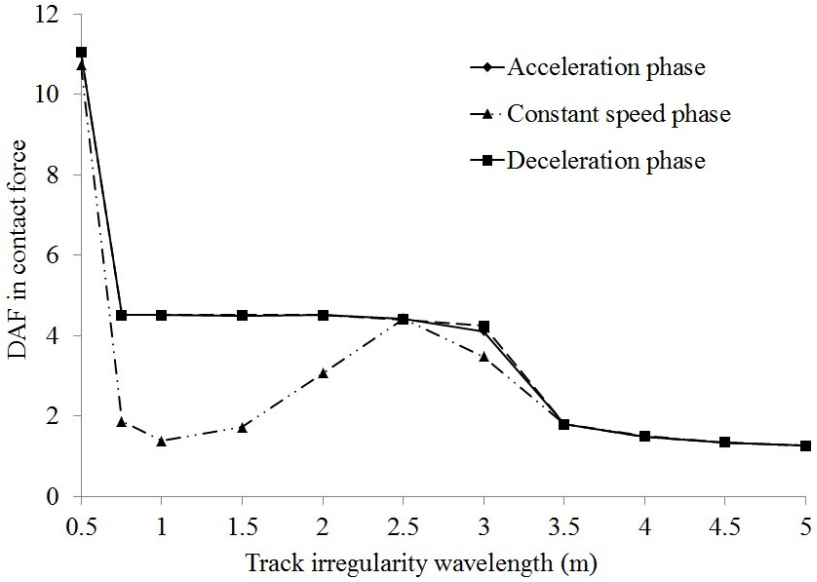

Figure 4.11. Effect of track irregularity wavelength on the DAF.

4.6.2.3 Effect of wheel load

The effect of wheel load on the dynamic response of the system was earlier investigated and discussed for the case when the train travels at constant speed. The conclusion then was that the wheel load effect could be considerable. It would thus be important to examine the effect of wheel load when the train travels at variable speed as in Case 1.

Figure 4.12 shows the variation of the DAF against track irregularity amplitude for various wheel loads. The track irregularity wavelength is fixed at 1.0 m for this study. The results show that the DAF during all phases for small wheel load is always larger as compared to large wheel load. Note that when the wheel load is large, it is expected that the dynamic effect is mitigated, which explains why the DAF is found to be larger for the case of the smaller wheel load. This finding is the same as that obtained by Herwig (2006). Figure 4.12 shows that there is virtually no difference in DAF for both cases of wheel loads when the track irregularity amplitude is below approximately 0.4 mm. Beyond this critical value, the DAF increases significantly during the acceleration/deceleration phases and the difference in DAF for the two wheel loads becomes more pronounced. However, during the constant speed phase, it is found that the DAF grows marginally for track irregularity amplitude beyond 0.4 mm and that there is virtually no difference in DAF for both cases of wheel loads. Wheel load is thus critical in affecting the response of the system for a brief time interval during the acceleration/deceleration phases as the train speed crosses the resonant speed of the linearized train model. A larger wheel load has the advantage of mitigating the dynamic response during the critical period of travel.

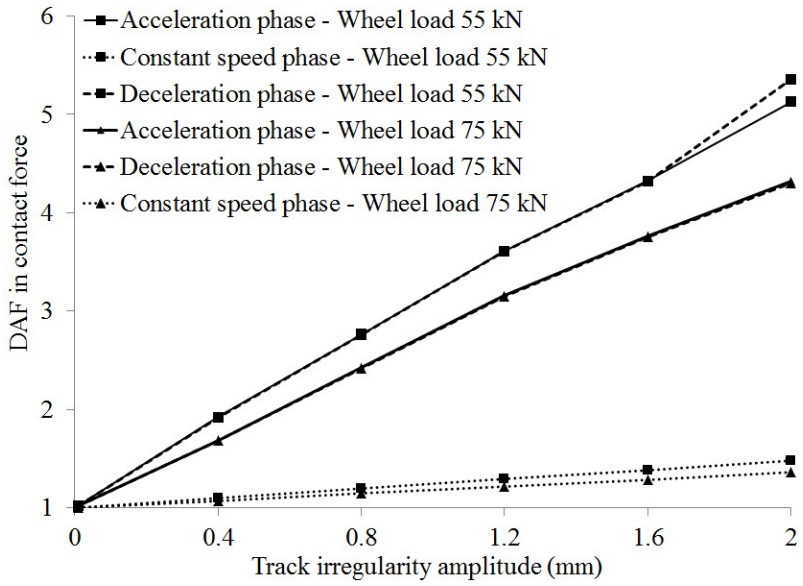

Figure 4.12. Effect of wheel load and track irregularity amplitude on DAF

4.6.2.4 Occurrence of jumping phenomenon

In this section, the jumping wheel phenomenon is also investigated when train travels at varying speed. Table 4.7 shows the occurrence or non-occurrence of the jumping wheel phenomenon for various track irregularity amplitudes. Note that "Y" and "N" denote occurrence and non-occurrence of jumping wheel phenomenon, respectively. The track irregularity wavelength is fixed at 1.0 m in this study. It can be seen that when the track irregularity amplitude is less than 0.4 mm corresponding to a near smooth track condition, there is no occurrence of the jumping wheel phenomenon. Beyond this critical value, the jumping wheel phenomenon may or may not occur during the acceleration/deceleration phase. When the track condition is considered to be severe, the jumping wheel phenomenon occurs briefly during the critical period of travel of the acceleration/deceleration phase. As the exciting

frequency is close to the natural frequency of the wheel-set, there is occurrence of resonant phenomenon during these phases. With such condition and large amplitude, the jumping wheel phenomenon occurs, as it is anticipated that the dynamic effect is large. Note that there is non-occurrence of jumping wheel phenomenon regardless of track irregularity amplitude during constant speed phase.

Table 4.8 shows the occurrence or non-occurrence of the jumping wheel phenomenon for various track irregularity wavelengths. The track irregularity amplitude is fixed at 2.0 mm in this study. The jumping wheel phenomenon is noted to occur in all phases of travel when the track irregularity wavelength is small, such as at 0.5 m, since this value corresponds to the case of a more severe track condition and hence high dynamic effects. At a wavelength of 2.5 m, the frequency of the wheel-set is close to the exciting frequency and thus there is expected occurrence of resonance resulting in the occurrence of the jumping wheel phenomenon too. For wavelengths higher than the critical value of 3 m, the track condition matches closer to a near smooth case. Consequently, there is no occurrence of the jumping wheel phenomenon. Non-occurrence of jumping wheel phenomenon also is found at critical wavelengths, i.e. 1 m and 1.5 m when the train travels during constant speed phase. At these wavelengths, the frequency of the wheel-set is not close to the exciting frequency and thus there is non-occurrence of resonance resulting in the non-occurrence of the jumping wheel phenomenon.

Table 4.7. Occurrence of jumping wheel phenomenon ($\lambda_t = 1$ m)

Phase	Track irregularity amplitude (mm)					
	0.01	0.4	0.8	1.2	1.6	2
Acceleration	N	N	Y	Y	Y	Y
Constant	N	N	N	N	N	N
Deceleration	N	N	Y	Y	Y	Y

Table 4.8. Occurrence of jumping wheel phenomenon ($a_t = 2$ mm)

Phase	Track irregularity wavelength (m)							
	0.5	1	1.5	2	2.5	3	3.5	4
Acceleration	Y	Y	Y	Y	Y	Y	N	N
Constant	Y	N	N	Y	Y	Y	N	N
Deceleration	Y	Y	Y	Y	Y	Y	N	N

4.7 Concluding remarks

In this chapter, the proposed MEM is employed to investigate the response of non-uniform motion of high-speed train, in which the speed-time profile of the train is given. The profile consists of three phases, namely (1) an accelerating phase in which the train accelerates uniformly to attain an operational speed, (2) a constant-speed phase and (3) a decelerating phase in which the train decelerates uniformly from operational speed to a halt. The results obtained using the proposed MEM is found to agree well with results found in the literature using the MEM as well as FEM solutions. The magnitude of train acceleration/deceleration is found to be significant effect on the dynamic response of the system when the train travels at a theoretical acceleration/deceleration on a soft foundation.

Two computational schemes, one implicit and the other explicit, to treat the nonlinear normal wheel-rail contact force are discussed and presented. The implicit scheme is simpler to implement but is restricted only to simple train models. The other explicit scheme is more complicated and requires generally more computational effort. Due to the simple 3-DOF train model employed, it is thus recommended that the implicit scheme be employed to investigate the dynamic response of non-uniform motion of the HSR. A parametric study is carried out to understand the effects of various factors on the dynamic response of HSR including the occurrence of jumping wheel phenomenon. Parameters considered include the magnitude of train acceleration or deceleration, the severity of railhead roughness (track irregularity) and the wheel load.

To account for the wheel-rail interaction, two normal contact models were employed and their accuracy and suitability evaluated. It is found that the computationally cheaper linearized contact model is accurate enough to be used whenever the expected dynamic effect of the system is not large. In general, when the train speed is low, track irregularity is near smooth and/or wheel load is large, the DAF in contact wheel force is expected to be small, and hence the use of the linearized contact model would be acceptable. On the other hand, it should be emphasized that the computationally more expensive but more accurate nonlinear contact model must be employed whenever the dynamic effect of the HSR system is expected to be significant. A combination of small wheel load, high train speed and severe track condition

promotes larger dynamic effects and hence the greater chance of occurrence of the jumping wheel phenomenon.

Subject to ensuring that the comfort level of passengers is attained, it is recommended that HSR trains should travel at its highest possible acceleration/deceleration to attain its final speed in order to minimize the duration of the jumping wheel phenomenon. However, it is important to note that other ill effects relating to high acceleration/deceleration have not been considered. Also, such a major recommendation to the operation of HSR be confirmed experimentally on a real line.

When a train travels at a cruising speed higher than the resonant speed of the HSR, the dynamic response is found to be significantly larger when the speed of the train crosses the resonant speed as the train decelerates to come to a halt. The momentary spike in the dynamic response, including the higher chance of occurrences of the jumping wheel phenomenon, needs to be considered in the safe operation of the HSR.

CHAPTER 5. SINGLE-RAILCAR TRAIN SUBJECT TO BRAKING

5.1 Introduction

In the previous chapter, the computational method for analysing the dynamic response of non-uniform motion of the HSR is presented. To capture the vertical inertia effect of the moving train mass, a simple train model such as the 3-DOF model was presented. However, the above simple train model cannot be employed for the study of railway vehicle braking. Thus, a more realistic 15-DOF train model that accounts for the effect of pitching moment arising from the longitudinal inertia effects and wheel adhesion forces is necessary.

Under emergency situations that require the train to come to a halt quickly to avoid other possible catastrophes, high-speed trains may undergo high deceleration. Unlike normal braking, when a train decelerates under moderate to heavy braking condition, there may be possible occurrence of instability due to train wheels sliding over the rails. The lack of research might be cited as the reason why there are many unfortunate catastrophic accidents involving HSRs all over the world. Thus, there would be a need to study the dynamic response of the HSR subject to braking with posibile occurrence of wheel sliding.

5.2 Literature review

Railway vehicle braking is an important research topic in view of the catastrophic nature of any failure of any structural components that may arise, collision when the safe braking distance is exceeded and heightened instability due to wheel sliding over the rails. A derailment study (China Academy of Railway Science 1998) revealed that 30% of derailments in Russia occurred due to emergency braking under poor wheel-rail contact condition. Lixin and Haitao (2001) studied the 3-D dynamic response of heavy trains travelling at a low speed and subject to normal braking, in which the occurrence of wheel sliding was not investigated. Handoko and Dhanasekar (2007) predicted the dynamics of simplified two-axle bogies of low-speed train both under constant speed and under variable speed due to traction and braking. Zhang and Dhanasekar (2009) presented a low-speed train model under braking conditions in order to investigate car body pitch, derailment, and wheel-set skid. The influence of wheel-rail contact condition and track geometry defects on car body pitch was also discussed.

In the above-cited research works, researchers mostly focused on a heavy train traveling at low-speed under normal braking conditions with the railhead assumed to be perfectly smooth. However, real train-track systems are likely to have various degrees of railhead roughness. High-speed trains may undergo high deceleration under emergency situations that require the train to come to a halt quickly to avoid other possible catastrophes. Such trains would then be subject to so-called ‘abnormal’ braking. Unlike normal braking, when

a train decelerates under moderate to heavy braking conditions, instability due to train wheels sliding over the rails could occur. Due to track irregularity and the high speed of the train, it cannot be assumed that the wheel is always in contact with the railway track. The jumping wheel phenomenon needs to be accounted for. Simple train models such as a moving load or moving sprung-mass cannot be employed for the study of railway vehicle braking. A more realistic train model that accounts for the effect of pitching moment arising from the longitudinal inertia effects and wheel adhesion forces is necessary.

5.3 Problem definition

5.3.1 15-DOF train model

Consider a 15-DOF half-train model traveling at a distance s as shown in Figure 5.1. Without loss of generality, the locomotive of the train is modelled as a system of interconnected car body, two bogies and four wheels. In the model, $m_c = 4m_1$ and J_c denote the mass and moment of inertia about the pitch of the car body, respectively. For brevity, the terms car body and bogie refer to half of these components in view of the half-train model adopted. The car body is supported through secondary suspensions to two identical bogies. The mass and moment of inertia about the pitch of each bogie are $m_b = 2m_2$ and J_b, respectively. The secondary suspension consists of two spring-damping units, each modelled by a spring $k_s = 2k_1$ and dashpot $k_p = k_2$. The bogies are supported through primary suspensions to the four wheels, each of

mass $m_w = m_3$ and moment of inertia about the pitch J_w. The primary suspension system consists of four spring-damping units, each comprising a spring k_p and dashpot c_p. The nonlinear Hertz contact force and adhesion force between the i^{th} wheel and rail beam are F_{ci} and f_i, respectively. The positions of the secondary and primary suspension spring-damping units measured with respect to the centre of mass of car body and the bogies are specified by l_1 and l_2, respectively, as shown in Figure 5.1.

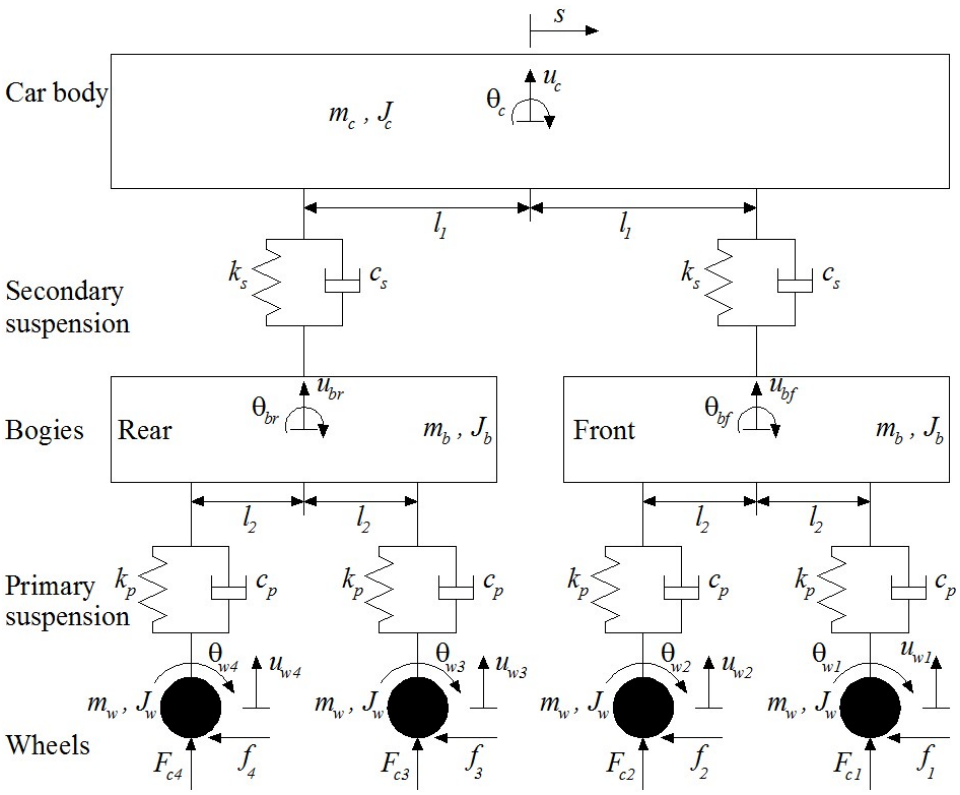

Figure 5.1. A 15-DOF train model.

The governing equations of the car body, bogies and wheels may be derived from Newton's second law of motion

$$m_c\ddot{u}_c + c_s\left(2\dot{u}_c - \dot{u}_{br} - \dot{u}_{bf}\right) + k_s\left(2u_c - u_{br} - u_{bf}\right) = -m_c g \tag{5.1}$$

$$J_c\ddot{\theta}_c + c_s l_1\left(\dot{u}_{bf} + 2l_1\dot{\theta}_c - \dot{u}_{br}\right) + k_s l_1\left(u_{bf} + 2l_1\theta_c - u_{br}\right) + m_c h_1\ddot{s} = -F_r h_1 \tag{5.2}$$

$$\begin{aligned} &m_b\ddot{u}_{bf} + c_s\left(\dot{u}_{bf} + l_1\dot{\theta}_c - \dot{u}_c\right) + c_p\left(2\dot{u}_{bf} - \dot{u}_{w2} - \dot{u}_{w1}\right) \\ &+k_s\left(u_{bf} + l_1\theta_c - u_c\right) + k_p\left(2u_{bf} - u_{w2} - u_{w1}\right) = -m_b g \end{aligned} \tag{5.3}$$

$$\begin{aligned} &m_b\ddot{u}_{br} + c_s\left(\dot{u}_{br} - l_1\dot{\theta}_c - \dot{u}_c\right) + c_p\left(2\dot{u}_{br} - \dot{u}_{w4} - \dot{u}_{w3}\right) \\ &+k_s\left(u_{br} - l_1\theta_c - u_c\right) + k_p\left(2u_{br} - u_{w4} - u_{w3}\right) = -m_b g \end{aligned} \tag{5.4}$$

$$\begin{aligned} &J_b\ddot{\theta}_{bf} + c_p l_2\left(\dot{u}_{w1} + 2l_2\dot{\theta}_{bf} - \dot{u}_{w2}\right) + k_p l_2\left(u_{w1} + 2l_2\theta_{bf} - u_{w2}\right) \\ &-\left[2m_w\left(h_2 + h_3\right) + m_b h_2\right]\ddot{s} = \left(f_1 + f_2\right)\left(h_2 + h_3\right) \end{aligned} \tag{5.5}$$

$$\begin{aligned} &J_b\ddot{\theta}_{br} + c_p l_2\left(\dot{u}_{w3} + 2l_2\dot{\theta}_{br} - \dot{u}_{w4}\right) + k_p l_2\left(u_{w3} + 2l_2\theta_{br} - u_{w4}\right) \\ &-\left[2m_w\left(h_2 + h_3\right) + m_b h_2\right]\ddot{s} = \left(f_3 + f_4\right)\left(h_2 + h_3\right) \end{aligned} \tag{5.6}$$

$$m_w\ddot{u}_{w1} + c_p\left(\dot{u}_{w1} + l_2\dot{\theta}_{bf} - \dot{u}_{bf}\right) + k_p\left(u_{w1} + l_2\theta_{bf} - u_{bf}\right) = F_{c1} - m_w g \tag{5.7}$$

$$m_w\ddot{u}_{w2} + c_p\left(\dot{u}_{w2} - l_2\dot{\theta}_{bf} - \dot{u}_{bf}\right) + k_p\left(u_{w2} - l_2\theta_{bf} - u_{bf}\right) = F_{c2} - m_w g \tag{5.8}$$

$$m_w\ddot{u}_{w3} + c_p\left(\dot{u}_{w3} + l_2\dot{\theta}_{br} - \dot{u}_{br}\right) + k_p\left(u_{w3} + l_2\theta_{br} - u_{br}\right) = F_{c3} - m_w g \tag{5.9}$$

$$m_w\ddot{u}_{w4} + c_p\left(\dot{u}_{w4} - l_2\dot{\theta}_{br} - \dot{u}_{br}\right) + k_p\left(u_{w4} - l_2\theta_{br} - u_{br}\right) = F_{c4} - m_w g \tag{5.10}$$

$$J_w\ddot{\theta}_{w1} = f_1 R_w - T_b \tag{5.11}$$

$$J_w\ddot{\theta}_{w2} = f_2 R_w - T_b \tag{5.12}$$

$$J_w\ddot{\theta}_{w3} = f_3 R_w - T_b \tag{5.13}$$

$$J_w\ddot{\theta}_{w4} = f_4 R_w - T_b \tag{5.14}$$

$$\left(m_c + 2m_b + 4m_w\right)\ddot{s} = -\left(\sum_{i=1}^{4} f_i + F_r\right) \tag{5.15}$$

where u_c and θ_c are the vertical and pitch displacements of the car body, respectively; $\left(u_{br},\theta_{br}\right)$ and $\left(u_{bf},\theta_{bf}\right)$ the vertical and pitch displacements of the rear and front bogies, respectively; $\left(u_{wi},\theta_{wi}\right)$ the vertical and pitch displacements of the i^{th} wheel; F_r the total running resistance force acting on car body; g the gravitational acceleration; T_b the applied braking torque; h_1 the vertical distance between car body's center of mass and longitudinal internal forces interlocking between car body and bogies; h_2 the vertical distance between the longitudinal internal forces and center of mass of bogies; and h_3 the vertical distance between the center of mass of bogies and the longitudinal internal forces connecting bogies to wheels.

5.3.2 Running resistance

Running resistance generally includes aerodynamic drag and the rolling resistance. Based on an experimental study by Yang and Sun (2001), the running resistance of a high-speed train may be written as

$$R = c_0 + c_v\dot{s} + c_a\dot{s}^2 \tag{5.16}$$

where the coefficients c_0, c_v, c_a are obtained from the wind tunnel test. The third term $c_a\dot{s}^2$ denotes the aerodynamic drag and the first two terms are considered to be rolling mechanical resistance. The total running resistance force F_r, acting on the locomotive, is obtained by multiplying the running resistance R with the total mass of the train $\left(m_c + 2m_b + 4m_w\right)$.

5.3.3 Wheel-rail contact force

Based on the nonlinear Hertz contact model (Esveld 2001), the contact force F_{ci} between the i^{th} wheel and rail may be expressed as

$$F_{ci} = \begin{cases} K_H \Delta y_i^{\frac{3}{2}} & for \quad \Delta y_i \geq 0 \\ 0 & for \quad \Delta y_i < 0 \end{cases} \tag{5.17}$$

where Δy_i denotes the indentation at the contact surface at the i^{th} wheel, which may be expressed as

$$\Delta y_i = y_{ri} + y_{ti} - u_{wi} \tag{5.18}$$

where y_{ri} and y_{ti} denote the vertical displacement of the rail and track irregularity at the i^{th} contact point, respectively, and u_{wi} the vertical displacement of the i^{th} wheel. The track irregularity is widely assumed to take the following sinusoidal form (Nielsen and Abrahamsson 1992)

$$y_{ti} = a_t \sin \frac{2\pi x_i}{\lambda_t} \tag{5.19}$$

where a_t and λ_t denote the amplitude and wavelength of track irregularity, respectively.

5.3.4 Wheel-rail adhesion force

The adhesion force f_i between the wheel and rail significantly affects the performance of the drive dynamics. A simplified wheel-rail contact model for the computation of the adhesion force has been introduced by Polach (2005). This adhesion model, which will be employed in this study, is suitable

for accounting the dynamics of wheel sliding resulting from braking where there may be an occurrence of large creep conditions.

The simplified wheel-rail contact model for the adhesion force f_i is given by

$$f_i = \frac{2\mu_i F_{ci}}{\pi}\left(\frac{k_A \varepsilon_i}{1+\left(k_A \varepsilon_i\right)^2} + \tan^{-1}\left(k_S \varepsilon_i\right)\right) \tag{5.20}$$

where ε_i is the gradient of tangential stress in the longitudinal direction and k_A and k_S refer to the reduction factors in the adhesion and slip areas, respectively. Based on Kalker's linear theory (Kalker 1967), ε_i may be expressed as

$$\varepsilon_i = \frac{G\pi a_i b_i c_{11}}{4F_{ci}\mu_i} c_{li} \tag{5.21}$$

in which a_i and b_i denote the semi-axes of the contact ellipse at the i^{th} wheel, c_{11} a coefficient from Kalker's linear theory, G the shear modulus of rigidity, μ_i the friction coefficient between the i^{th} wheel and rail given by

$$\mu_i = \mu_0\left[\left(1-A\right)e^{-B\left|\dot{s}-R_w\dot{\theta}_{wi}\right|} + A\right] \tag{5.22}$$

and c_{li} the longitudinal creep at the i^{th} wheel

$$c_{li} = \frac{\left|\dot{s} - R_w\dot{\theta}_{wi}\right|}{\dot{s}} \tag{5.23}$$

In Eq. (5.22), A denotes the ratio of limit friction coefficient μ_∞ at infinity slip velocity to maximum friction coefficient μ_0 at the zero slip velocity and B the coefficient of the exponential friction decrease.

5.3.5 Track-foundation model

The rail track is modeled as an infinite Euler-Bernoulli beam resting on a two-parameter elastic damped foundation. The beam is subject to the typical wheel-rail contact forces F_{ci}, as illustrated in Figure 5.2. The track-foundation is discretized into finite moving elements, in which the formulation of the element equations is based on adopting a convected coordinate r-axis with origin fixed at the centre of mass of the moving train, as shown in Figure 5.2. The differential governing equation of motion of the track-foundation may be rewritten as

$$EI\frac{\partial^4 y}{\partial x^4}+\phi EI\frac{\partial^4 \dot{y}}{\partial x^4}-\lambda\frac{\partial^2 \dot{y}}{\partial x^2}-k_{sm}\frac{\partial^2 y}{\partial x^2}+m\ddot{y}+\alpha\dot{y}+ky=-\sum_{i=1}^{4}F_{ci}\delta\left(x-s-r_i\right) \quad (5.24)$$

where r_i denotes the r-coordinate of the i^{th} wheel.

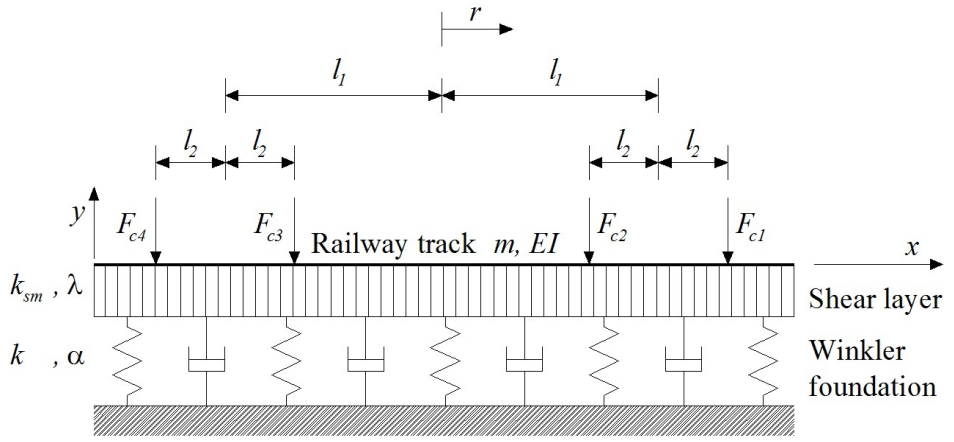

Figure 5.2. Track-foundation model.

5.4 Proposed computational technique

The MEM is also employed to model the track-foundation, where element matrices are formulated based on the convected coordinate system

attached to the center of mass of the moving train. In view of Eq. (3.1), Eq. (5.24) may be rewritten as

$$\begin{aligned} &EI\frac{\partial^4 y}{\partial r^4}+\phi EI\frac{\partial^4}{\partial r^4}\left(\dot{y}-\dot{s}\frac{\partial y}{\partial r}\right)-\lambda\frac{\partial^2}{\partial r^2}\left(\dot{y}-\dot{s}\frac{\partial y}{\partial r}\right)-k_{sm}\frac{\partial^2 y}{\partial r^2} \\ &+m\left(\dot{s}^2\frac{\partial^2 y}{\partial r^2}-2\dot{s}\frac{\partial \dot{y}}{\partial r}-\ddot{s}\frac{\partial y}{\partial r}+\ddot{y}\right)+\alpha\left(\dot{y}-\dot{s}\frac{\partial y}{\partial r}\right)+ky=-\sum_{i=1}^{4}F_{ci}\delta(r-r_i) \end{aligned} \tag{5.25}$$

By adopting Galerkin's approach, the generalized mass $\mathbf{M}_e$, damping $\mathbf{C}_e$ and stiffness $\mathbf{K}_e$ matrices for a typical moving element of length L may be proposed as:

$$\mathbf{M}_e=m\int_0^L \mathbf{N}^{\mathrm{T}}\mathbf{N}\,\mathrm{d}r \tag{5.26}$$

$$\mathbf{C}_e=\phi EI\int_0^L \mathbf{N}_{,rr}^{\mathrm{T}}\mathbf{N}_{,rr}\,\mathrm{d}r+\lambda\int_0^L \mathbf{N}_{,r}^{\mathrm{T}}\mathbf{N}_{,r}\,\mathrm{d}r-2m\dot{s}\int_0^L \mathbf{N}^{\mathrm{T}}\mathbf{N}_{,r}\,\mathrm{d}r+\alpha\int_0^L \mathbf{N}^{\mathrm{T}}\mathbf{N}\,\mathrm{d}r \tag{5.27}$$

$$\begin{aligned} \mathbf{K}_e=&EI\int_0^L \mathbf{N}_{,rr}^{\mathrm{T}}\mathbf{N}_{,rr}\,\mathrm{d}r-\dot{s}\lambda\int_0^L \mathbf{N}_{,r}^{\mathrm{T}}\mathbf{N}_{,rr}\,\mathrm{d}r-\dot{s}\phi EI\int_0^L \mathbf{N}_{,rr}^{\mathrm{T}}\mathbf{N}_{,rrr}\,\mathrm{d}r \\ &-\left(m\dot{s}^2-k_{sm}\right)\int_0^L \mathbf{N}_{,r}^{\mathrm{T}}\mathbf{N}_{,r}\,\mathrm{d}r-\left(m\ddot{s}+\alpha\dot{s}\right)\int_0^L \mathbf{N}^{\mathrm{T}}\mathbf{N}_{,r}\,\mathrm{d}r+k\int_0^L \mathbf{N}^{\mathrm{T}}\mathbf{N}\,\mathrm{d}r \end{aligned} \tag{5.28}$$

where $\mathbf{N}$ is the shape function based on Hermitian cubic polynomials and $(\ )_{,r}$ denotes partial derivative with respect to r.

By assembling the element matrices, the equation of motion for the combined train-track-foundation (HSR) model can be written as

$$\mathbf{M}\ddot{\mathbf{z}}+\mathbf{C}\dot{\mathbf{z}}+\mathbf{K}\mathbf{z}=\mathbf{P} \tag{5.29}$$

where $\ddot{\mathbf{z}}$, $\dot{\mathbf{z}}$, $\mathbf{z}$ denote the global acceleration, velocity and displacement vectors of the train-track-foundation system, respectively; $\mathbf{M}$, $\mathbf{C}$ and $\mathbf{K}$ the global mass, damping and stiffness matrices, respectively; and $\mathbf{P}$ the global

load vector. The above dynamic equation can be solved by using the Newmark's constant acceleration method (Bathe 1996).

Two computational schemes, one implicit and the other explicit, to treat the nonlinear normal wheel-rail contact force were discussed and presented in Chapter 4. It may be recalled that the implicit scheme is simpler to implement but restricted only to simple train models. The other explicit scheme is more complicated and requires generally more computational effort but needs to be employed when dealing with more complicated train models. Where braking is involved, there is the additional complication arising from the nonlinear wheel-rail adhesion force. Thus, it is necessary to employ the explicit scheme in dealing with single-railcar train subject to braking. For the given condition, it is found that a time step size less than 0.0002 s is necessary to achieve the convergence requirement, which is consistent with the time step size found in the Chapter 4.

5.5 Verification of results

As there are no available results in the literature on the dynamic response of high-speed single-railcar train subject to braking, the effectiveness and accuracy of the proposed MEM are verified through comparison with results obtained via the FEM. A FEM code was written that is matched in capability as the MEM code. As previously explained, the FEM code is not suited to solving problems involving moving loads. The computational effort required by the FEM is significantly higher than the MEM.

In the FEM model, a sufficiently long segment of the railway track is discretized uniformly with 0.25 m size elements, which has been found to be adequately small enough to attain converged accurate results. The segment may be divided into three sub-portions, a central portion and two end portions. The central portion, where the train travels during the period considered, is taken to be 140.5 m. The central portion is padded by two end portions of sufficient length in order to mitigate the erroneous boundary effects due to the moving train load approaching the boundaries of the FEM model. Through a convergence study, the length of the end portions is taken to be 24 m. Due to the advantage enjoyed by the MEM in dealing with moving load problems, a relatively shorter segment is required. Also from a convergence study made, the length required for the truncated railway track in the MEM model is 68.5 m that is discretized non-uniformly with elements ranging from a coarse 1 m to a more refined 0.25 m size.

The train is assumed to be cruising at 70 m s^{-1} before braking torques T_b of 25 kN m are applied at all the wheels of the train. The properties of track-foundation are summarized in Table 5.1 (Wu et al. 2001) and the parameters associated with the train are given in Table 3.1. The condition of the wheel-rail contact is taken to be dry. The degree of severity of track irregularity is assumed to be moderate, with the irregularity amplitude and wavelength equal to 1.5 mm and 4 m, respectively. The coefficients c_0, c_v, c_a used to compute the resistance force in Eq. (5.16) are 1176×10^{-5} N kg^{-1}, 77.616×10^{-5} N s m^{-1} kg^{-1} and 1.6×10^{-5} N s^2 m^{-2} kg^{-1} (Yang and Sun 1999), respectively. The nonlinear

Hertz spring constant used to model the contact between wheels and rail are computed from Eq. (2.4) with the radii of the wheel R_w, railhead R_r and the Poisson's ratio of the wheel/rail material υ taken to be 460 mm, 300 mm and 0.3, respectively. Typical parameters for wheel-rail contact condition used to compute the adhesion force from Eq. (5.20) are given in Table 5.2.

Table 5.1. Parameters for train model (Wu et al. 2001).

Notation	Value
m_c	23.4×10^3 kg
k_s	265×10^3 N m^{-1}
c_s	45.1×10^3 N s m^{-1}
J_c	1040×10^3 kg m^2
m_b	1.52×10^3 kg
k_p	590×10^3 N m^{-1}
c_p	19.6×10^3 N s m^{-1}
J_b	1.965×10^3 kg m^2
m_w	0.89×10^3 kg
J_w	92.126 kg m^2
l_1	8.75 m
l_2	1.25 m
h_1	0.75 m
h_2	0.42 m
h_3	0.20 m

Table 5.2. Typical parameters for wheel-rail contact conditions (Polach 2005).

Notation	Wheel-rail contact condition	
	Dry	Wet
k_A	1.00	0.30
k_S	0.40	0.10
μ_0	0.55	0.30
A	0.40	0.40
B	0.60	0.20

Figures 5.3(a) and (b) show the rail displacement profiles obtained by FEM and MEM in the vicinity of the wheel-rail contact point at the instants

0.5 s and 1.0 s after the application of wheel brakes, respectively. Note that there is no occurrence of wheel sliding at the first instance. At the second instant, wheel sliding have been found to occur at all wheels. As can be seen in Figure 5.3, both results are found to be virtually the same. In view that the FEM requires a longer domain length as compared to the MEM, it is not surprising that the computational time required is 11.5 times higher than that needed in the MEM using a desktop computer (Intel(R) Core(TM) i7-2600 CPU @3.40GHz 3.40GHz), with a memory usage of 16.0 GB". This comparison study clearly illustrated that the MEM is accurate as well as computationally efficient and is thus superior to the FEM for dealing with the dynamic response of high-speed single-railcar train subject to braking.

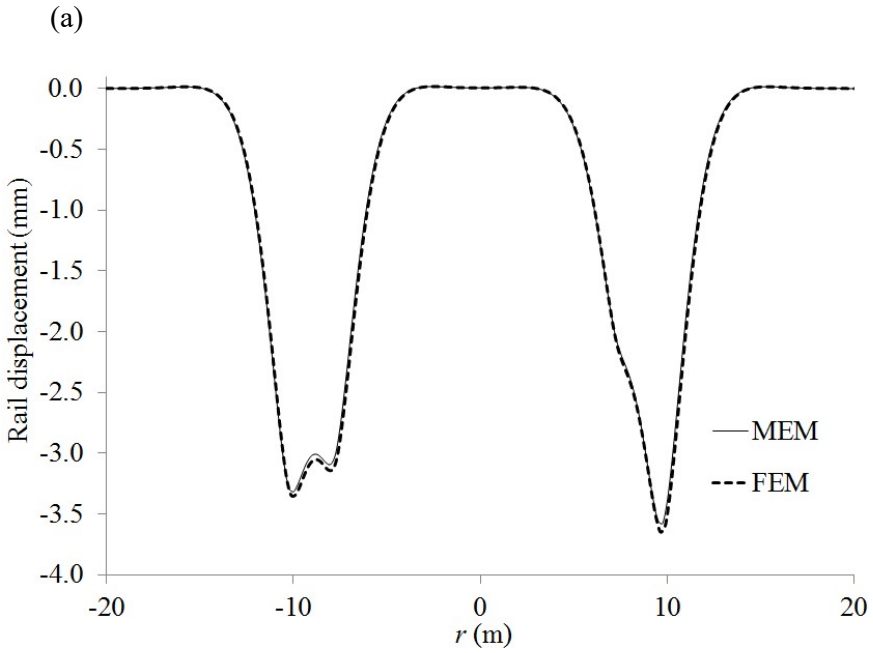

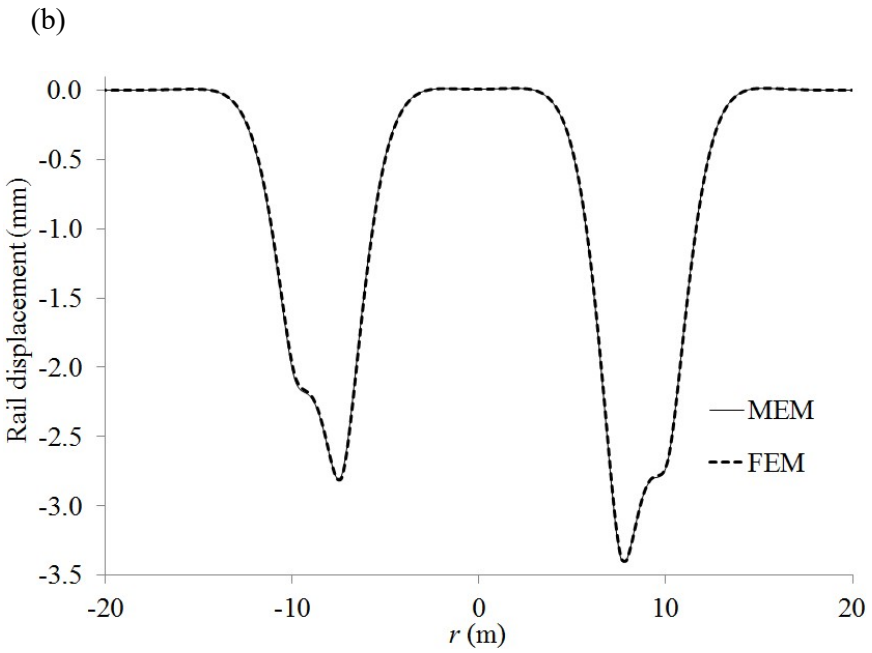

Figure 5.3. Comparison of rail displacement profiles at the instants: (a) 0.5 s and (b) 1.0 s, after the application of wheel brakes.

5.6 Numerical results

5.6.1 Effect of braking on wheel sliding

The magnitude of the braking torque applied to decelerate a train will undoubtedly affect the stability and safety of the train. If the braking torque is high enough, some or all the wheels may slide, which is a cause for concern as possible rail derailment may occur. On the other hand, if the braking torque is too low, all wheels tend to roll but the braking distance, which is the total distance taken by the train to halt, may exceed the required safe braking distance. Other factors that govern the motion of the train upon application of braking torque, in particular the mode of motion of each train wheel, include

the initial train speed, wheel-rail contact condition and severity of track irregularity.

The case of a train travelling at an initial speed of 70 m s^{-1} and subject to the sudden application of various braking torques to halt the train is investigated. For high-speed trains, it has been reported that the magnitude of the braking torque, T_b, can reach a value as high as 25 kN m (Kim 2011). In this study, the torque considered ranges from as low as 1 kN m to as high as 25 kN m, corresponding to light and heavy braking conditions, respectively. Heavy braking may arise due to emergency conditions in which the train needs to halt within a certain short distance. Note that braking torques of constant magnitude are assumed to be applied at all four wheels of the train throughout the period of motion of train as it comes to a halt. The condition of the wheel-rail contact is taken to be dry. The severity of track irregularity is assumed to be the same for all cases, with the irregularity amplitude and wavelength equal to 1.5 mm and 4 m, respectively.

To examine the mode of motion of each wheel under a braking condition, wheel angular speed-time history plots of all wheels are presented in Figure 5.4(a) for a typical case in which a moderate magnitude of braking torque of 11 kN m is applied. Superimposed in the figure is the train speed-history plot. Note that the left axis shows the wheel angular speed whilst the right axis shows the train speed. It can be seen that the train speed varies almost linearly from the initial train speed to zero throughout the train motion. For this case, the train took about 26.6 s to come to a halt after traveling 932 m

since the start of braking. To examine why the train speed varies almost linearly, it is necessary to view the corresponding train deceleration-time history plot shown in Figure 5.4(b). As can be seen in the figure, the train's deceleration fluctuates at high frequency. The mean deceleration increases sharply from zero shortly after the application of braking torque. It then decreases sharply before attaining a virtually constant magnitude. The fluctuation in deceleration arises due to the effect of track irregularity. In view that the mean train deceleration is virtually constant throughout the motion except for a brief duration initially, the train speed is expected to vary almost linearly too.

Upon closer examination of Figure 5.4(a), it can be seen that the angular speed of the fourth wheel reduces to zero very quickly after the application of braking torque. The angular speed remains zero thereafter throughout the motion of the train till it comes to a halt. Thus, the fourth wheel is noted to roll initially for a brief duration and then slides thereafter for the rest of the journey. The second wheel is noted to behave similarly to the fourth wheel. The only minor difference is that it is noted to roll for a slightly longer duration than the fourth wheel. The angular speed-history plots of the other two wheels are virtually the same whereby the speed is seen to reduce almost linearly to zero from the start of braking till the train halts. Thus, there is no occurrence of wheel sliding for these two wheels.

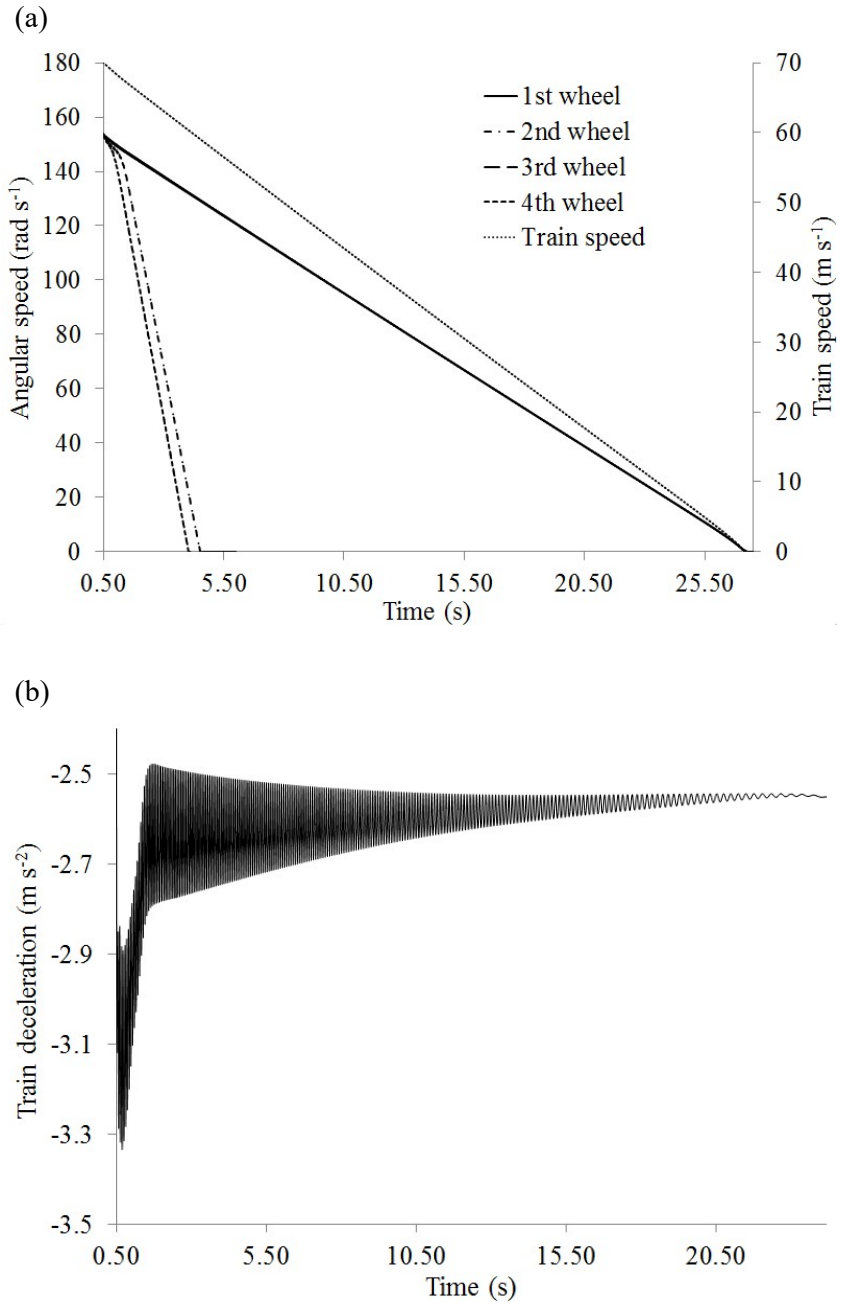

Figure 5.4. Time history of: (a) train speed and angular wheel speed; and (b) train deceleration.

The mode of behaviour of a train wheel with regards to whether it does slide for any part of the train journey depends on its position within the wheel-

set, the magnitude of the applied braking torque, the initial train speed and the condition of the wheel-rail contact. For the case study considered, Table 5.3 summarizes the mode of behaviour of each wheel for various magnitudes of applied braking torques. The notation t_s denotes the time lapse since the start of braking before wheel sliding occurs for the rest of the journey. Note that no value is indicated for t_s if the wheel does not slide at all. Also presented in the Table are the corresponding braking time, which is the time taken for the train to come to a halt.

For the case of light braking torque of 1 kN m, wheel sliding does not occur for all the wheels. When braking torque is increased, the modes of behaviour of all wheels are found to remain the same till the magnitude reaches approximately 10.5 kN m. At this moderately high magnitude of braking torque, it is interestingly found that only the fourth wheel begins to slide after a brief period of rolling. When the braking torque is increased slightly by only 0.5 kN m, the second wheel is found to slide shortly after the fourth wheel began to slide. No sliding is noted to occur for the other two wheels. When the braking torque is increased further to 13 kN m, it is found that the fourth and second wheels began to slide first at almost the same instant, followed shortly after by the sliding of the third wheel. No wheel sliding is noted to occur for the first wheel. With only a slight increase in braking torque to approximately 13.5 kN m, the mode of behaviour of the wheels is similar to the previously described case except that the first wheel is found to slide too at virtually the same instant as the third wheel. For any

braking torque higher than 13.5 kN m, the mode of behaviour of wheels remains similar i.e. the fourth and second wheels slide first followed briefly later by the simultaneous sliding of the third and first wheels. As to be expected, the duration of initial rolling decreases when the applied torque increases. In other words, the duration of wheel sliding increases with any increase in applied braking torque beyond the critical value of 13.5 kN m.

For a low braking torque of 1 kN m, the braking time required is expectedly very long as shown in Table 5.3. As the torque is increased, the braking time decreases initially and attains a minimal value when the torque reaches the optimal braking torque. The latter refers to that magnitude of torque in which one of the wheels, namely the fourth wheel, is at an impending sliding condition. For the case study considered, the optimal braking torque is found to be approximately 10.0 kN m. As the torque is increased slightly beyond the optimal value, say 10.5 kN m, the 4^{th} wheel starts to slide and as a result the braking time is increased. Any further increase in torque results in further increase in braking time, which ensues due to the occurrence of wheel sliding at other wheels, hence leading to a lesser resistance at the wheels to decelerate the train. As can be seen from Table 5.3, the larger the braking torque above the optimal value, the longer the duration of wheel sliding which results in a longer braking time. When the braking torque reaches the magnitude of 13.5 kN m, the last of the four wheels begins to slide too. This magnitude may be termed as the critical braking torque which is the smallest torque to cause wheel sliding in all four wheels. It may

be useful to classify braking torques less than the optimal value as normal braking where no wheel sliding occurs at all wheels and in which the braking time and hence the braking distance attainable is smallest. On the other hand, torques larger than the critical torque may be termed as heavy braking. Torques in between are classified as moderately heavy braking in which wheel sliding occurs at some but not all wheels.

Table 5.3. The mode of behavior of each wheel.

Braking torque T_b (kN m)	Braking time t_b (s)	Time t_s (s)			
		4th wheel	3rd wheel	2nd wheel	1st wheel
1.0	203.5	-	-	-	-
6.0	40.5	-	-	-	-
10.0	24.7	-	-	-	-
10.5	25.3	4.65	-	-	-
11.0	26.6	3.53	-	4.00	-
13.0	26.9	2.31	3.40	2.34	-
13.5	30.1	2.14	2.88	2.20	3.29
20.0	30.3	1.08	1.20	1.09	1.23
25.0	30.3	0.78	0.84	0.79	0.86

It is necessary to explain that there is the sequence of occurrence of wheel sliding, ie. from fourth wheel, second wheel, three wheel to first wheel. Figure 5.5 shows the free body diagram of the train subject to braking with effect of longitudinal inertial force. Note that $2P_1$ is the component induced by the car body pitching moment arising from the inertia force and shear force of the car body; and P_2 the component produced from the bogie pitching moment arising from the inertia force and shear force of the bogie.

The contact force at wheels may be obtained as

$$\begin{aligned} F_{c1} &= P + P_2 + P_1 \\ F_{c2} &= P - P_2 + P_1 \\ F_{c3} &= P + P_2 - P_1 \\ F_{c4} &= P - P_2 - P_1 \end{aligned} \tag{5.30}$$

where P is the wheel load including static and dynamic components.

Due to the fact that P_1 is smaller than P_2, the relationship between contact forces may be written as $F_{c4} < F_{c2} < F_{c3} < F_{c1}$ and hence wheel-rail adhesion $f_4 < f_2 < f_3 < f_1$. Consequently, for the same braking torque, there is a higher tendency for the fourth wheel to slide. When the braking torque is increased slightly, the second wheel is found to slide shortly after the fourth wheel began to slide. When the braking torque is increased further, it is found that the fourth and second wheels began to slide first at almost the same instant, followed shortly after by the sliding of the third wheel. No wheel sliding is noted to occur for the first wheel. For any higher braking torque, the mode of behaviour of wheels remains similar i.e. the fourth and second wheels slide first followed briefly later by the simultaneous sliding of the third and first wheels.

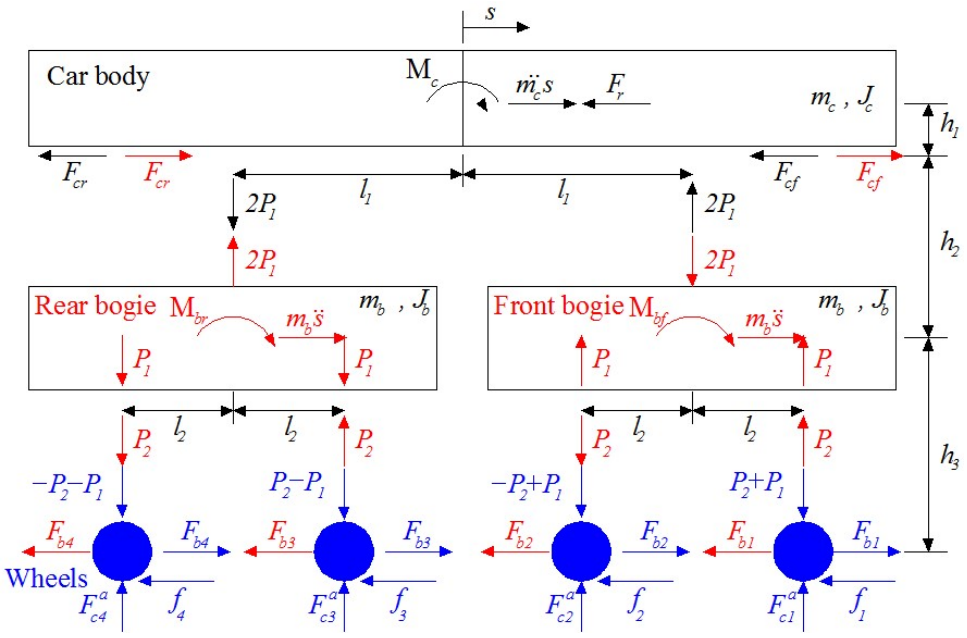

Figure 5.5. Free body diagram of the train.

5.6.2 Effect of initial train speed

The dynamic response of a high-speed rail (HSR) experiencing deceleration under a braking condition is dependent on many factors, including the initial train speed. Figure 5.6 presents the duration of wheel sliding against the magnitude of applied braking torque for three values of initial train speed. In view that the fourth and second wheels behave similarly, results are shown only for the fourth wheel (trailing wheel) in Figure 5.6(a). For a similar reason, only results for the first wheel (leading wheel) are presented in Figure 5.6(b).

The minimum braking torque required to cause wheel sliding is dependent on the position of the wheel and the initial train speed. The minimum torque is smaller at higher speed and vice-versa, as can be seen from

Figure 5.6. This result is to be expected in view that a higher initial train speed poses a more serious safety situation when braking is applied where a relatively smaller braking torque would induce wheel sliding. Also, upon examining Figures 5.6(a) and (b), it can be seen that the minimum torque is smaller for the trailing wheel as compared to the leading wheel for the same initial train speed. This can be explained as being due to the additional pitching moment induced by the effect of longitudinal inertia and wheel adhesion force that results in a reduction of normal contact force at the trailing wheel as compared to the leading wheel. Consequently, there is lesser wheel-rail adhesion at the trailing wheel and therefore a higher tendency for the wheel to slide for the same braking torque as compared to the leading wheel.

The duration of wheel sliding depends on the initial train speed and braking torque, being longer for higher train speed and larger braking torque. Generally, the results in Figure 5.6 show that once wheel sliding has been initiated due to the application of a braking torque larger than a certain value, the duration of sliding is virtually constant and is not dependent on the magnitude of braking torque.

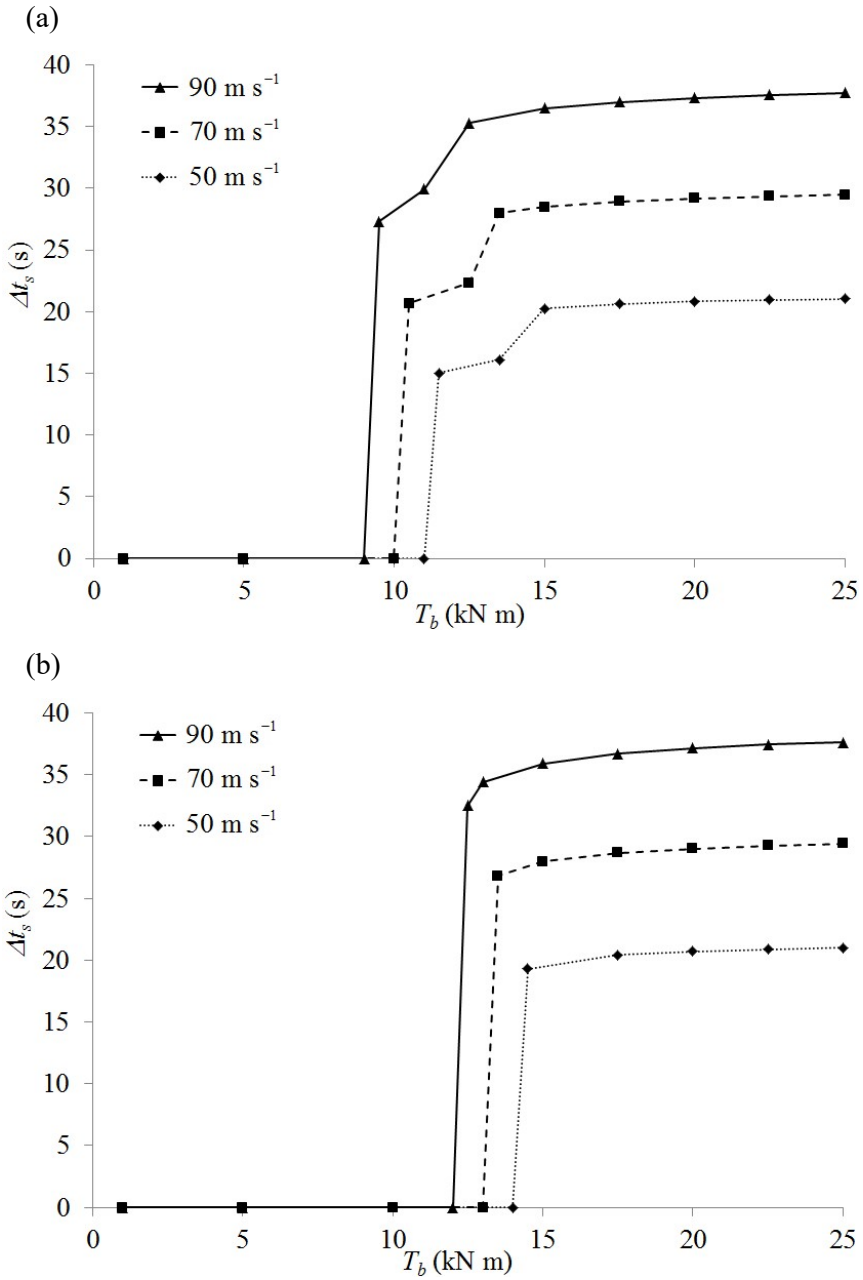

Figure 5.6. Effect of initial train speed on the duration of wheel sliding: (a) in the trailing wheel and (b) in the leading wheel.

It is obvious that to avoid wheel sliding and the high dynamic effects encountered during train braking, the braking torque applied should be as low as possible and the train speed prior to the onset of braking should be low too.

However, light braking would result in longer braking distance, which is the distance taken by the train to come to a complete halt. Thus, besides strength and instability concerns relating to structural failure and train derailment, respectively, it is also necessary to consider the safe braking distance, which is the maximum distance allowed for the train to halt safely under emergency braking conditions.

The braking distance attained is dependent on the initial train speed and the magnitude of applied braking torque. Figure 5.7 presents plots of the braking distance s_b against applied braking torque for various initial train speeds. As is to be expected, the braking distance is larger for higher initial train speed for a given braking torque. In other words, to attain the desired braking distance, the applied braking torque needs to be larger for higher initial train speed.

As the braking torque applied is increased from zero, the braking distance decreases sharply initially as shown in Figure 5.7. As presented in earlier results in Table 5.3, the braking time, and hence braking distance, reaches a minimum value when the braking torque applied is at the optimal magnitude. The optimal torque is noted to depend on the initial train speed, being larger for smaller speed. However, for the three cases of initial train speed considered, the optimal torque for each case is noted to differ only slightly. These are approximately 9.0 kN m, 10.0 kN m and 11.0 kN m for the initial train speed of 90 m s^{-1}, 70 m s^{-1} and 50 m s^{-1}, respectively. As the braking torque is increased beyond the optimal magnitude, there is initially a

slight increase in the braking distance. It is interesting to note that any further increase in the braking torque does not result in any perceptible change in the braking distance.

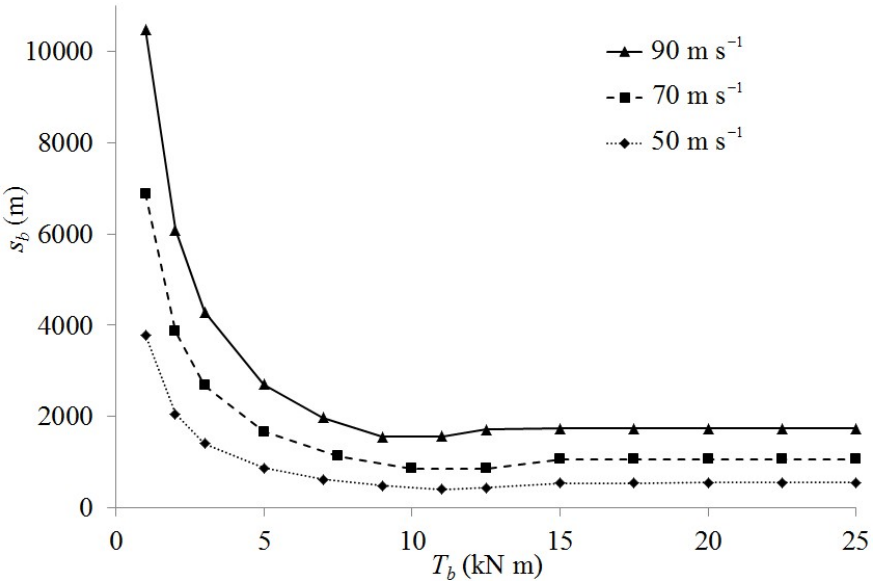

Figure 5.7. Effect of initial train speed and braking torque on the braking distance.

The dynamic response of the HSR is significantly affected by the severity of track irregularity as well as the speed of the train, as shown in Chapter 4. When there is a deceleration of the train due to the application of braking torques at the wheels, the dynamic wheel-rail contact force may be influenced by the longitudinal inertia effects. Thus, it is important to evaluate the dynamic amplification factor (DAF) in contact force at the wheels when the train is subject to braking.

Figure 5.8 shows plots of the DAF in contact force at both the trailing and leading wheels against the applied braking torque for three initial train speeds. As can be seen in the figure, the DAF in contact force depends on the

initial train speed, the position of the wheel and possibly the magnitude of applied braking torque. As is to be expected, the DAF increases as the initial train speed increases. The DAFs at both wheels are noted to be virtually the same when the train is not subject to any braking for both the 50 and 70 m s^{-1} initial train speed cases. This is however not true for the case of the higher initial train speed of 90 m s^{-1}, where it is noted that there is an abrupt difference in DAF between both wheels when braking torque is zero. For all cases of initial train speed, the DAF in the wheels begins to differ when braking torque is increased. For a given initial train speed, the DAF is found to be always larger at the leading wheel as compared to the trailing wheel. The magnitude of the braking torque is noted to have a small effect on the DAF produced in the trailing wheel, unlike the leading wheel. In the latter, the DAF is noted to increase to a peak by approximately 9% as braking torque is increased from zero to a moderate magnitude of approximately 12.5 kN m.

When a train is subject to braking, the effect of longitudinal inertia and wheel adhesion force causes the train to experience a pitching moment. This results in the leading wheel experiencing a higher than normal contact force as compared to the trailing wheel. This explains why the DAF in the contact force at the leading wheel tends to be larger than at the trailing wheel. For a given initial train speed, wheel sliding occurs sequentially in the four wheels starting with the trailing wheel, the intermediate wheels and finally the leading wheel as braking torque is increased. When the applied braking torque reaches a certain critical value, wheel sliding occurs at all wheels when the leading

wheel finally starts to slide. These critical braking torques are approximately 12.5 kN m, 13.5 kN m and 14.5 kN m for initial train speed of 90 m s^{-1}, 70 m s^{-1} and 50 m s^{-1}, respectively. When braking torque applied is at the critical magnitude, the pitching moment acting on the train is also the maximum, resulting therefore in a peak in the DAF.

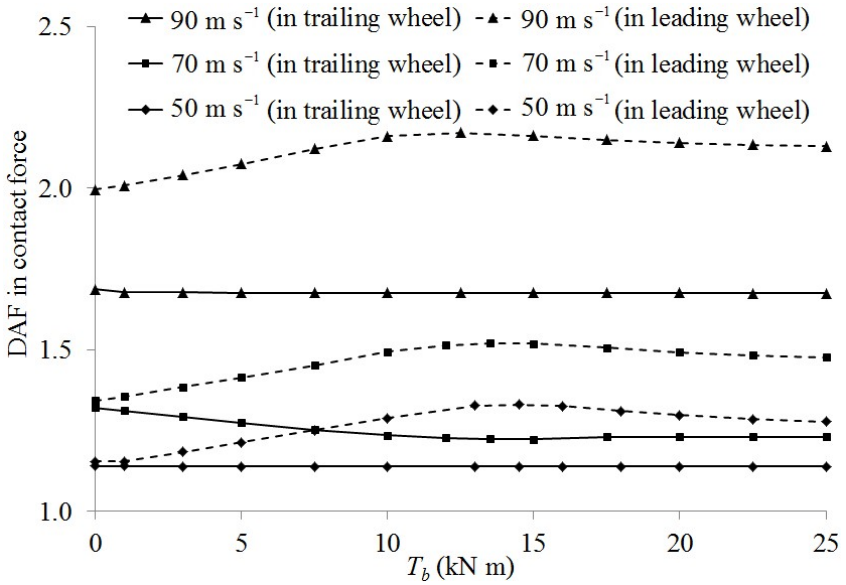

Figure 5.8. Effect of initial train speed on the DAF in contact force.

5.6.3 Effect of wheel-rail contact condition

Earlier results presented correspond only to dry wheel-rail contact condition. It is expected that the dynamic response of HSR would be appreciably increased if the condition is wet. To investigate the magnitude of influence of the wheel-rail contact condition on the dynamic response, the case of a train traveling at an initial speed of 70 m s^{-1} before experiencing sudden deceleration due to the application of braking torques is considered.

Figure 5.9 shows the duration of wheel sliding at the trailing wheel plotted against the braking torque for both the dry and wet wheel-rail contact conditions. The minimum braking torque required to cause wheel sliding is dependent on the wheel-rail contact condition. This optimal braking torque magnitude is approximately 6.0 kN m and 10.0 kN m for the wet and dry wheel-rail contact conditions, respectively. Thus, a smaller optimal braking torque would induce wheel sliding for the wet condition. This result is to be expected in view that a wet wheel-rail contact condition causes lesser wheel-rail adhesion and hence a higher tendency for the wheel to slide for the same braking torque as compared to the dry case. This is also the underlying reason why the duration of wheel sliding for the wet case is always longer as compared to the dry case.

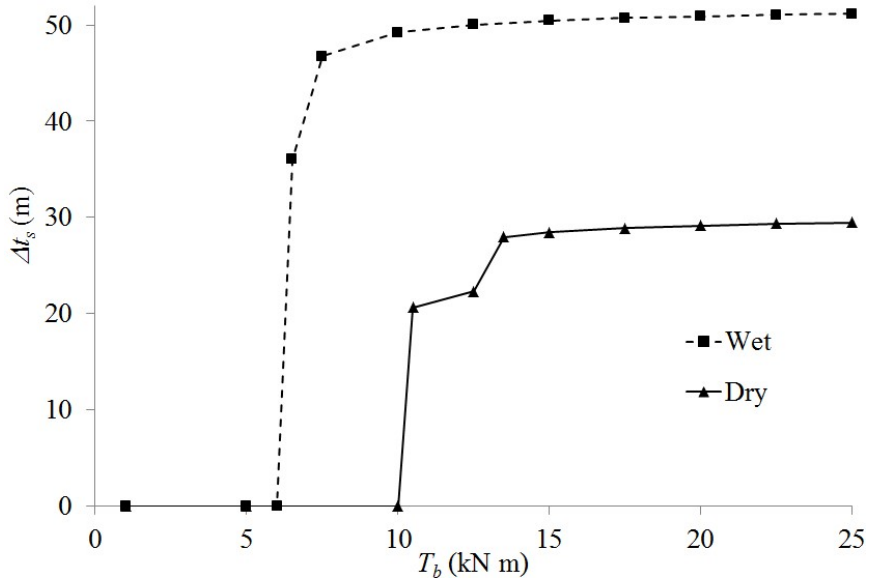

Figure 5.9. Effect of wheel-rail contact condition on the duration of wheel sliding.

Figure 5.10 shows the train braking distance for the wet and dry wheel-rail contact conditions plotted against the applied braking torque. The braking distance for both dry and wet wheel-rail contact conditions is noted to be virtually the same for braking torque less than the optimal value of 6.0 kN m, where there is no wheel sliding in both cases. The braking distance decreases as the braking torque increases till it reaches the optimal value. Beyond this optimal value, some or all wheels will slide during the deceleration of the train for the wet case. This explains why the braking distance increases abruptly and then remains virtually constant for a braking torque larger than the optimal value. In the case of a dry condition, no wheel sliding occurs till the braking torque reaches 10.0 kN m as stated earlier. Thus, the braking distance continues to decrease as the braking torque increases and reaches the smallest value when the braking torque is equal to the optimal value when one of the wheels is at an impending sliding condition. In both cases of wet and dry conditions when the braking torque applied is greater than their respective optimal values, the braking distance is virtually constant. As is to be expected, Figure 5.10 shows that the braking distance achievable is always larger for the wet condition whenever wheel sliding occurs.

Figure 5.11 shows the variation of the DAF in the leading wheel against the applied braking torque for the wet and dry wheel-rail contact conditions. It can be seen that the DAF in the dry case is generally larger as compared to the wet condition. In the latter case, lesser adhesion is generated at the wheel resulting in smaller pitching moment and hence smaller DAF in the wheel

contact force. The maximum difference in DAF between dry and wet conditions is noted to occur when the braking torque is approximately 13.5 kN m.

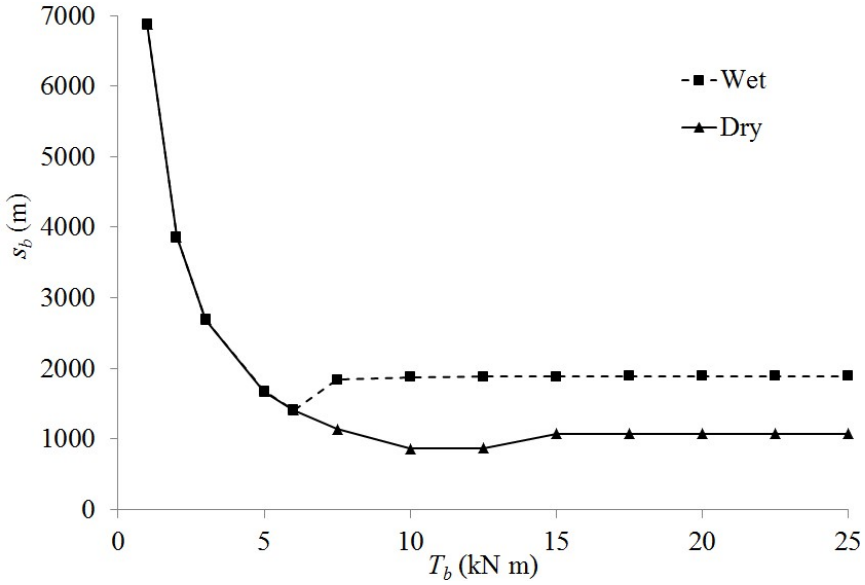

Figure 5.10. Effect of wheel-rail contact condition on the braking distance.

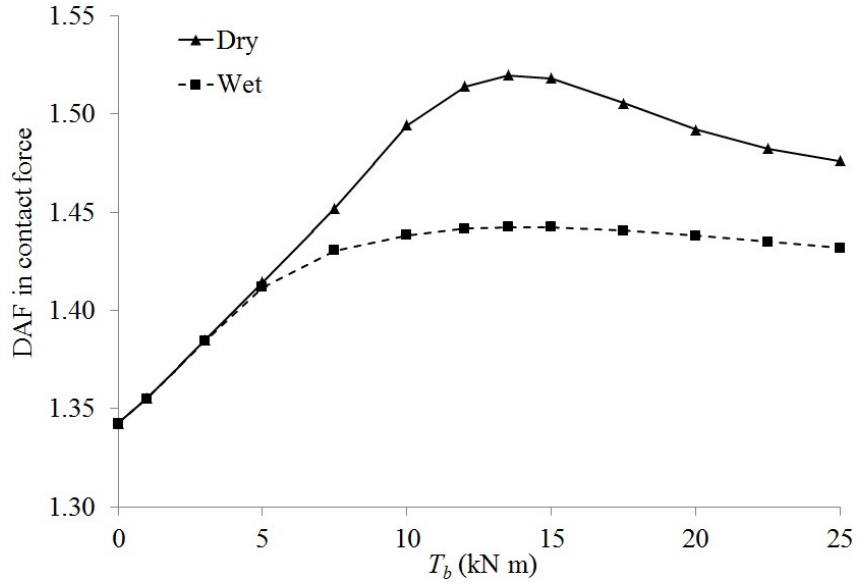

Figure 5.11. Effect of wheel-rail contact condition on the DAF in the leading wheel.

5.7 Concluding remarks

In this chapter, a numerical study of the dynamic response of high-speed single-railcar train subject to braking, with possible wheel sliding, using the proposed MEM is carried out. Braking torques of constant magnitude are applied at all wheels in order to decelerate the train from its operational train speed to a halt. A realistic train model that accounts for the effect of pitching moment arising from the longitudinal inertia effects and wheel adhesion forces is employed. The modified nonlinear Hertz contact theory and Polach adhesive model are employed to account for the normal and tangential wheel-rail contact forces, respectively. The formulation of the governing equations includes the possibility of wheel sliding over the rail. The effects of various factors on the dynamic response of single-railcar train subject to braking, including the DAF in wheel-rail contact force as well as the occurrence of wheel sliding and jumping wheel phenomenon, have been examined. Parameters considered include the magnitude of braking torque, wheel-rail contact condition and initial train speed.

The magnitude of braking torque applied to decelerate a train to bring it to a halt plays an important role in the stability and safety of the train. If the torque is too high, some or all the wheels may slide, which is a cause for concern, as train instability resulting from possible rail derailment may occur. On the other hand, if the torque is too low, no wheel sliding occurs but the resistance to decelerate the train is reduced, leading to a longer braking distance which may exceed the required safe braking distance.

As to be expected, all wheels roll at low braking torque. At a sufficiently high torque, namely the optimal torque, all train wheels are rolling with one at an impending sliding condition. The wheel that is at an impending sliding condition occurs at the trailing wheel. When a train is subject to braking employing the optimal braking torque, the braking distance achieved is the smallest possible. Since there is no wheel sliding and the braking distance is the smallest, the optimal braking torque therefore represents a good compromise between train instability and safety. For braking torque greater than the optimal torque, some or all wheels of the train are in sliding condition. The critical braking torque refers to the smallest braking torque that results in the situation when all wheels are sliding. Braking below the optimal torque may be termed as normal braking. Braking higher than the critical torque may be termed as heavy braking. Braking between optimal and critical torques may be termed as moderately heavy braking.

Besides initial train speed, another important parameter that has a considerable influence on the stability and safety of a train subject to braking is the wheel-rail contact condition, i.e. whether dry or wet. It is found that the contact condition affects the magnitude of the optimal braking torque, being reduced when the contact condition changes from dry to wet. For a given braking torque, the braking distance is increased when the condition changes from dry to wet. Likewise, when the train is subject to braking at their respective optimal torque values for both cases, the braking distance is also increased when the condition changes from dry to wet.

The DAF in the wheel contact force is governed by the initial train speed as well as the magnitude of the applied braking torque. The DAF is found to be always larger at the leading wheel as compared to the trailing wheel when the train is subject to braking. The difference in DAF between trailing and leading wheels is larger for higher initial train speed and also tends to increase as the magnitude of braking torque increases. The braking torque is noted to have a small effect on the DAF in the trailing wheel unlike the leading wheel. Wheel sliding at all wheels occurs when the torque applied is at a certain critical magnitude where it is found that the DAF in contact force at the leading wheel reaches a peak. The critical braking torque depends on the initial train speed, being smaller for higher initial train speed. The braking torque applied should not match the critical torque value as this increases the chance of failure in train structural components due to the development of high DAF in contact force.

CHAPTER 6. MULTIPLE-RAILCAR TRAIN SUBJECT TO BRAKING

6.1 Introduction

In Chapter 5, a computational study on the dynamic response of single-railcar train subject to braking with possible wheel sliding is presented. The train model employed comprises only one railcar, namely the locomotive, modelled as a 15-DOF system of interconnected car body, two bogies and four wheels. As a typical train comprises of several railcars, it is important to investigate the longitudinal interaction between multiple railcars connected by couplers, especially when the train is subject to braking. The relative motion between railcars, known as "slack action", plays a significant effect on the response of the train-track system. During braking, the coupler between consecutive railcars develops cyclical compressive and tensile forces. The maximum compressive force developed in the coupler depends on many factors, such as the coupler stiffness and the coupler gap. Under adverse conditions, the coupler force developed may be large enough to cause failure in the couplers resulting in catastrophic train derailments (Garg and Dukkipati 1984). This chapter presents the results of a study on the dynamics of a multiple-railcar train subject to abrupt braking with allowance for possible wheel sliding.

6.2 Literature review

Multiple-railcar train dynamics, which is defined as the motion of the rolling stock railcars in the direction of the track (Iwnicki 2006), is a subject of critical interests to many researchers. Pugi et al. (2007) developed a simple model of the longitudinal dynamics of a freight train due to normal braking. Vehicles are modeled as simple lumped masses connected by coupling system subject to normal braking. Dhanasekar et al. (2007) studied the longitudinal bogie dynamics of low-speed train under applied braking torque using an experimental method. In this study, controlling braking pressure and its application time were used to evaluate the occurrence of wheel sliding. Ansari et al. (2009) presented a comprehensive parametric study on the longitudinal dynamics of low-speed freight trains subject to traction and braking. The effect of the coupler properties on the dynamic response of a ten-railcar train model was investigated. Recently, Ahmad (2013) developed a dynamic model of a low-speed freight train due to normal braking. A three-railcar train model was used for performing a parametric study to investigate the effect of various factors on the braking distance.

The above-cited research works on multiple-railcar train dynamics are mostly focused on heavy long train model traveling at low-speed over a smooth track subject to normal braking. However, as stated in previous chapters, real train-track systems are likely to have various degrees of railhead roughness. High-speed trains may undergo high deceleration under emergency situations that require the train to come to a halt quickly to avoid other

possible catastrophes. Such trains would then be subject to unplanned abrupt braking with possible detrimental outcomes. Unlike normal braking, when a train decelerates under moderate to heavy braking condition, instability due to train wheels sliding over the rails could occur.

When a multiple-railcar train decelerates due to braking, neighbouring railcars interact with each other due to their relative motion and the coupler gap distance. As a result of this interaction, the force in the train coupler experiences a cyclical change in its magnitude ranging from tension to compression. This interaction between neighbouring railcars may lead to significant spikes in the time history plots of the train deceleration and bogie's pitching motion.

6.3 Problem definition

In this study, the train is assumed to comprise of a locomotive as the leading railcar and several passenger railcars connected to each other through train couplers. The train and track-foundation are coupled through the normal and tangential wheel-rail interactions. The railhead is assumed to have some imperfections which are termed as "track irregularity". The multiple-railcar train is assumed to be cruising at a constant speed and subsequently subject to unplanned abrupt braking causing the train to decelerate to quickly come to a halt.

6.3.1 Train model

A generalized train model comprising of multiple railcars is shown in Figure 6.1. The leading railcar is the locomotive and all others are passenger railcars. The railcars are connected to each other by couplers.

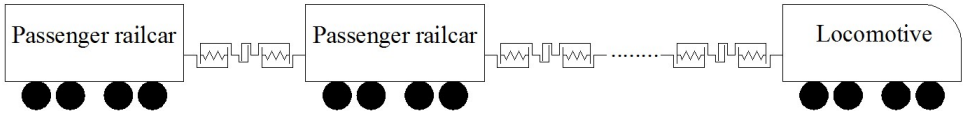

Figure 6.1. A multiple-railcar train.

Each railcar is modelled as a 15-DOF system of interconnected car body, two bogies and four wheels, as shown in Figure 6.2, where m_c and J_c denote the mass and moment of inertia about the pitch of the car body, respectively. The car body is supported through secondary suspensions to two identical bogies. The mass and moment of inertia about the pitch of each bogie are m_b and J_b, respectively. The secondary suspension consists of two spring-damping units, each modelled by a spring k_s and dashpot c_s. The bogies are supported through primary suspensions to the four wheels, each of mass m_w and moment of inertia about the pitch J_w. The primary suspension system consists of four spring-damping units, each comprising a spring k_p and dashpot c_p. The nonlinear Hertz contact force and adhesive force between the i^{th} wheel and rail beam are denoted by F_{ci} and f_i, respectively. The car body is connected to the car bodies of the front and rear railcars by couplers. The coupler forces exerted on the car body at the front and rear are denoted by F_{cf}

and F_{cr}, respectively. The vertical distance between the coupler and the car body's centre of mass is denoted by h_4. The positions of the secondary and primary suspension spring-damping units measured with respect to the centre of mass of car body and the bogies are specified by l_1 and l_2, respectively, as shown in Figure 6.2.

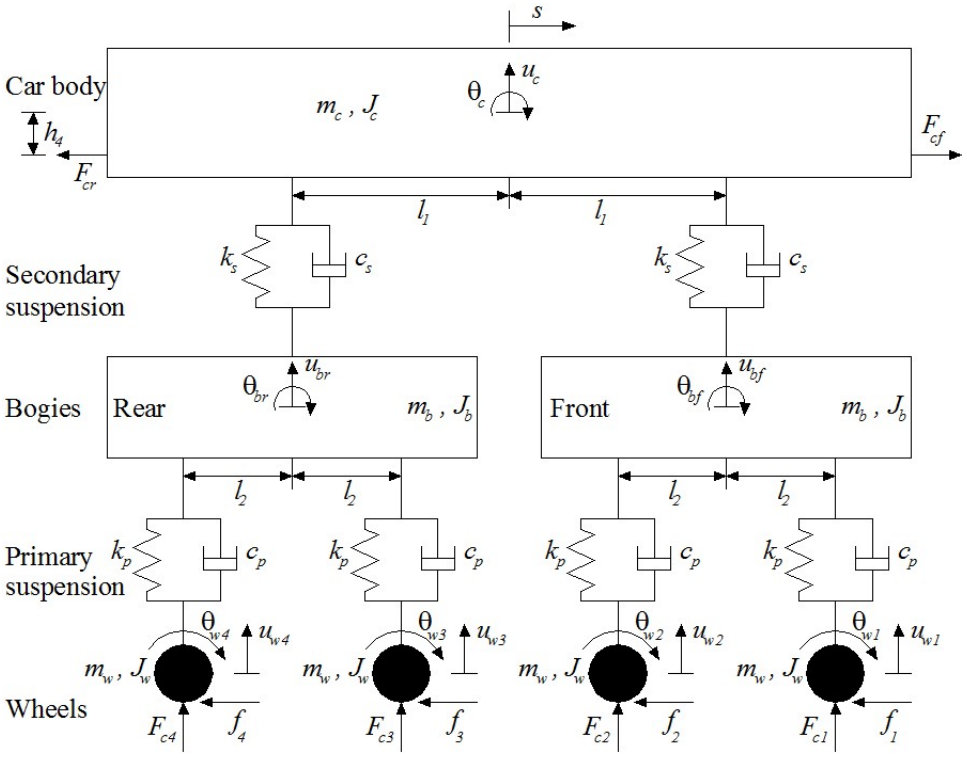

Figure 6.2. A typical railcar model.

The governing equations of the car body, bogies and wheels are similar to Eqs. (5.1) to (5.15) presented earlier for a single-railcar train. For a multiple-railcar train, some of these equations need to be modified to account for the effect of the coupler forces. The set of modified governing equations for a typical railcar may be written as

$$m_c\ddot{u}_c + c_s\left(2\dot{u}_c - \dot{u}_{br} - \dot{u}_{bf}\right) + k_s\left(2u_c - u_{br} - u_{bf}\right) = -m_c g \tag{6.1}$$

$$\begin{aligned} J_c\ddot{\theta}_c + c_s l_1\left(\dot{u}_{bf} + 2l_1\dot{\theta}_c - \dot{u}_{br}\right) + k_s l_1\left(u_{bf} + 2l_1\theta_c - u_{br}\right) + m_c h_1\ddot{s} \\ = -F_r h_1 + \left(F_{cf} - F_{cr}\right)\left(h_1 - h_4\right) \end{aligned} \tag{6.2}$$

$$\begin{aligned} & m_b\ddot{u}_{bf} + c_s\left(\dot{u}_{bf} + l_1\dot{\theta}_c - \dot{u}_c\right) + c_p\left(2\dot{u}_{bf} - \dot{u}_{w2} - \dot{u}_{w1}\right) \\ & + k_s\left(u_{bf} + l_1\theta_c - u_c\right) + k_p\left(2u_{bf} - u_{w2} - u_{w1}\right) = -m_b g \end{aligned} \tag{6.3}$$

$$\begin{aligned} & m_b\ddot{u}_{br} + c_s\left(\dot{u}_{br} - l_1\dot{\theta}_c - \dot{u}_c\right) + c_p\left(2\dot{u}_{br} - \dot{u}_{w4} - \dot{u}_{w3}\right) \\ & + k_s\left(u_{br} - l_1\theta_c - u_c\right) + k_p\left(2u_{br} - u_{w4} - u_{w3}\right) = -m_b g \end{aligned} \tag{6.4}$$

$$\begin{aligned} & J_b\ddot{\theta}_{bf} + c_p l_2\left(\dot{u}_{w1} + 2l_2\dot{\theta}_{bf} - \dot{u}_{w2}\right) + k_p l_2\left(u_{w1} + 2l_2\theta_{bf} - u_{w2}\right) \\ & -\left[2m_w\left(h_2 + h_3\right) + m_b h_2\right]\ddot{s} = \left(f_1 + f_2\right)\left(h_2 + h_3\right) \end{aligned} \tag{6.5}$$

$$\begin{aligned} & J_b\ddot{\theta}_{br} + c_p l_2\left(\dot{u}_{w3} + 2l_2\dot{\theta}_{br} - \dot{u}_{w4}\right) + k_p l_2\left(u_{w3} + 2l_2\theta_{br} - u_{w4}\right) \\ & -\left[2m_w\left(h_2 + h_3\right) + m_b h_2\right]\ddot{s} = \left(f_3 + f_4\right)\left(h_2 + h_3\right) \end{aligned} \tag{6.6}$$

$$m_w\ddot{u}_{w1} + c_p\left(\dot{u}_{w1} + l_2\dot{\theta}_{bf} - \dot{u}_{bf}\right) + k_p\left(u_{w1} + l_2\theta_{bf} - u_{bf}\right) = F_{c1} - m_w g \tag{6.7}$$

$$m_w\ddot{u}_{w2} + c_p\left(\dot{u}_{w2} - l_2\dot{\theta}_{bf} - \dot{u}_{bf}\right) + k_p\left(u_{w2} - l_2\theta_{bf} - u_{bf}\right) = F_{c2} - m_w g \tag{6.8}$$

$$m_w\ddot{u}_{w3} + c_p\left(\dot{u}_{w3} + l_2\dot{\theta}_{br} - \dot{u}_{br}\right) + k_p\left(u_{w3} + l_2\theta_{br} - u_{br}\right) = F_{c3} - m_w g \tag{6.9}$$

$$m_w\ddot{u}_{w4} + c_p\left(\dot{u}_{w4} - l_2\dot{\theta}_{br} - \dot{u}_{br}\right) + k_p\left(u_{w4} - l_2\theta_{br} - u_{br}\right) = F_{c4} - m_w g \tag{6.10}$$

$$J_w\ddot{\theta}_{w1} = f_1 R_w - T_b \tag{6.11}$$

$$J_w\ddot{\theta}_{w2} = f_2 R_w - T_b \tag{6.12}$$

$$J_w\ddot{\theta}_{w3} = f_3 R_w - T_b \tag{6.13}$$

$$J_w\ddot{\theta}_{w4} = f_4 R_w - T_b \tag{6.14}$$

$$\left(m_c + 2m_b + 4m_w\right)\ddot{s} = -\left(F_r + F_{cr} - F_{cf} + \sum_{i=1}^{4} f_i \right) \tag{6.15}$$

where it can be seen that all equations are the same as those in Eqs. (5.1) to (5.15) except for Eqs. (6.2) and (6.15) which have been modified to account for the effect of the coupler forces, F_{cf} and F_{cr}. Note that F_r denotes the total running resistance force acting on car body.

6.3.2 Running resistance

Based on an experimental study by Yang and Sun (2001), the running resistance of high-speed train may be written as

$$R = c_0 + c_v\dot{s} + c_a\dot{s}^2 \tag{6.16}$$

where the coefficients c_0, c_v, c_a are obtained from wind tunnel test. The total running resistance force F_r acting on the car body is obtained by multiplying the running resistance R with the total mass of the railcar $\left(m_c + 2m_b + 4m_w\right)$.

6.3.3 Wheel-rail contact force

Based on the nonlinear Hertz contact model (Esveld 2001), the contact force F_{ci} between the i^{th} wheel and rail may be expressed as

$$F_{ci} = \begin{cases} K_H\left(\Delta y_i\right)^{\frac{3}{2}} & for \quad \Delta y_i \geq 0 \\ 0 & for \quad \Delta y_i < 0 \end{cases} \tag{6.17}$$

where Δy_i denotes the indentation at the contact surface at the i^{th} wheel, which may be expressed as

$$\Delta y_i = y_{ri} + y_{ti} - u_{wi} \tag{6.18}$$

where y_{ri}, y_{ti} denote the vertical displacement of the rail and track irregularity at the i^{th} contact point, respectively, and u_{wi} the vertical displacement of the i^{th} wheel of the railcar. The track irregularity is widely assumed to take the following sinusoidal form (Nielsen and Abrahamsson 1992)

$$y_{ti} = a_t \sin \frac{2\pi x_i}{\lambda_t} \tag{6.19}$$

where a_t and λ_t denote the amplitude and wavelength of track irregularity, respectively.

6.3.4 Wheel-rail adhesion force

The simplified wheel-rail contact model for the adhesion force f_i (Polach 2005) is given by

$$f_i = \frac{2\mu_i F_{ci}}{\pi}\left(\frac{k_A \varepsilon_i}{1+\left(k_A \varepsilon_i\right)^2} + \tan^{-1}\left(k_S \varepsilon_i\right)\right) \tag{6.20}$$

where ε_i is the gradient of tangential stress in the longitudinal direction and k_A, k_S refer to the reduction factors in the adhesion and slip areas, respectively. Based on Kalker's linear theory (Kalker 1967), ε_i may be expressed as

$$\varepsilon_i = \frac{G\pi a_i b_i c_{11}}{4F_{ci}\mu_i} c_{li} \tag{6.21}$$

in which a_i and b_i denote the semi-axes of the contact ellipse at the i^{th} wheel, c_{11} a coefficient from Kalker's linear theory, G the shear modulus of rigidity, μ_i the friction coefficient between the i^{th} wheel and rail given by

$$\mu_i = \mu_0 \left[(1-A) e^{-B\left|\dot{s} - R_w \dot{\theta}_{wi}\right|} + A \right] \tag{6.22}$$

and c_{li} the longitudinal creep at the i^{th} wheel

$$c_{li} = \frac{\left|\dot{s} - R_w \dot{\theta}_{wi}\right|}{\dot{s}} \tag{6.23}$$

In Eq. (6.22), A denotes the ratio of limit friction coefficient μ_∞ at infinity slip velocity to maximum friction coefficient μ_0 at the zero slip velocity and B the coefficient of the exponential friction decrease.

6.3.5 Coupler force

The connection between railcars of a high-speed train comprises of a coupler with slack action, as shown schematically in Figure 6.3. The linkage system between the first passenger railcar and locomotive, termed the first coupler, is shown Figure 6.3(a). Figure 6.3(b) shows the corresponding linkage system between the last passenger railcar and the passenger railcar in front and is termed the last coupler. In these figures, g_{cf}, g_{cr} denote the coupler gap sizes of the first and last couplers, respectively, and s_f, s_r the travels of the front and rear railcars, respectively.

A typical linkage system comprises of a coupler with specified gap size connected at each end to a draft gear. The draft gears are in turn connected to

the respective ends of neighbouring railcars. Should the relative motion between railcars be large enough to cause the closure of the coupler, longitudinal forces are transmitted through the draft gears to the railcars. Note that the coupler could close in the positive or negative sense. Consequently, the force in the coupler could be compressive or tensile. If the relative motion between railcars is not large enough to cause closure of the coupler, then no coupler force is produced and hence the railcars do not interact longitudinally.

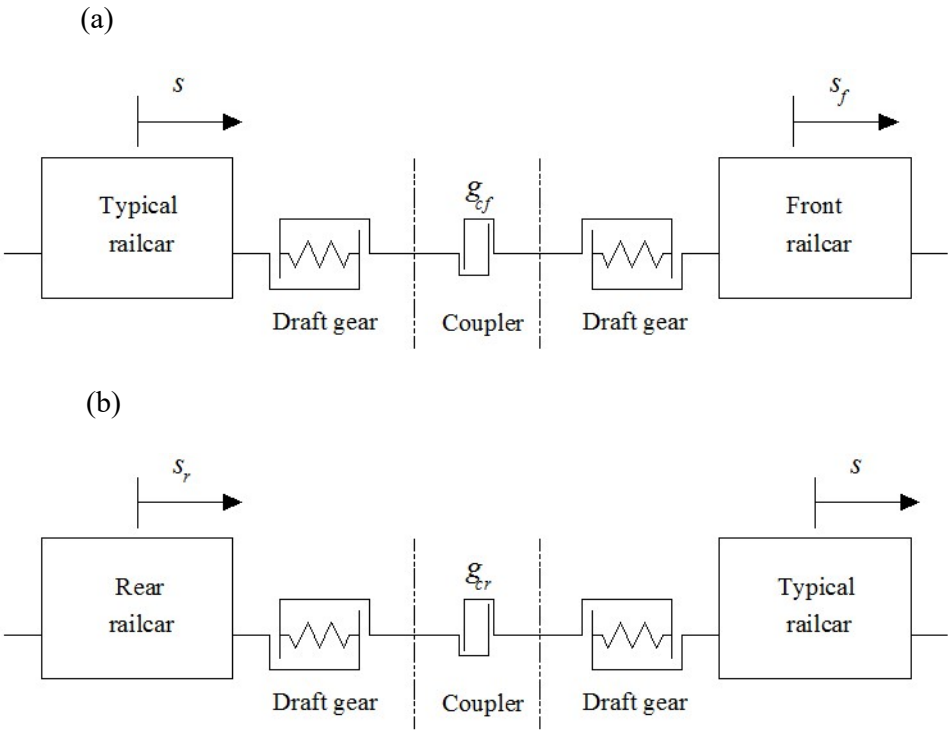

Figure 6.3. Linkage systems between: (a) Typical and front railcars; and (b) Rear and typical railcars.

To simplify the calculations, the coupler is assumed as a spring and damper with considering the effect of slack action. Thus, the coupler forces F_{cf} and F_{cr} may be written as

$$F_{cf} = \begin{cases} c_{cf}\left(\dot{s}_f - \dot{s}\right) + k_{cf}\left(s_f - s\right) & \text{if} \quad s - s_f \le 0 \\ 0 & \text{if} \quad s - s_f \le g_{cf} \\ c_{cf}\left(\dot{s}_f - \dot{s}\right) + k_{cf}\left(s_f - s + g_{cf}\right) & \text{if} \quad s - s_f > g_{cf} \end{cases} \tag{6.24}$$

$$F_{cr} = \begin{cases} c_{cr}\left(\dot{s} - \dot{s}_r\right) + k_{cr}\left(s - s_r\right) & \text{if} \quad s_r - s \le 0 \\ 0 & \text{if} \quad s_r - s \le g_{cr} \\ c_{cr}\left(\dot{s} - \dot{s}_r\right) + k_{cr}\left(s - s_r + g_{cr}\right) & \text{if} \quad s_r - s > g_{cr} \end{cases} \tag{6.25}$$

where c_{cf}, k_{cf} denote the damping and stiffness of the coupler between the typical railcar and front neighbouring railcar, respectively; c_{cr}, k_{cr} the corresponding properties of the coupler between the typical railcar and rear neighbouring railcar. Note that for the locomotive, $F_{cf} = 0$ in view that there is no railcar connected ahead of the locomotive. Similarly, for the last passenger railcar, $F_{cr} = 0$ in view that there is no railcar connected at its rear.

6.3.6 Track-foundation model

The track is modeled as an infinite Euler-Bernoulli beam resting on a two-parameter elastic damped foundation. The beam is subject to the typical wheel-rail contact forces F_{ci}, as illustrated in Figure 6.4. The track-foundation is discretized into finite moving elements, in which the formulation of the element equations are based on adopting a convected coordinate r-axis with origin fixed at the centre of mass of the car body, as shown in Figure 6.4. Based on Eq. (2.12), the differential governing equation of motion of the track-foundation may be rewritten as

$$EI\frac{\partial^4 y}{\partial x^4}+\phi EI\frac{\partial^4 \dot{y}}{\partial x^4}-\lambda\frac{\partial^2 \dot{y}}{\partial x^2}-k_{sm}\frac{\partial^2 y}{\partial x^2}+m\ddot{y}+\alpha\dot{y}+ky=-\sum_{i=1}^{4}F_{ci}\delta\left(x-s-r_i\right) \quad (6.26)$$

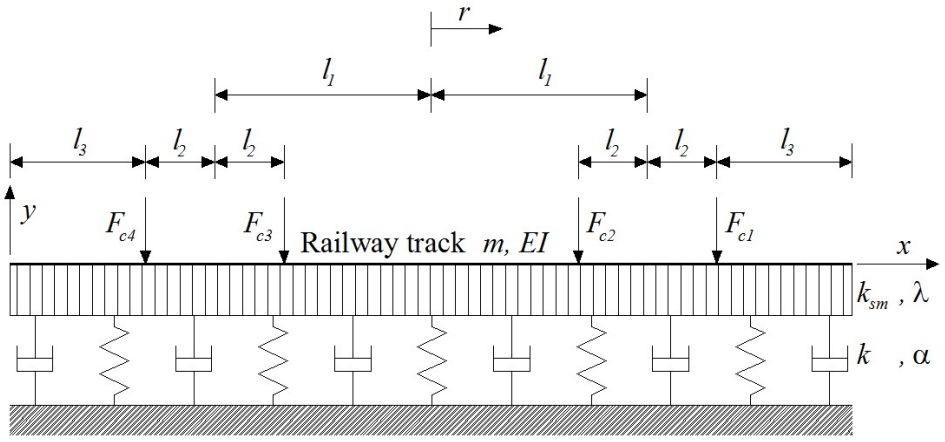

Figure 6.4. Track-foundation model.

6.4 Proposed computational technique

The relationship of the fixed and the moving coordinate system r is given by

$$r=x-s \quad (6.27)$$

In view of Eq. (6.27), Eq. (6.26) may be rewritten as

$$\begin{aligned}&EI\frac{\partial^4 y}{\partial r^4}+\phi EI\frac{\partial^4}{\partial r^4}\left(\dot{y}-\dot{s}\frac{\partial y}{\partial r}\right)-\lambda\frac{\partial^2}{\partial r^2}\left(\dot{y}-\dot{s}\frac{\partial y}{\partial r}\right)-k_{sm}\frac{\partial^2 y}{\partial r^2}\\&+m\left(\dot{s}^2\frac{\partial^2 y}{\partial r^2}-2\dot{s}\frac{\partial \dot{y}}{\partial r}-\ddot{s}\frac{\partial y}{\partial r}+\ddot{y}\right)+\alpha\left(\dot{y}-\dot{s}\frac{\partial y}{\partial r}\right)+ky=-\sum_{i=1}^{4}F_{ci}\delta\left(r-r_i\right)\end{aligned} \quad (6.28)$$

By adopting Galerkin's approach, the element mass $\mathbf{M}_e$, damping $\mathbf{C}_e$ and stiffness $\mathbf{K}_e$ matrices for a typical moving element of length L can be proposed:

$$\mathbf{M}_e=m\int_0^L \mathbf{N}^{\mathrm{T}}\mathbf{N}\,\mathrm{d}r \quad (6.29)$$

$$\mathbf{C}_e = \phi EI\int_0^L \mathbf{N}_{,rr}^{\mathrm{T}}\mathbf{N}_{,rr}\,\mathrm{d}r + \lambda\int_0^L \mathbf{N}_{,r}^{\mathrm{T}}\mathbf{N}_{,r}\,\mathrm{d}r - 2m\dot{s}\int_0^L \mathbf{N}^{\mathrm{T}}\mathbf{N}_{,r}\,\mathrm{d}r + \alpha\int_0^L \mathbf{N}^{\mathrm{T}}\mathbf{N}\,\mathrm{d}r \tag{6.30}$$

$$\begin{aligned}\mathbf{K}_e = {} & EI\int_0^L \mathbf{N}_{,rr}^{\mathrm{T}}\mathbf{N}_{,rr}\,\mathrm{d}r - \dot{s}\lambda\int_0^L \mathbf{N}_{,r}^{\mathrm{T}}\mathbf{N}_{,rr}\,\mathrm{d}r - \dot{s}\phi EI\int_0^L \mathbf{N}_{,rr}^{\mathrm{T}}\mathbf{N}_{,rrr}\,\mathrm{d}r \\ & -\left(m\dot{s}^2 - k_{sm}\right)\int_0^L \mathbf{N}_{,r}^{\mathrm{T}}\mathbf{N}_{,r}\,\mathrm{d}r - \left(m\ddot{s} + \alpha\dot{s}\right)\int_0^L \mathbf{N}^{\mathrm{T}}\mathbf{N}_{,r}\,\mathrm{d}r + k\int_0^L \mathbf{N}^{\mathrm{T}}\mathbf{N}\,\mathrm{d}r\end{aligned} \tag{6.31}$$

where $\mathbf{N}$ is the shape function based on Hermitian cubic polynomials; $(\ )_{,r}$ denotes partial derivative with respect to r.

By assembling the element matrices, the equation of motion for a typical railcar-track-foundation model can be written as

$$\mathbf{M}_j\ddot{\mathbf{z}}_j + \mathbf{C}_j\dot{\mathbf{z}}_j + \mathbf{K}_j\mathbf{z}_j = \mathbf{F}_j \tag{6.32}$$

where $\mathbf{z}_j$ denote the assembled displacement vector; $\mathbf{M}_j$, $\mathbf{C}_j$ and $\mathbf{K}_j$ the assembled mass, damping and stiffness matrices, respectively; and $\mathbf{F}_j$ the assembled load vector. Note that the index j denotes the relative order of the railcar in a multiple-railcar train. For a train comprising of N railcars, $j=1$ refers to the last passenger railcar, $j=N-1$ the first passenger railcar just before the locomotive and $j=N$ refers to the locomotive. The governing equation of the train-track-foundation is obtained by assembling Eq. (6.32) as follows

$$\mathbf{M}\ddot{\mathbf{z}} + \mathbf{C}\dot{\mathbf{z}} + \mathbf{K}\mathbf{z} = \mathbf{F} \tag{6.33}$$

where $\mathbf{M}$, $\mathbf{C}$, $\mathbf{K}$ the global mass, damping, stiffness matrices, $\mathbf{F}$ the global generalized load vector, and $\mathbf{z}$ the global displacement vector are assembled as follows

$$\mathbf{M} = \sum_{j=1}^{N} \mathbf{M}_j \tag{6.34}$$

$$\mathbf{C} = \sum_{j=1}^{N} \mathbf{C}_j \tag{6.35}$$

$$\mathbf{K} = \sum_{j=1}^{N} \mathbf{K}_j \tag{6.36}$$

$$\mathbf{F} = \sum_{j=1}^{N} \mathbf{F}_j \tag{6.37}$$

$$\mathbf{z} = \sum_{j=1}^{N} \mathbf{z}_j \tag{6.38}$$

The equation of motion of the multiple-railcar HSR in Eq. (6.33) can be solved by using Newmark's constant acceleration method (Bathe 1996).

Two computational schemes, one implicit and the other explicit, to treat the nonlinear normal wheel-rail contact force were discussed and presented in Chapter 4. It may be recalled that the implicit scheme is simpler to implement but restricted only to simple train models. The other explicit scheme is more complicated and requires generally more computational effort but needs to be employed when dealing with more complicated train models. Where braking is involved, there is the additional complication arising from the nonlinear wheel-rail adhesion force. In the study on single-railcar train subject to braking presented in Chapter 5, it was explained that it is necessary to employ the explicit scheme in dealing with the nonlinear wheel-rail normal contact and adhesion forces. In the study on multiple-railcar train subject to braking,

the complexity of the train model adopted is further increased and it is therefore necessary to employ the explicit scheme.

6.5 Verification of results

As there are no available results in the literature on the dynamic response of high-speed multiple-railcar train subject to braking, the effectiveness and accuracy of the proposed MEM are verified through comparison with results obtained via the FEM. A FEM code was written that is matched in capability as the MEM code. As previously explained, the FEM code is not suited to solving problems involving moving loads. The computational effort required by the FEM is significantly higher than the MEM.

For the purpose of verification, the case of a two-railcar train comprising of a locomotive and a passenger railcar is considered. The two railcars are connected to each other by a coupler. The stiffness and damping property of the coupler are 0.605×10^{8} N m^{-1} and 0.605×10^{6} N s m$^{-1,}$ respectively, and the coupler gap is 0.04 m (Chou et al. 2007). The train is assumed to be cruising at 70 m s^{-1} before braking torques T_b of 25 kN m are applied at all the wheels of the train. The properties of track-foundation are summarized in Table 3.1 and the parameters associated with the locomotive are given in Table 5.1. Note that all parameters related to the passenger railcar are taken to be the same with the locomotive except for only the mass of the car body, which is lighter and taken to be $m_c = 20875$ kg (Wu et al. 2001). The wheel-rail contact

condition is assumed to be dry. The degree of severity of track irregularity is assumed to be moderate, with the irregularity amplitude and wavelength equal to 1.5 mm and 4 m, respectively. The coefficients c_0, c_v, c_a used to compute the resistance force in Eq. (6.16) are 1176×10^{-5} N kg^{-1}, 77.616×10^{-5} N s m^{-1} kg^{-1} and 1.6×10^{-5} N s^2 m^{-2} kg^{-1} (Yang and Sun 1999), respectively.

In the FEM model, a sufficiently long segment of the railway track is discretized uniformly with 0.25 m size elements, which has been found to be adequately small enough to attain converged accurate results. The segment may be divided into three sub-portions, a central portion and two end portions. The central portion, where the train travels during the period considered, is taken to be 140.5 m. The central portion is padded by two end portions of sufficient length in order to mitigate the erroneous boundary effects due to the moving train load approaching the boundaries of the FEM model. Through a convergence study, the length of the end portions is taken to be 24 m. Due to the advantage enjoyed by the MEM in dealing with moving load problems, a relatively shorter segment is required. Also from a convergence study made, the length required for the truncated railway track in the MEM model is 95 m that is discretized non-uniformly with elements ranging from a coarse 1 m to a more refined 0.25 m size.

Figures 6.5(a) and (b) show the rail displacement profiles predicted by FEM and MEM in the vicinity of the wheel-rail contact point at the instants 0.5 s and 1.0 s after the application of wheel brakes, respectively. Note that there is no occurrence of wheel sliding at the first instance. At the second

instant, wheel sliding have been found to occur at all wheels. As can be seen in Figure 6.5, both results are virtually the same. In view that the FEM requires a longer domain length as compared to the MEM, it is not surprising that the computational time required is 11.5 times higher than that needed in the MEM using a desktop computer (Intel(R) Core(TM) i7-2600 CPU @3.40GHz 3.40GHz), with a memory usage of 16.0 GB". This comparison study clearly illustrated that the MEM is accurate as well as computationally efficient and is thus superior to the FEM for dealing with the dynamic response of multiple-railcar HSRs subject to braking.

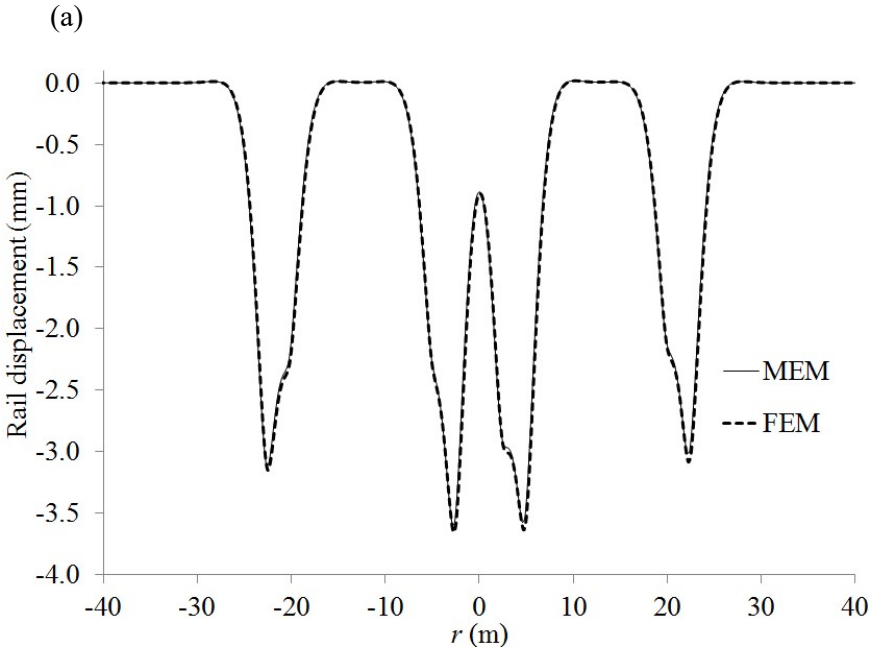

(b)

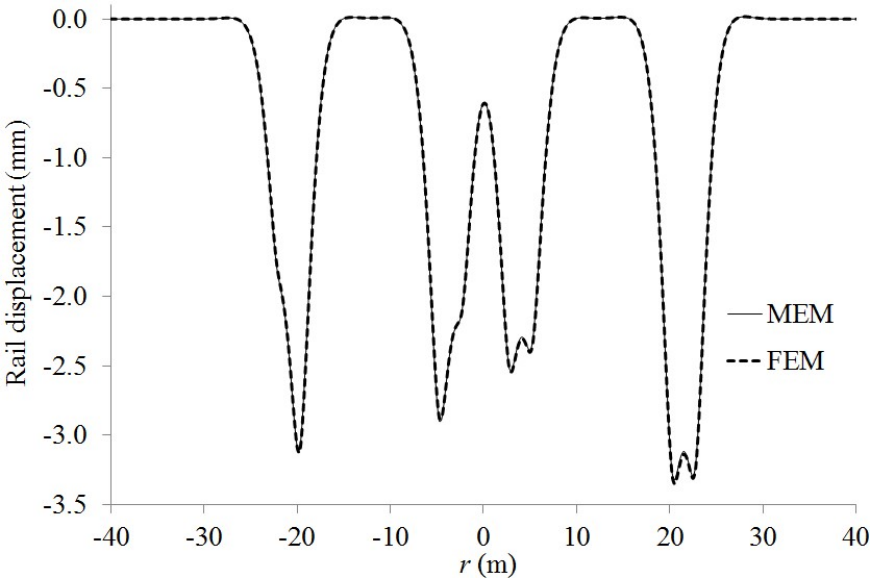

Figure 6.5. Comparison of rail displacement profiles at the instants: (a) 0.5 s and (b) 1.0 s, after the application of wheel brakes.

6.6 Numerical results

Numerical results obtained by the proposed MEM investigating the dynamic response of multiple-railcar train are presented and discussed in this section. For all cases investigated, the train comprises of several railcars of which the leading one is the locomotive and the others are passenger railcars. Neighbouring railcars are connected to each by coupler. The track irregularity is assumed to be moderate and taken to be the same in all cases investigated.

A realistic high-speed train would typically comprise of the locomotive and approximately fourteen passenger railcars (Chen and Li 2000). It seldom operates with less than two passenger railcars even under off-peak periods. Computational effort increases with the number of railcars. Thus, it would be useful to investigate the minimum number of railcars that would result in

similar dynamic response. The conclusion from this case study would then dictate the number of railcars to be employed for subsequent case studies. The effects of various parameters, such as braking torque, coupler stiffness, coupler gap, wheel load, wheel-rail contact condition, initial train speed and partial failure in braking mechanism on the dynamics of multiple-railcar HSR subject to braking are investigated and presented.

6.6.1 Representation of a multiple-railcar train

Before investigating the effects of multiple railcars on the dynamics of the HSR, it would be useful to investigate what is the minimum number of railcars that can safely represent a multiple-railcar train as this would result in great computational savings. The minimum number of railcars is one in which the dynamic response produced would be virtually the same as that produced for trains with more than the minimum number of railcars. For this purpose, three trains with different number of railcars are considered. The three are designated as 2-, 3-, 4-railcar trains, which comprises the locomotive and 1, 2, 3 additional passenger railcars, respectively. The lengths of the truncated railway track used in the MEM models of these trains are 95 m, 120 m and 145 m for the 2-, 3-, 4-railcar trains, respectively. The train is assumed to be cruising at 70 m s^{-1}, a typical speed of today's high-speed trains, before braking torques T_b of 13 kN m are applied at all the wheels of the train. At this magnitude of braking torque, sliding of wheels over the track is expected

to occur. The properties of the couplers connecting neighbouring railcars employed in the study are presented in Table 6.1 (Chou et al. 2007).

Table 6.1. The parameters of the couplers.

The coupler	Stiffness (N m^{-1})	Damping (N s m^{-1})	Gap (m)
Between locomotive and 1st passenger railcar	0.605×10^{8}	0.605×10^{6}	0.04
Between passenger railcars	0.245×10^{8}	0.245×10^{6}	0.04

Figures 6.6(a), (b) and (c) show the time history plots of the coupler force between the locomotive and 1st railcar, the acceleration/deceleration and bogie's pitching motion of the locomotive, respectively, for the three multiple-railcar trains considered. It also can be seen in Figure 6.6 that the responses of the 3- and 4-railcar trains are virtually the same, and differs from those of the 2-railcar train. The minimum number of railcars is thus 3. It is not surprising that the computational time required for the analysis of the 4-railcar train is significantly higher than that needed for the 3-railcar train. In view of this finding, it is adequate to investigate a realistic multiple-railcar train using only a 3-railcar train. Thus, subsequent studies on multiple-railcar train will be based on a 3-railcar train.

(a)

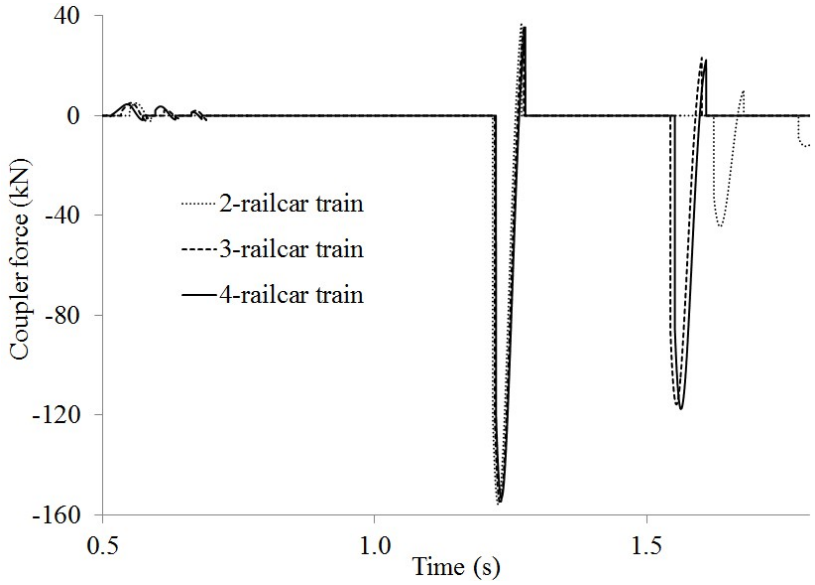
40
0
-40
-80
-120
-160
Coupler force (kN)
2-railcar train
3-railcar train
4-railcar train
0.5
1.0
1.5
Time (s)

(b)

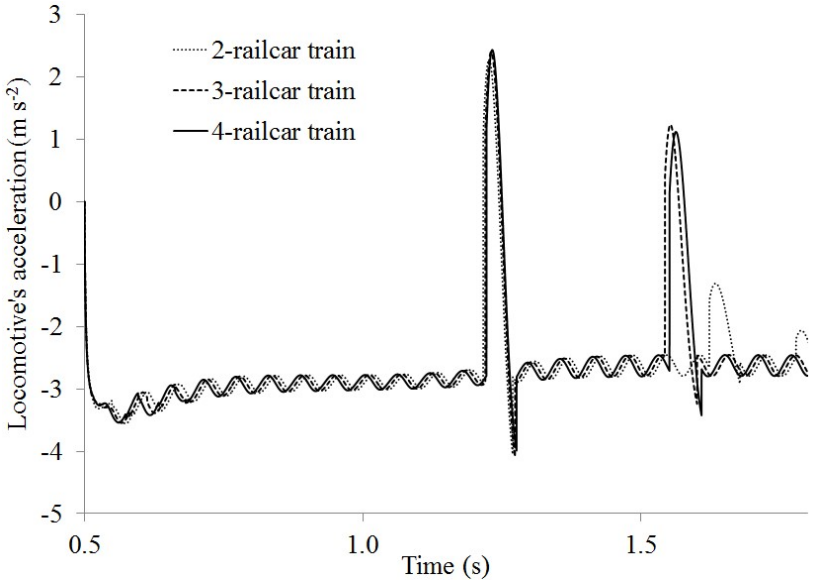
3
2
1
0
-1
-2
-3
-4
-5
Locomotive's acceleration (m s-2)
2-railcar train
3-railcar train
4-railcar train
0.5
1.0
1.5
Time (s)

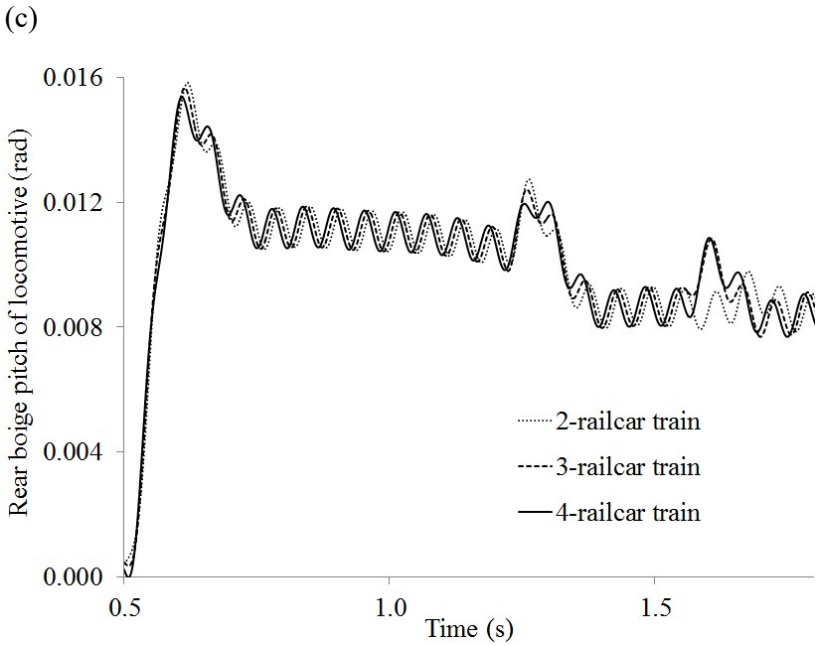

Figure 6.6. Time history for various train models of: (a) Coupler force; (b) Train deceleration and (c) Rear bogie pitch.

6.6.2 Single-railcar train vs. multiple-railcar train

Passenger railcars are expected to be lighter in weight, even when fully loaded with passengers, as compared to the locomotive which houses heavy engine and machineries. Consequently during braking, passenger railcars and the locomotive experience different magnitude of deceleration when the same magnitude of braking torque is applied to all wheels. Due to the difference in speeds of the passenger railcars and locomotive, there will be longitudinal interaction between railcars during the braking of a multiple-railcar train. The longitudinal interaction has a significant effect on the longitudinal and vertical responses of the multiple-railcar train. In order to understand the impact of the longitudinal interaction on the dynamic response of a multiple-railcar train, a

parametric study is carried out and the response is compared to the simple single-railcar train, where inherently there is no longitudinal interaction effect.

As already presented earlier in the preceding section, a multiple-railcar train shall comprise of three railcars, of which two are passenger railcars and the third is the locomotive. All train parameters, track foundation properties, coupler properties, track irregularity parameters, initial train speed and braking torque used for the parametric study are the same as described in the preceding section, unless otherwise stated.

Figures 6.7(a) and (b) show the time history plots of the acceleration and rear bogie's pitch motion of the locomotive, respectively, for both the single-railcar and multiple-railcar trains. After the application of brakes, the deceleration of the locomotive is nearly the same in both single- and multiple-railcar train initially. At a short time later, there is a significant increase in the acceleration of the locomotive of the multple-railcar train due to the development of large compressive coupler force acting on the locomotive when the relative motion between the neighbouring passenger railcar and locomotive results is larger than the coupler gap. The longitudinal interaction continues throughout the period of braking, during which the force in the train coupler experiences a cyclical change in its magnitude ranging from tension to compression. Thus, as can be seen in Fig. 6(a), there is periodical spiking in the acceleration of the locomotive which occurs whenever the relative motion between railcars results in the development of coupler force. The amplitude of the spikes decreases with time and finally disappears after a sufficient period

of braking. Obviously, there is no occurrence of acceleration spikes for the single-railcar train.

A similar occurrence of spikes is found for the pitching motion of the rear bogie of the locomotive, as can be seen from Fig. 6(b). Though not presented, the response of the passenger railcar is expected to be similar to that of the locomotive. Consequently, the comfort of passengers is expected to be affected by the occurrence of spikes due to the longitudinal interaction.

(a)

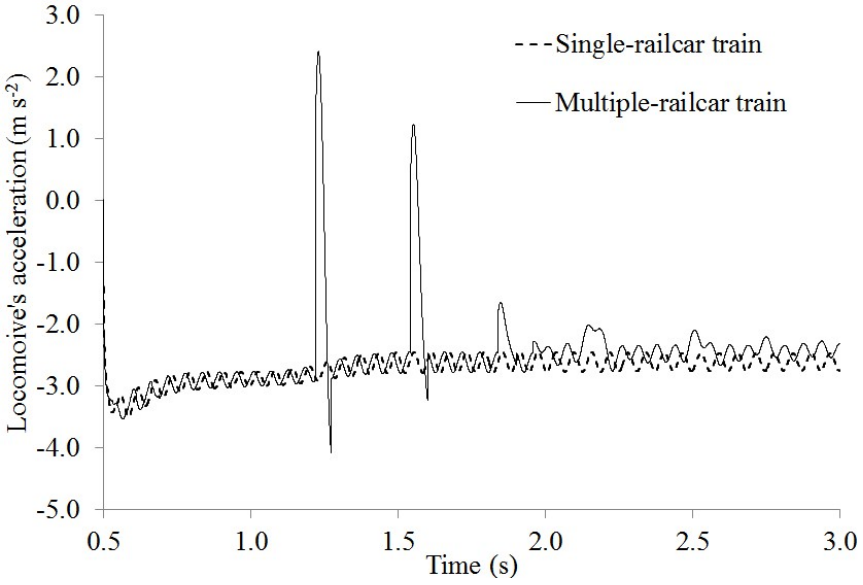

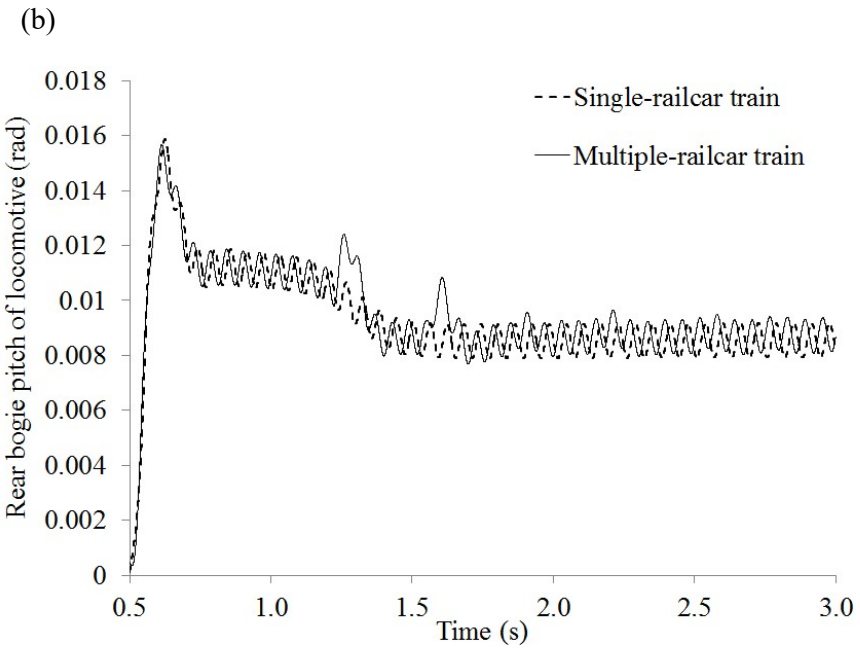

Figure 6.7. Time histories of (a) the locomotive's acceleration and (b) Rear bogie pitch of the locomotive.

Besides the longitudinal response, the longitudinal interaction between railcars may also have an effect on the vertical dynamic response of a multiple-railcar train subject to braking. Figures 6.8(a) and (b) show the time history plots of wheel-rail contact forces at the trailing and leading wheels of the locomotive for both single- and multiple-railcar trains. At the instant of time when there is occurrence of the first most significant spike in the locomotive's deceleration, it was found that the wheel-rail contact forces in the trailing and leading wheels are approximately 6.75% smaller and 3.75% larger, respectively, for a multiple-railcar train as compared to a single-railcar train. It may therefore be concluded that the longitudinal interaction between railcars does not result in a significant but nonetheless noticeable effect on the vertical dynamic response.

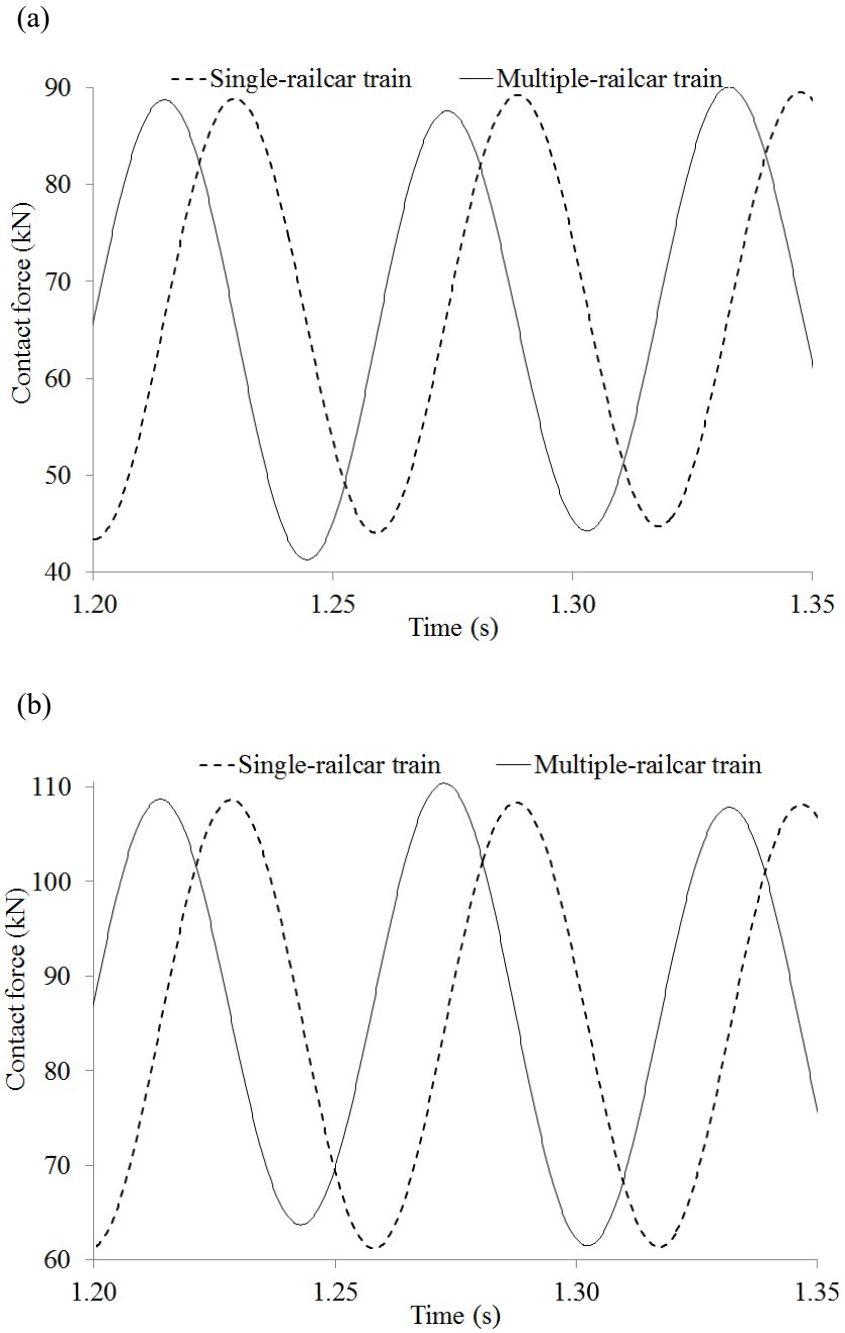

Figure 6.8. Time history of contact force in (a) the trailing wheel and (b) the leading wheel.

6.6.3 Effect of braking torque

In the study on single-railcar train subject to braking, which was presented in Chapter 5, it was found that there is an optimal and critical braking torque. The former refers to the maximum braking torque that can be applied without causing any of the wheels to slide, with one wheel at impending sliding condition. The braking distance of the train is minimal when the braking torque applied is at the optimal magnitude. The critical braking torque refers to the smallest torque that would result in all trains wheels to be sliding. Both the optimal and critical braking torques are dependent on the initial train speed. For a given initial train speed of 70 m s^{-1} and track irregularity considered, the study in Chapter 5 found that the optimal and critical braking torques are 10.0 kN m and 13.5 kN m, respectively. In view of the significance of the optimal and critical braking torques on the braking dynamics of the train, it is thus necessary to determine these corresponding torques for the multiple-railcar train.

Table 6.2 shows the optimal and critical torques for both single-railcar and multiple-railcar trains. As can be seen, the critical braking torque for the locomotive of the single- and multiple-railcar trains is the same. This is also true for the optimal braking torque. The critical braking torque for the two passenger railcars of the multiple-railcar train is the same and is about 7.4% lower than that of the locomotive. Similarly, the optimal braking torque for the two passenger railcars is also the same and is about 5.0% lower than that of the locomotive. It may therefore be concluded that the longitudinal interaction

between neighboring railcars has virtually no effect on the magnitude of the critical and optimal braking torques. The difference noted between passenger railcar and locomotive is due to the difference in mass of these two types of railcars.

Table 6.2. Optimal and critical torques

Torques (kN m)	Single-railcar train	Multiple-railcar train		
		2^{nd} railcar	1^{st} railcar	Locomotive
Optimal	10.0	9.5	9.5	10.0
Critical	13.5	12.5	12.5	13.5

The occurrence of sliding of wheels over rails may be affected by the longitudinal interaction between neighboring railcars. Figures 6.9(a) and (b) show the duration of wheel-sliding Δt_s of the trailing and leading wheels of the locomotive, respectively, plotted against the applied braking torque for both single- and multiple-railcar trains. As can be seen in Figure 6.9, there is virtually no difference in the period of wheel sliding for both trains for most values of applied braking torque. There is only some noticeable difference in the case of the trailing wheel when the magnitude of the braking torque is between the optimal and critical braking torques. It may be concluded that there appears to be negligible effect by the longitudinal interaction, which occurs in a multiple-railcar train, on the duration of wheel sliding. Only when the applied braking torque lies between the optimal and critical torques, the longitudinal interaction results in a noticeable increase in the duration of wheel sliding for the trailing wheel.

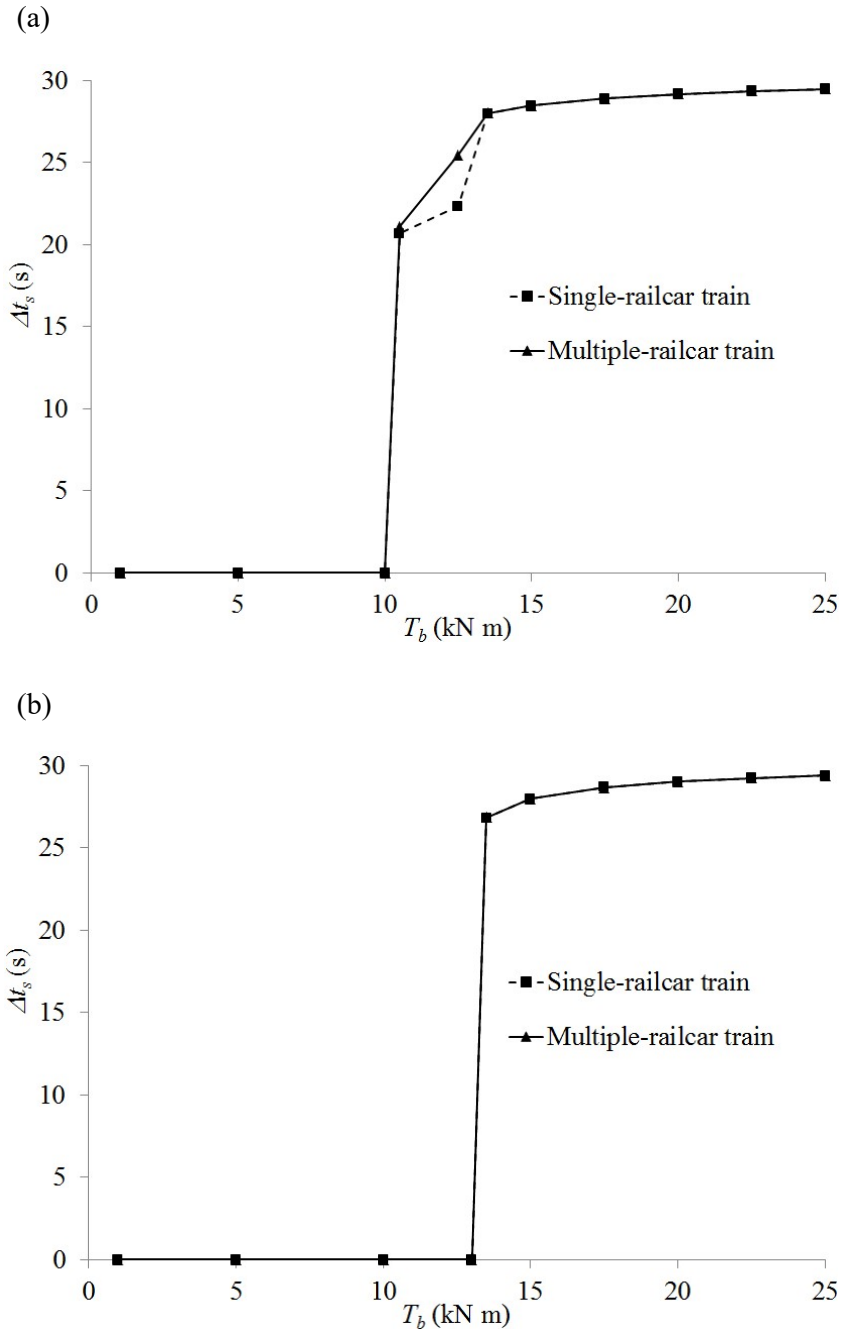

Figure 6.9. Comparison of duration of wheel-sliding in: (a) the trailing wheel and (b) the leading wheel.

The longitudinal interaction between neighboring railcars would induce force in the train coupler, which fluctuates between tension and compression

cyclically. The degree of interaction is obviously dependent on the magnitude of the applied braking torque as well as the relative masses of the connecting railcars. Since the masses between the two passenger railcars are the same, the dynamic motions of these railcars are expected to be virtually the same during braking. On the other hand, the mass of the locomotive is larger than the passenger railcar. Consequently, the dynamic motions of the locomotive and the first passenger railcar are different resulting in significant longitudinal interaction. In view that the coupler force is expected to be significantly higher in the train coupler between locomotive and the first passenger railcar than that between the two passenger railcars, results will only be presented for former.

Figure 6.10 presents the variation of the maximum tensile and compressive coupler forces plotted against the braking torque. It can be seen that the train coupler tends to experience higher magnitudes of compressive force than tensile force. The peak value of compressive coupler force is found to be approximately 4 times larger than that of tensile coupler force. Consequently, coupler tends to fail in compression than in tension when a train is subject to braking.

It can be seen from Figure 6.10 that there is virtually no force induced in the train coupler when the applied braking torque is smaller than the optimal value. When the braking torque is increased beyond the optimal torque, the force induced in the coupler increases significantly and reaches a peak at the torque of 13.0 kN m, which lies between the critical braking torques of the

locomotive and passenger railcar. The coupler force reduces sharply thereafter when the braking torque is increased further and stays virtually zero when the torque is higher than approximately 18.0 kN m.

When the braking torque applied is smaller than the passenger railcar's optimal torque, all wheels of the entire train tend to roll till the train comes to a halt. Under such a situation, the maximum relative motion between neighboring railcars is smaller than the coupler gap, resulting in zero force in the coupler. When the braking torque is increased beyond further into the range of moderate braking, the motions of the passenger railcar and locomotive become distinctly different. This occurs because the number of wheels sliding or rolling depends on the weight of the railcar as well as the braking torque. The passenger railcar with smaller weight tends to travel faster than the locomotive due to more wheels in sliding condition, resulting in relative motions between passenger railcar and locomotive that are larger than the coupler gap and inducement of high coupler force.

When the torque is increased further into the heavy braking range, all wheels of the entire train are in sliding condition. The train decelerates at a high magnitude and the speed of the train reduces rapidly. Due to decreased speed, the relative motion between railcars is also reduced and this leads to lesser longitudinal interaction and smaller coupler force. At a torque larger than approximately 18 kN m, there is apparently no more longitudinal interaction as the relative motion between railcars has reduced to a level smaller than the coupler gap.

Based on findings in the previous chapter as well as results presented in Fig. 6.10, it may be concluded that the braking torque should be applied at the optimal torque value. A train subject to braking at a torque equal to the optimal torque leads to the best safety in terms of smallest braking distance as well as ensuring structural stability and strength as there is no occurrence of wheel sliding and almost zero force in the train coupler. If the braking torque is applied unfortunately at a magnitude equal to the critical torque, the train coupler would experience peak compressive and tensile forces. There is therefore concern for the possible fatigue failure of the train coupler. Furthermore, all wheels of the train are in sliding motion almost throughout the period of deceleration. There is therefore additional unease over the overall stability of the train due to heightened chance of train derailment, especially if accompanied with occurrences of jumping wheel phenomenon.

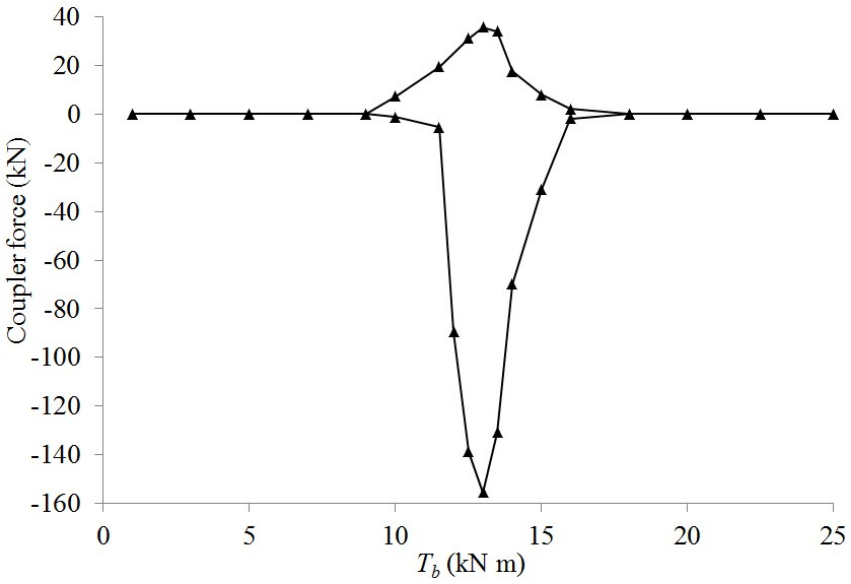

Figure 6.10. Effect of braking torque on the coupler force.

6.6.4 Effects of coupler stiffness and coupler gap

In railway engineering, slack action is the amount of free movement of one car before it transmits its motion to an adjoining coupled car. This free movement results from the fact that in railroad practice cars are loosely coupled. Loose coupling is necessary to enable the train to bend around curves and is an aid in starting trains, since the application of the locomotive power to the train operates on each car in the train successively, and the power is thus utilized to start only one car at a time. This explains why there is a need for a coupler gap. The design of the coupler gap size constitutes an important component for the practical and safe operation of the train.

In the previous section, it was also found that the coupler tends to experience higher magnitudes in compression than in tension. Furthermore, peak values of coupler force are experienced when the braking torque applied is equal to the critical torque value. The longitudinal interaction between the locomotive and first passenger railcar is also much more significant as compared between the first and second passenger railcars. Thus, results of parametric studies in subsequent sections will focus only on the coupler peak compressive force in the coupler between the locomotive and first passenger railcar due to train braking at the critical torque. As previously explained, the longitudinal interaction between railcars is dependent on the relative motion of the railcars, the coupler gap as well as the coupler stiffness. Thus, this section will investigate the influence of these key factors, namely the coupler stiffness

and coupler gap, on the coupler compressive force when a multiple-railcar train is subject to braking.

For the purpose of investigating the effect of coupler stiffness, a series of values that are in the vicinity of the practical range (Chou et al. 2007) is considered. In the literature, the damping property of the coupler is taken to be proportional to the stiffness [Chou et al. (2007); Zhuan and Xia (2006)]. Table 6.3 summarizes the range of coupler stiffness and corresponding coupler damping that is considered in the parametric study. The magnitude of the coupler gap ranges from 5 mm to 40 mm, which are also within the practical range. The special case where the gap is 0 mm is also considered. This special case is considered only for the purpose of comparison, as in reality, the coupler gap is always greater than 0 mm.

Table 6.3. Properties of couplers.

Cases	Coupler between locomotive and 1st passenger railcar		Couplers between passenger railcars	
	Stiffness $\times 10^7$ (N m^{-1})	Damping $\times 10^5$ (N s m^{-1})	Stiffness $\times 10^7$ (N m^{-1})	Damping $\times 10^5$ (N s m^{-1})
1	3.90	3.90	1.47	1.47
2	6.05	6.05	2.45	2.45
3	8.00	8.00	3.20	3.20
4	10.00	10.00	4.00	4.00
5	12.00	12.00	4.80	4.80
6	14.00	14.00	5.60	5.60
7	16.00	16.00	6.40	6.40
8	18.00	18.00	7.20	7.20

Figures 6.11(a) and (b) show the variation of the maximum spike in locomotive's acceleration and compressive coupler force, respectively, plotted against the coupler stiffness for various coupler gaps. When the coupler stiffness is increased, the maximum spike in acceleration and coupler force

also increases. The rate of increase is dependent on the size of the coupler gap, being higher for larger gap size and vice-versa. When the coupler gap is unrealistically 0 mm, there is no spike in the locomotive's deceleration and coupler force since there is no longitudinal interaction between railcars. This trend is to be expected since the effects of the coupler stiffness and gap both tend to amplify the effect of longitudinal interaction between railcars. Note that for certain range of values of coupler stiffness and gap, the maximum spike in locomotive's acceleration could be positive or negative. For the case of small coupler gap of 5 mm, the momentary increase in locomotive's acceleration due to longitudinal interaction between railcars is not large enough to cause the maximum spike to be in the positive range for all coupler stiffness considered.

Passenger safety becomes an issue when the acceleration/spike levels require passengers to take one or more steps to retain balance (Powell and Palacín 2015). Iwnicki (2006) as well as Powell and Palacín (2015) have recommended that the maximum acceleration of high-speed railcar under emergency braking be limited to 3 m s^{-2} in view of passenger comfort. In view of this recommendation, Figure 6.12 (a) shows that the stiffness of the coupler should not exceed a critical value. The critical stiffness depends on the coupler gap size, being smaller for larger gap size. For coupler gaps of 20 mm and 40 mm, these critical values are approximately 12×10^7 N m^{-1} and 8×10^7 N m^{-1}, respectively. As already mentioned, the spike in the locomotive's acceleration is not large enough and is always in the negative range when the coupler gap

is small at 5 mm. In view of this, the coupler stiffness need not be limited in order to meet the recommendation stated earlier.

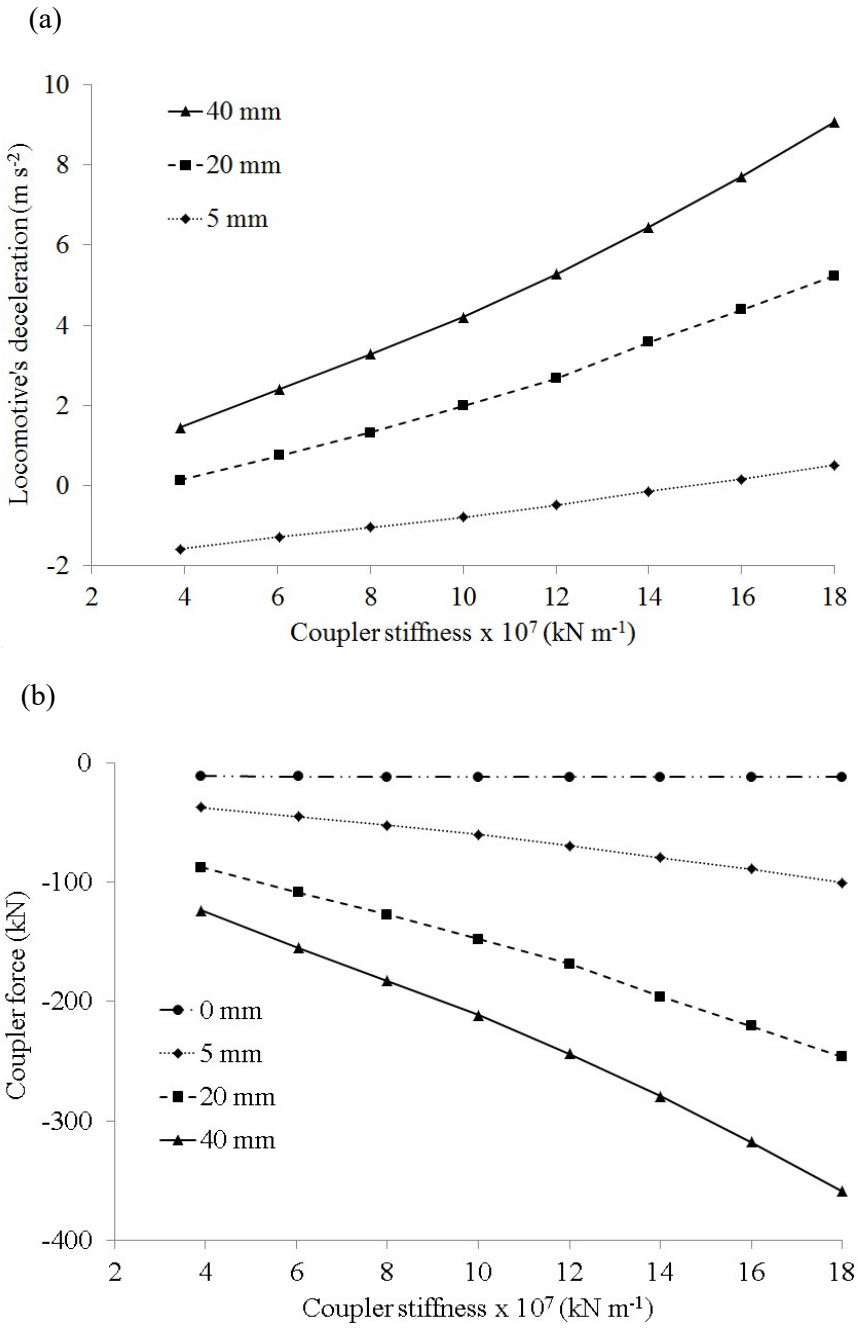

Figure 6.11. Effect of coupler stiffness and coupler gap on: (a) locomotive's acceleration and (b) compressive coupler force.

6.6.5 Effect of wheel load

Passenger railcars, even when filled to full capacity, are normally lighter than the locomotive which houses heavy machineries and engines. In view that wheel load is a key factor affecting the adhesion between the wheel and rail and hence the longitudinal interaction between railcars, it would be important to investigate the effect of wheel load on the longitudinal interaction in a multiple-railcar train. This section presents the results of a study in which the weight of the passenger railcar is varied from the smallest to the largest. The former occurs when the passenger railcar is empty and the latter occurs when the railcar is filled with passengers to the full capacity.

Figure 6.12 shows the variation of the force in the coupler between the locomotive and the 1st passenger railcar against the braking torque for two cases of wheel loads. Wheel loads of 55 kN (Tokunaga and Sogabe 2012) and 69 kN (Chen and Li 2000) correspond to the empty and full capacity passenger railcars, respectively. In both cases, wheel loads of 75 kN (Chen and Li 2000) are assumed for the locomotive. The properties of the couplers connecting neighbouring railcars employed in the study are presented in Table 6.1 (Chou et al. 2007). As can be seen in Figure 6.12, the coupler force in the case of full capacity railcars is noted to be generally smaller than that of empty railcars. There is a wider range of braking torques in which there is longitudinal interaction between railcars when the passenger railcars are empty as compared to the case when they are full capacity. This can be explained as due to the lesser adhesion between the wheels and rail for the

case of empty passenger railcars, which then tends to travel faster than the locomotive resulting in longitudinal interaction.

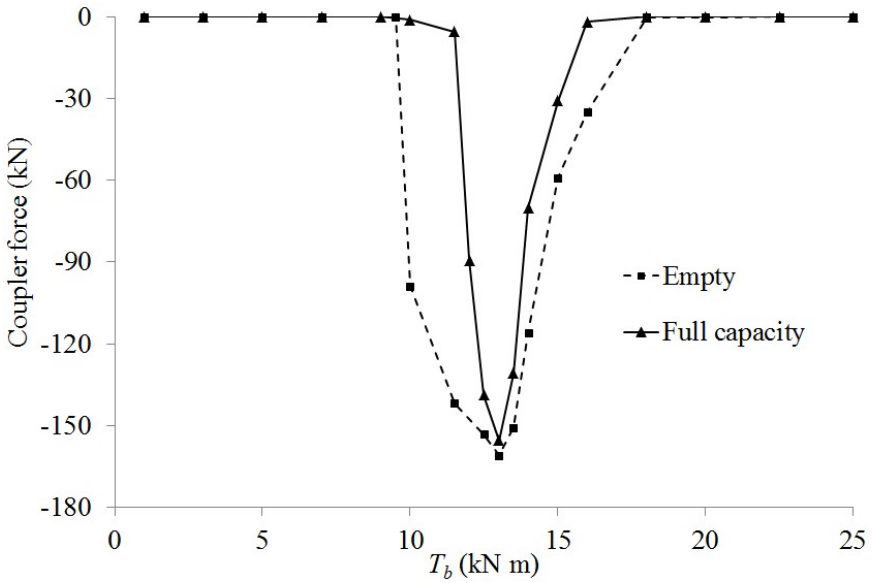

Figure 6.12. Effect of passenger railcar's wheel load on coupler force.

6.6.6 Effect of wheel-rail contact condition

The adhesion wheel-rail force depends on the wheel-rail contact condition, which ultimately affects the response of the multiple-railcar train subject to braking. Earlier results presented correspond only to dry contact condition. It is expected that the multiple-railcar train dynamics would be affected if the wheel-rail contact condition is wet. This section presents the results of a study comparing the response of the train subject to braking under wet and dry contact conditions.

Figure 6.13 shows the variation of the compressive coupler force against the applied braking torque for both dry and wet wheel-rail contact conditions. Under wet condition, longitudinal interaction between railcars occurs at a

smaller braking torque as compared to the dry case condition. The peak value in the compressive coupler force is lower in the wet condition as compared to the dry case. In both cases, the peak coupler force is attained when the braking torque is at the corresponding critical value, namely, 7.5 kN m and 13.5 kN m for the wet and dry conditions, respectively.

The wheel-rail adhesion depends on the wheel-rail condition, being smaller when it is wet. In view there is smaller adhesion, railcars tend to be moving independently which explains why there is less longitudinal interaction and hence smaller peak compressive coupler force. While it appears 'favourable' that the wet condition results in smaller interaction and coupler force, it is important to take note of the unfavourable conclusions made earlier in Chapter 5 regarding the safe braking distance and duration of wheel sliding.

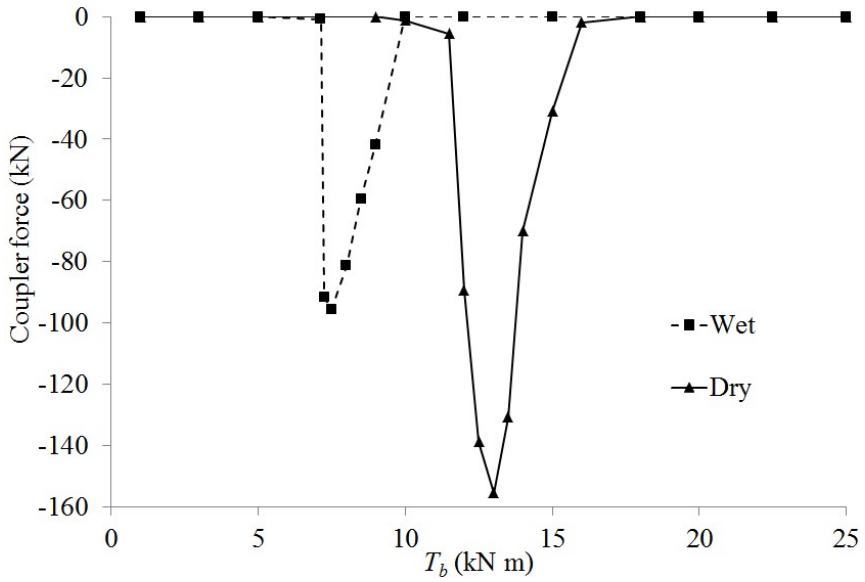

Figure 6.13. Effect of wheel-rail contact condition on the coupler force.

6.6.7 Effect of initial train speed

Earlier chapters have demonstrated that the initial train speed plays a significant factor on the dynamics of the HSR when a single-railcar train is subject to braking. It is therefore expected that the initial train speed will also be a key factor in the case of a multiple-railcar train subject to braking, in particular the longitudinal interaction between railcars. This section presents the results of a study in which three typical speeds of today's high-speed trains are selected as the initial speed of the train prior to the application of wheel braking torque.

Figure 6.14 shows the variation of the maximum compressive coupler force between the locomotive and 1st railcar against the braking torque for various initial train speeds. It can be seen that the magnitude of the peak coupler force is inversely affected by the magnitude of the initial train speed. In other words, the peak is smaller when the initial train speed is higher and vice-versa. The coupler force attains its peak when the braking torque is applied at the critical value. As explained in earlier chapters, the critical braking torque is the smallest torque that results in the condition when all wheels are sliding. Figure 6.14 shows that the critical braking torque is also inversely affected by the initial train speed, being smaller for higher initial train speed and vice-versa.

The adhesion between the wheels and rail is dependent on initial train speed, being smaller for higher initial train speed. As explained in the previous section, the lesser adhesion between wheel and rail results in railcars tending

to travel independently. There is therefore lesser longitudinal interaction and hence smaller peak compressive coupler force. Thus, while it appears 'favourable' that higher initial train speed results in smaller interaction and coupler force, it is important to take note that there is also accompanying unfavourable effects due to high initial train speed, including longer braking distance, longer duration of wheel sliding, high DAF in wheel contact force and higher possibility of wheel jumping.

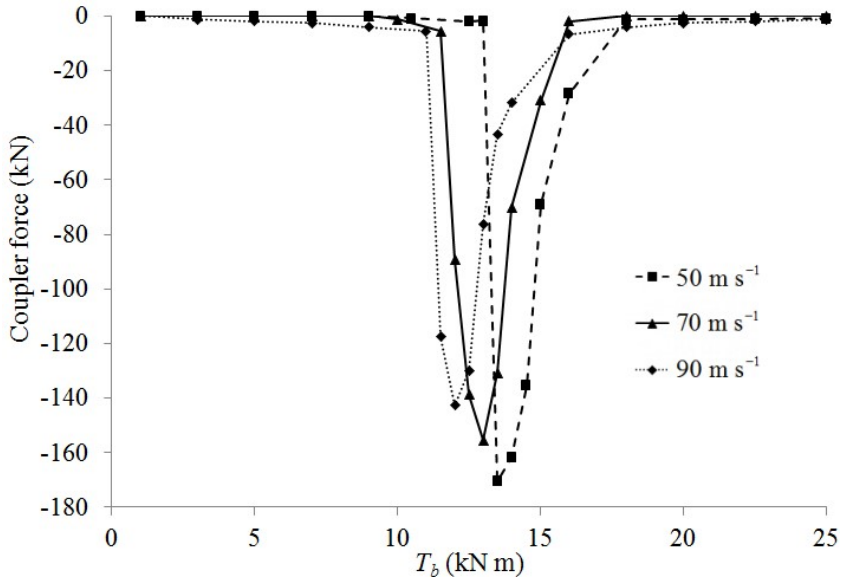

Figure 6.14. Effect of train speed and braking torque on the coupler force.

6.6.8 Effect of partial failure in braking mechanism

In all previous studies, the train is subject to braking through the application of braking torque to all wheels of the train. This is the normal mode of braking to bring a train from a high speed to a halt. For the unfortunate incidence where there is partial failure in the braking mechanism, it is expected that there will be substantial effect on the longitudinal

interaction between railcars. This section presents the results of the scenario of partial failure in the braking mechanism of the train in which there is failure in the braking mechanisms of the passenger railcars. Therefore, the braking of the train is dependent solely on the braking mechanism of the locomotive.

Figure 6.15 shows the variation of maximum compressive coupler force between the locomotive and 1st passenger railcar against various braking torques, which is applied to at all wheels of the entire train (Case 1) and all wheels of the locomotive only (Case 2). It can be seen from the figure that there is virtually no force induced in the train coupler when the applied braking torque is smaller than approximately 8.5 kN m for the two cases considered. When the braking torque is further increased, the coupler force induced in Case 2 increases significantly whilst there is no corresponding immediate increase in the coupler force for Case 1. In both cases, the coupler force reaches a peak when the applied braking torque reaches approximately 13.0 kN m. The peak value for Case 2 is noticeably larger than Case 1. The coupler force reduces rapidly from the peak value to virtually 0 and a smaller non-zero value when the braking torque is increased further for Cases 1 and 2, respectively. From Figure 6.15, it can be seen that there is a wider range of braking torque that will induce high values of coupler force when there is partial failure in the train's braking mechanism as compared to the case where there is no failure.

The trend in the results presented in Figure 6.15 can be readily explained. When the braking torque is smaller than 8.5 kN m, all wheels of the

entire train tend to roll till the train comes to a halt for both cases. Under such a situation, the maximum relative motion between neighboring railcars is smaller than the coupler gap. There is thus no longitudinal interaction between railcars and no development of force in the coupler. When the braking torque is increased, the passenger railcars in Case 2 tend to move faster than the locomotive as there are no brakes applied to the passenger railcars' wheels unlike in Case 1. Consequently, there is more longitudinal interaction and hence larger coupler force in Case 2 as compared to Case 1.

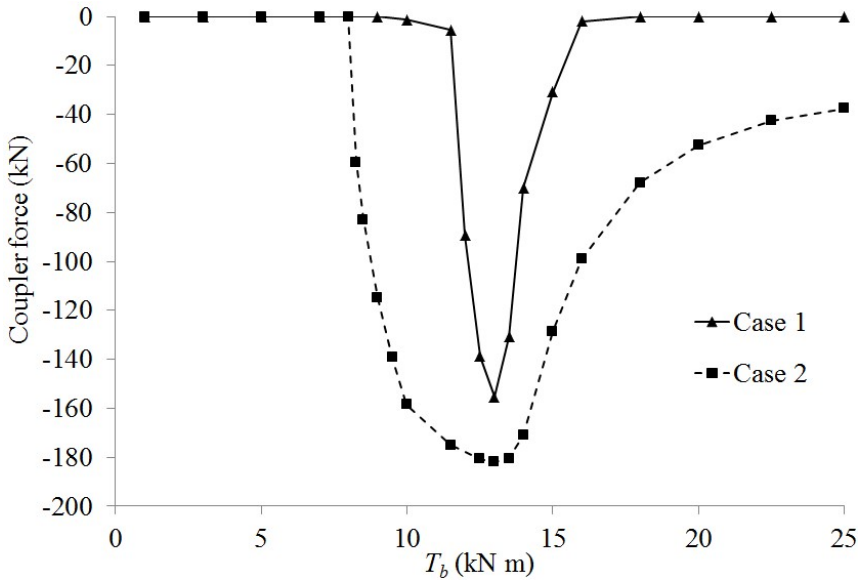

Figure 6.15. Effect of braking mechanisms on the coupler force.

6.7 Concluding remarks

This chapter is concerned with the dynamic response of multiple-railcar train subject to braking using the MEM, where longitudinal interaction between railcars is of major concern. The mathematical model of a multiple-railcar train subject to braking is presented. The model considers the

interaction between railcars connected to each other through train coupler. Slack action due to relative motion between railcars is considered. The model also considers the possibility of wheel sliding, which may occur sequentially when the braking torque applied is large enough. The model also considers the effect of the coupler gap, which tends to cause cyclical variation in the coupler force ranging from compression to tension.

The MEM solutions obtained in this study are verified through comparison with results obtained via the FEM due to the lack of available results in the literature. Both methods gave results which are found to be virtually the same. As highlighted throughout this thesis, the MEM enjoys significant computational efficiency over the FEM. The minimum number of railcars that can accurately model a multiple-railcar train is found to be 3. In other words, the response of a 3-railcar train would give nearly the same response of a train comprising of more railcars. In view of significant computational cost savings, it is therefore recommended that any study of a multiple-railcar train need to consider only 3 railcars.

Results of a parametric study to investigate the effects of various factors on the dynamic response of high-speed multiple-railcar train subject to braking have been presented. Parameters considered include the magnitude of braking torque, coupler stiffness, coupler gap size, wheel load, wheel-rail contact condition and initial train speed. The effect of partial failure in the braking mechanism of the train was also investigated.

When a multiple-railcar train decelerates due to braking, the longitudinal interaction between neighbouring railcars results in periodic significant spikes in the time histories of the deceleration and bogie's pitching motion of the locomotive. The longitudinal interaction does not result in a significant but nonetheless noticeable effect on the vertical dynamic response. The longitudinal interaction has virtually no effect on the magnitude of the critical and optimal braking torques. The difference noted between passenger railcar and locomotive is due to the difference in mass of these two types of railcars. The longitudinal interaction has negligible effect on the duration of wheel sliding. Only when the applied braking torque lies between the optimal and critical torques, the longitudinal interaction results in a noticeable increase in the duration of wheel sliding for the trailing wheel.

There is a wider range of braking torque that will induce high longitudinal interaction when the passenger railcars are empty as compared to the case when they are full capacity. The same finding is also found when there is partial failure in the train's braking mechanism as compared to the case where there is no failure. The longitudinal interaction in the case of full capacity railcars and no failure in the train's braking mechanism is noted to be generally smaller as compared to the case of empty railcars and partial failure in the train's braking mechanism, respectively. While it appears 'favourable' that the wet condition and higher initial train speed result in smaller interaction between railcars and coupler force, it is important to take note of the unfavourable conclusions made earlier in Chapter 5 regarding the safe braking

distance, duration of wheel sliding, DAF in contact force and higher possibility of occurrences of the jumping wheel phenomenon.

Similar to a single-railcar train, the magnitude of the applied braking torque controls significantly the dynamic response of a multiple-railcar train. The braking torque should be applied at the optimal torque value as this would lead to the best safety in terms of smallest braking distance as well as ensuring structural stability and strength as there is no occurrence of wheel sliding and almost zero force in the train coupler.

When the braking torque applied is at the critical torque value, the DAF in wheel contact force and the compressive force developed in the train coupler both reached their peak values. Thus, in both single and multiple-railcar trains, the present study reveals that the braking torque applied should not match the critical torque value as this increases the chance of failures in train structural components. In the case of multiple-railcar train, the train coupler would experience peak compressive and tensile forces. The peak compressive force is found to be higher than the peak tensile force, which has implications in the design of the train coupler. As there are the repetitive cyclical variations between peak compressive and peak tensile force, there is therefore an increased concern in the fatigue failure of the train coupler. In addition, all wheels of the train are in sliding motion almost throughout the period of deceleration. Thus, there is additional unease over the overall stability of the train due to heightened chance of train derailment, especially if accompanied with occurrences of jumping wheel phenomenon.

CHAPTER 7. CONCLUSIONS AND RECOMMENDATIONS FOR FUTURE WORK

The key points and conclusions from the present study are summarized in the next section. Finally, this chapter concludes with a section on the recommendations for future work.

7.1 Summary of key points

The main objective of the present study is to investigate the dynamic response of high-speed train subject to braking. Overall, the thesis represents a significant contribution to the subject in the context of the relatively new method of MEM. Compared to previous works on the MEM, the main findings in enhancing the method can be summarized as follows:

(1) A solution strategy to deal with non-uniform speed, instead of using the previous method of piecewise constant speed (Chapters 3 and 4). This is necessary to solve problems where acceleration or deceleration is not a priori known, which is the case for braking (especially unplanned deceleration due to emergency braking).

(2) In achieving point 1 above, the system dynamics has to include forces on moving train such as running resistance, wheel-rail contact force

(nonlinear Hertz model), wheel-rail adhesion force (Chapter 5). This enables the study of effects of braking on wheel sliding.

(3) Extended to include interaction of multiple railcars accounting for couplers with slack action (Chapter 6). This enables parametric studies of more realistic train-track dynamics due to braking.

The fundamental novel features of MEM remain largely the same, i.e. let the elements flow with the moving train and computational efficiency is thus improved substantially. The above enhancements indeed expand the applicability of MEM in a significant way to solve practical train-track dynamic problems. The thesis confirms that the MEM outperforms the FEM by presenting many numerical examples with good results.

7.2 Conclusions

The proposed computational scheme based on the MEM for the treatment of HSR subject to braking are verified against available analytical, MEM solutions as well as FEM solutions wherever necessary. Results from all methods are found to be agreeable thereby validating the proposed MEM adopted in the present study. The MEM, which is a variation of the FEM, however enjoys significant computational efficiency over the FEM and overcomes the inherent complications faced by the FEM.

Two computational schemes, one implicit and the other explicit, to treat the nonlinear normal wheel-rail contact force were discussed and presented. The implicit scheme is simpler to implement but is restricted only to simple

train models. The other explicit scheme is more complicated and requires generally more computational effort. This must be employed when dealing with more complicated train models. Where braking is involved, there is the additional complication arising from the nonlinear wheel-rail adhesion force. Thus, it is recommended that the explicit scheme be employed to investigate the dynamic response of single- and multiple-railcar train subject to braking.

To account for the wheel-rail interaction, two normal contact models were employed and their accuracy and suitability evaluated. It is found that the computationally cheaper linearized contact model is accurate enough to be used whenever the expected dynamic effect of the system is not large. On the other hand, it should be emphasized that the computationally more expensive but more accurate nonlinear contact model must be employed whenever the dynamic effect of the HSR system is expected to be significant. A combination of small wheel load, high train speed and severe track condition promotes larger dynamic effects and hence the greater chance of occurrence of the jumping wheel phenomenon. This has important implication on the track maintenance program. It is critical that track maintenance be properly exercised and/or the train operational speed be moderated to avoid any occurrence of the jumping wheel phenomenon, especially for old tracks where track corrugation is likely to be severe.

When a train travels at a cruising speed higher than the resonant speed of the HSR, the dynamic response is found to be significantly larger when the speed of the train crosses the resonant speed as the train decelerates to come to

a halt. The momentary spike in the dynamic response, including the higher chance of occurrences of the jumping wheel phenomenon, needs to be considered in the safe operation of the HSR. From an engineering view point, it is therefore important to design the train-track-foundation system and propose a track maintenance program such that the resonant speed of the system is sufficiently higher than the maximum operational speed of the train.

When the train is subject to braking under emergency situation, the braking torque should be applied at the optimal torque value as this would lead to the best safety in terms of smallest braking distance as well as ensuring structural stability and strength as there is no occurrence of wheel sliding and almost zero force in the train coupler. The study also revealed that the braking torque applied should not match the critical torque value as this increases the chance of failure in train structural components due to the development of high DAF in contact force as well as peak compressive and tensile coupler forces.

The minimum number of railcars that can accurately model a multiple-railcar train is 3. In other words, the response of a 3-railcar train would give nearly the same response of a train comprising of more railcars. In view of significant computational cost savings, it is therefore recommended that any study of a multiple-railcar train need to consider only 3 railcars.

It was found that the peak compressive force is higher than the peak tensile force, which has implications in the design of the train coupler. Due to the repetitive cyclical variations between peak compressive and peak tensile

force, there is therefore an increased concern in the fatigue failure of the train coupler.

7.3 Recommendations for future work

The present study focused on the 2-D train model travelling over a straight railway beam resting on two-parameter elastic damped foundation. The train is assumed to be cruising at a typical speed of today's high-speed trains, before braking torques are applied at all wheels of entire train to decelerate the train to a halt. The railhead roughness is assumed to be sinusoidal. In view of the above scopes of the present study, some recommendations are given for further works on this subject:

(1) Dynamic analysis of a curved HSR subject to braking

The Spain derailment (2013) occurred when the train travels over a curved track at a speed that is 2.5 times higher than the design speed. This presents a good motivation for the study of high-speed train subject to braking as it travels over a curved track segment. Various parameters to be investigated include the initial train speed, the curvature and superelevation of the track and the magnitude of braking torque.

(2) Three-dimensional MEM study of the dynamics of HSR

In reality, train-track-foundation problems are three-dimensional (3-D) in nature. However, 2-D models are frequently employed by various researchers to solve such problems due to the high computational costs involved in employing 3-D models. Furthermore, 2-D models are generally

accepted to be able to provide reasonable estimates of the dynamic response. When would 3-D modeling be necessary is an important question to be investigated. Parameters such as train speed, track irregularity conditions, track-gauge and foundation properties would obviously affect the response and hence the accuracy of a 2-D model as compared to a 3-D model.

(3) Dynamic response of HSR over a curved rail in 3-D space

As rail tracks are often laid over realistic terrain, the tracks are typically curved in 3-D space. The dynamic response of HSR over a curved rail in 3-D space would therefore be useful. In addition to the parameters that are important for HSR over a straight track, other parameters that can be included in the study are associated with the 3-D nature of the problem including the angles of inclination and curvatures of the track. It is envisaged that the degree of curvature and angle of inclination have an appreciable effect on the stability and safety of the train carriage as well as the level of comfort to the passengers.

(4) Dynamic response of HSR over a floating bridge

Due to land scarcity in many parts of the world, there is increasing interests to harvest useable space from the sea. Many researches are presently carried out to investigate the feasibility of employing very large floating structures (VLFS) for various purposes, such as oil storage facility, floating city and floating wind-mill farm. These platforms are very large and infrastructures such as roads and train-tracks are needed to complement the

platform. Floating bridges are also increasingly being considered to increase the network of roads and rails. Thus, a study on the dynamics of HSR over a floating platform or bridge would provide useful results in the research into the use of VLFS and floating bridges.

PUBLICATIONS

Some of my research findings were reported in the following journal and conference papers:

1. SCI Journal papers

Ang, K. K., Dai, J., **Tran, M. T.** and Luong, V.H. (2014). Analysis of high-speed rail accounting for jumping wheel phenomenon. International Journal of Computational Methods, 11(3), 1343007-1–1343007-12.

Tran, M. T., Ang, K. K. and Luong, V. H. (2014). Vertical dynamic response of non-uniform motion of high-speed rails. Journal of Sound and Vibration, 333, 5427–5442.

Tran, M. T., Ang, K. K. and Luong, V. H. (2016). Dynamic response of high-speed rails due to heavy braking. Journal of Rail and Rapid Transit (DOI: 10.1177/0954409716639997).

Tran, M. T., Ang, K. K. and Luong, V. H. (2017). Vertical dynamic response of high-speed rails during sudden deceleration. International Journal of Computational Methods, 14(1), 1750014-1–1750014-24.

Tran, M. T., Ang, K. K. and Luong, V. H. (2017). Multiple-railcar high-speed train subject to braking. International Journal of Structural Stability and Dynamics, 17(7) (In Proof).

Tran, M. T., Ang, K. K., Luong, V. H. and Dai, J. (2016). High-speed trains subject to abrupt braking. Vehicle System Dynamics. (Accepted)

2. Conference papers

Ang, K. K., Dai, J. and **Tran, M. T.** (2012). Analysis of high-speed rail accounting for jumping wheel phenomenon. The International Conference on Advances in Computational Mechanics (ACOME), August 14-16, Ho Chi Minh City,

Vietnam. (**Keynote lecture**)

Ang, K. K., **Tran, M. T.** and Luong, V. H. (2013). Track vibrations during accelerating and decelerating phases of high-speed rails, The 13th East Asia-Pacific Conference on Structural Engineering and Construction (EASEC-13), September 11-13, Sapporo, Japan.

Tran, M. T., Ang, K. K. and Luong, V.H. (2013). Dynamic analysis of high-speed rail system on two-parameter elastic damped foundation. International Conference on Advanced Computing and Applications (ACOMP), October 23-25, Ho Chi Minh City, Vietnam.

Tran, M. T., Ang, K. K., Dai, J. and Luong, V. H. (2013). Moving frame method for dynamic analysis of high speed train-slab track system. The Conference on Computational Solid Mechanics (CSM), November 7-9, Ho Chi Minh City, Vietnam.

Ang, K. K., Dai, J., **Tran, M. T.** and Luong, V. H. (2013). Moving element analysis of elastic beams on visco-elastic foundation under moving loads. The Conference on Computational Solid Mechanics (CSM), November 7-9, Ho Chi Minh City, Vietnam. (**Keynote lecture**).

Tran, M. T., Ang, K. K. and Luong, V. H. (2016). Response of high-speed rails subject to braking. The 14th East Asia-Pacific Conference on Structural Engineering and Construction (EASEC-14), January 6-8, Ho Chi Minh City, Vietnam.

REFERENCES

Ahmad, H. A. (2013). Dynamic Braking Control for Accurate Train Braking Distance Estimation under Different Operating Conditions. Thesis, Blacksburg, VA, USA.

Andersen, L., Nielsen, S. R. K. and Kirkegaard, P. H. (2001). Finite element modelling of infinite Euler beams on Kelvin foundations exposed to moving loads in convected co-ordinates. Journal of Sound and Vibration, 241(4), 587–604.

Andersen, L., Nielsen, S. R. K. and Krenk, S. (2007). Numerical methods for analysis of structure and ground vibration from moving loads. Computers and Structures, 85, 43–58.

Ang, K. K. and Dai, J. (2013). Response analysis of high-speed rail system accounting for abrupt change of foundation stiffness. Journal of Sound and Vibration, 332, 2954–2970.

Ansari, M., Esmailzadeh, E. and Younesian, D. (2009). Longitudinal dynamics of freight trains. International Journal of Heavy Vehicle Systems, 16(1), 102–131.

Bathe, K. J. (1996). Finite Element Procedures. Prentice-Hall, Englewood Cliffs, N.J.

Chen, Y. H. and Li, C. Y. (2000). Dynamic response of elevated high-speed railway. Journal of bridge engineering, 5(2), 124–130.

China Academy of Railway Science (1998). Translation Collection of Safety of Running Trains: Derailment Study.

Chou, M., Xia, X. and Kayser, C. (2007). Modelling and model validation of heavy-haul trains equipped with electronically controlled pneumatic brake systems. Control Engineering Practice, 15, 501–509.

Clark, R. A., Dean, P. A., Elkins, J. A. and Newton, S. G. (1982). An investigation into the dynamic effects of railway vehicles running on corrugated rails. Journal of Mechanical Engineering Science, 24, 65–76.

Clough, R. W. and Penzien, J. (1993). Dynamics of structures (2nd edition). McGraw-Hill, Inc, New York.

Cole, C. and Sun, Y. Q. (2006). Simulated comparisons of wagon coupler systems in heavy haul trains. Proceedings of the Institution of Mechanical Engineers, Part F:

Journal of Rail and Rapid Transit, 220(3), 247–255.

Dai, J. and Ang, K. K. (2014). Steady-state response of a curved beam on a viscously damped foundation subjected to a sequence of moving loads. Proceedings of the Institution of Mechanical Engineers, Part F: Journal of Rail and Rapid Transit, 229(4), 375–394.

Dhanasekar, M., Cole, C. and Handoko, Y. (2007). Experimental evaluation of the braking torque on bogie dynamics. International Journal of Heavy Vehicle Systems, 14(3), 308–330.

Dimitrovova´, Z. and Varandas, J. N. (2009). Critical velocity of a load moving on a beam with a sudden change of foundation stiffness: Applications to high speed trains. Computers and Structures, 87, 1224–1232.

Esveld, C. (2001). Modern Railway Track (2nd edition). MRT Productions: Duisburg.

Feng, Z. and Cook, R. (1983). Beam elements on two-parameter elastic foundations. Journal of Engineering Mechanics, 109, 1390–1402.

Filonenko-Borodich, M. M. (1940). Some approximate theories of the elastic foundation. Scientific Notes of the Moscow State University, Mechanics, 46, 3–18. (in Russian)

Frýba, L., Nakagiri, S. and Yoshikawa, N. (1993). Stochastic finite element for a beam on a random foundation with uncertain damping under a moving force. Journal of Sound and Vibration, 163, 31–45.

Garg, V. K. and Dukkipati, R. V. (1984). Dynamics of Railway Vehicle Systems. Ontario, Canada: Academic Press.

Grassie, S. L. and Kalousek, J. (1993). Rail corrugation: characteristics, causes and treatments. Proceedings of the institution of Mechanical Engineerings, 207, 57–68.

Handoko, Y. and Dhanasekar, M. (2007). Wheelset skid in railway bogies. Journal of Rail Rapid Transit, 221, 237–245.

Herrmann, L. (2008). Vibration of the Euler-Bernoulli beam with allowance for damping, Proceedings of the World congress on Engineering, 2, London, U.K.

Herwig, A. (2006). Consideration of the dynamic effect of increased train loads for the fatigue examination of concrete bridges. The 6th International PhD Symposium in Civil Engineering, Zurich.

Iwnicki, S. (2006). Handbook of Railway Vehicle Dynamics. CRC Press, Boca Raton.

Kalker, J. J. (1967). On the rolling contact of two elastic bodies in the presence of dry friction. Thesis, Delft.

Karlstrom, A. (2006). An analytical model for ground vibrations from accelerating trains. Journal of Sound and Vibration, 293, 587–598.

Kerr, A. D. (1964). Elastic and viscoelastic foundation models. Journal of Applied Mechanics, 31, 491–498.

Kim, M. S. (2011). Dynamometer tests of brake shoes under wet conditions for the high speed trains. International Journal of Systems Applications, Engineering and Development, 5(2), 143–150.

Koh, C. G., Chiew, G. H. and Lim, C. C. (2007). A numerical method for moving load on continuum. Journal of Sound and Vibration, 300, 126–138.

Koh, C. G., Ong, J. S. Y., Chua, D. K. H. and Feng, J. (2003). Moving element method for train-track dynamics. International Journal for Numerical Methods in Engineering, 56, 1549–1567.

Koh, C. G., Sze, P. P. and Deng, T. T. (2006). Numerical and analytical methods for in-plane dynamic response of annular disk. International Journal of Solids and Structures, 43, 112–131.

Krenk, S., Kellezi, L., Nielsen, S. R. K. and Kirkegaard, P. H. (1999). Finite elements and transmitting boundary conditions for moving loads. Proceedings of the 4th European Conference on Structural Dynamics, Eurodyn '99, 447–452.

Kumari, S., Sahoo, P. P. and Sawant, V. A. (2012). Dynamic response of railway track using two parameter model. International Journal of Science and Engineering Applications, 1(2), 2319–7560.

Lei, X. and Wang, J. (2013). Dynamic analysis of the train and slab track coupling system with finite elements in a moving frame of reference. Journal of Vibration and Control, 20(9), 1301–1317.

Lixin, Q. and Haitao, C. (2001). Three dimension dynamics response of car in heavy haul train during braking mode. 7th International Heavy Haul Conference, Brisbane, Australia, 231–238.

Nielsen, J. C. O. and Abrahamsson, T. J. S. (1992). Coupling of physical and modal components for analysis of moving non-linear dynamic systems on general beam structures. International Journal for Numerical Methods in Engineering, 33, 1843–1859.

Nielsen, J. C. O. and Igeland, A. (1995). Vertical dynamic interaction between train

and track influence of wheel and track imperfections. Journal of Sound and Vibration, 187(5), 825–839.

Pasternak, P. L. (1954). On a new method of analysis of an elastic foundation by means of two foundation constants. State Publications on Construction Literature, Architecture, Moscow 1954. (in Russian).

Polach, O. (2005). Creep forces in simulations of traction vehicles running on adhesion limit. Wear, 258, 992–1000.

Powell, J. P. and Palacín, R. (2015). Passenger Stability Within Moving Railway Vehicles: Limits on Maximum Longitudinal Acceleration. Urban Rail Transit, 1(2), 95–103.

Pugi, L., Fioravanti, D. and Rindi, A. (2007). Modelling the longitudinal dynamics of long freight trains during the braking phase. 12th IFToMM World Congress, France.

Suzuki, S. I. (1977). Dynamic behavior of a finite beam subjected to travelling loads with acceleration. Journal of Sound and Vibration, 55(1), 65–70.

Thambiratnam, D. and Zhuge, Y. (1996). Dynamic analysis of beams on an elastic foundation subjected to moving loads. Journal of Sound and Vibration, 198(2), 149–169.

Thompson, D. J. (2008). Railway Noise and Vibration: Mechanisms, modelling and means of control. Elsevier science, Oxford, 506.

Timoshenko, S. P. (1926). Statical and dynamical stresses in rails. Proceedings of the 2nd International Congress for Applied Mechanics, Zurich, Switzerland, 407–418.

Tokunaga, M. and Sogabe, M. (2012). Effect of dynamic interaction between train vehicle and structure on seismic response of structure. The 15th World Conference on Earthquake Engineering, Portugal, 7, 5617–5627.

Vlasov, V. Z. and Leont'ev, N. N. (1966). Beams, plates and shells on elastic foundations. Israel Program for Scientific Translations, Jerusalem, Israel, 1966; IPST Cat. No. 1453.

Wu, T. X. and Thompson, D. J. (2000). Theoretical investigations of wheel/rail non-linear interaction due to roughness excitation. ISVR Technical Memorandum No. 582.

Wu, Y. S., Yang, Y. B. and Yau, J. D. (2001). Three-dimensional analysis of train-rail-bridge interaction problems. Vehicle System Dynamics, 36, 1–35.

Yadav, D. (1991). Non-stationary dynamics of train and flexible track over inertial

foundation during variable velocity. Journal of Sound and Vibration, 147(1), 57–71.

Yang, C. D. and Sun, Y. P (2001). Mixed H_2/H cruise controller design for high speed train. International Journal of Control, 74(9), 905–920.

Zhang, Z. and Dhanasekar, M. (2009). Dynamics of railway wagons subjected to braking/traction torque. Vehicle System Dynamics, 47(3), 285–307.

Zhuan, X. and Xia, X. (2006). Optimal Scheduling and Control of Heavy Haul Train Equipped with Electronically Controlled Pneumatic Braking Systems. Proceedings of the 6th World Congress on Intelligent Control and Automation, Dalian, China, 8168–8172.